



**EXPERIMENTAL METHODS TO CHARACTERIZE NONLINEAR  
VIBRATION OF FLAPPING WING MICRO AIR VEHICLES**

THESIS

Adam P. Tobias, Captain, USAF  
AFIT/GAE/ENY/07-M23

DEPARTMENT OF THE AIR FORCE  
AIR UNIVERSITY

**AIR FORCE INSTITUTE OF TECHNOLOGY**

Wright-Patterson Air Force Base, Ohio

APPROVED FOR PUBLIC RELEASE; DISTRIBUTION UNLIMITED

The views expressed in this thesis are those of the author and do not reflect the official policy or position of the United States Air Force, Department of Defense, or the United States Government.

AFIT/GAE/ENY/07-M23

EXPERIMENTAL METHODS TO CHARACTERIZE NONLINEAR  
VIBRATION OF FLAPPING WING MICRO AIR VEHICLES

THESIS

Presented to the Faculty

Department of Aeronautics and Astronautics

Graduate School of Engineering and Management

Air Force Institute of Technology

Air University

Air Education and Training Command

In Partial Fulfillment of the Requirements for the  
Degree of Master of Science in Aeronautical Engineering

Adam P. Tobias, BS

Captain, USAF

March 2007

APPROVED FOR PUBLIC RELEASE; DISTRIBUTION UNLIMITED

AFIT/GAE/ENY/07-M23

EXPERIMENTAL METHODS TO CHARACTERIZE NONLINEAR  
VIBRATION OF FLAPPING WING MICRO AIR VEHICLES

Adam P. Tobias, BS  
Captain, USAF

Approved:

\_\_\_\_\_  
Anthony N. Palazotto (Chairman)

\_\_\_\_\_  
Date

\_\_\_\_\_  
Phillip S. Beran (Member)

\_\_\_\_\_  
Date

\_\_\_\_\_  
Richard G. Cobb (Member)

\_\_\_\_\_  
Date

## **Abstract**

**For urban combat reconnaissance, the flapping wing micro air vehicle concept is ideal because of its low speed and miniature size, which are both conducive to indoor operations. The focus of this research is the development of experimental methods best suited for the vibration testing of the wing structure of a flapping wing micro air vehicle. This study utilizes the similarity of a beam resonating at its first bending mode to actual wing flapping motion. While computational finite element analysis based on linear vibration theory is employed for preliminary beam sizing, an emphasis is placed on experimental measurement of the nonlinear vibration characteristics introduced as a result of large movement. Beam specimens fabricated from 2024-T3 aluminum alloy and IM7/5250-4 carbon-epoxy were examined using a high speed optical system and a scanning laser vibrometer configured in both three and one dimensions, respectively.**

AFIT/GAE/ENY/07-M23

*To my wife, and our inspiration*

## **Acknowledgments**

I would like to express my sincere appreciation to my thesis advisor, Dr. Anthony Palazotto, for his support during the course of this research effort. Dr. Palazotto offered a lifetime of experience and immeasurable guidance, and for that I am grateful. I would also like to thank Dr. Richard Cobb and Dr. Phillip Beran for their support and feedback throughout this project.

Additionally, I would like to extend my gratitude to Dean Bryson, an undergraduate student from Purdue University. Dean was extremely helpful in many facets of the beginning stages of this project. Next, I would like to mention my appreciation for the moment's notice assistance that Dr. Greg Schoeppner provided in creating the carbon-epoxy beam specimens; a very large part of this project. Finally, I would like to thank the AFIT laboratory staff members Dwight, Wilbur, and Jay. They provided continuous assistance through the entirety of the experimental stages of this thesis.

Adam P. Tobias

## Table of Contents

Abstract .....	iv
Acknowledgments.....	vi
Table of Contents.....	vii
List of Figures .....	ix
List of Tables.....	xii
<b>I Introduction.....</b>	<b>1</b>
<i>1.1 Motivation .....</i>	<i>1</i>
<i>1.2 Relevance to the USAF.....</i>	<i>2</i>
<b>II Problem Formulation.....</b>	<b>6</b>
<i>2.1 Beam Theory and Analysis of Methods .....</i>	<i>6</i>
<i>2.2 Beam Sizing .....</i>	<i>9</i>
2.2.1 Matlab Eigenvalue Determinations.....	9
2.2.2 ABAQUS Finite Element Analysis .....	16
<b>III Experimental Investigation .....</b>	<b>23</b>
<i>3.1 Laser Vibrometry Theory .....</i>	<i>23</i>
<i>3.2 High Speed Camera Methodology .....</i>	<i>25</i>
<i>3.3 Experimental Equipment.....</i>	<i>26</i>
3.3.1 Aluminum Beam Design .....	27
3.3.2 Carbon-Epoxy Beam Design.....	28
3.3.3 Aluminum Clamp Design.....	29
3.3.4 Laboratory Test Support Equipment .....	31
3.3.5 Laser Vibrometer Setup and Procedure.....	37
3.3.6 High Speed Camera Setup and Procedure .....	48
<i>3.4 Three Dimensional Laser Vibrometer Experimentation .....</i>	<i>54</i>
3.4.1 Aluminum Beam - Asymmetric Shaker Configuration.....	55
3.4.2 IM7/5250-4 Carbon-Epoxy Beam - Asymmetric Shaker Configuration .....	60
<i>3.5 One Dimensional Laser Vibrometer Experimentation .....</i>	<i>64</i>
3.5.1 Aluminum Beam - Asymmetric Shaker Configuration.....	65
3.5.2 Aluminum Beam - Symmetric Shaker Configuration .....	70
3.5.3 IM7/5250-4 Carbon-Epoxy Beam - Asymmetric Shaker Configuration .....	73
3.5.4 IM7/5250-4 Carbon-Epoxy Beam - Symmetric Shaker Configuration .....	76
<i>3.6 High Speed Optical Experimentation .....</i>	<i>106</i>
<b>IV Conclusions.....</b>	<b>110</b>



<i>4.1 Experimental Methods</i> .....	110
<i>4.2 Proposed Topics for Further Study</i> .....	113
<b>Appendix A</b> .....	<b>114</b>
<i>A.1 Matlab Code to Calculate Beam Length for an Aluminum Beam</i> .....	114
<i>A.2 Matlab Code to Calculate Beam Length for a Carbon-Epoxy Beam</i> .....	116
<i>A.3 Matlab Code to Plot PSV FRFs and Displacement Frequency Spectrums</i> .....	120
<i>A.4 Matlab Code to Plot PSV Phase Plots</i> .....	123
<i>A.5 Matlab Code to Plot Vibrometer &amp; Accelerometer FRF Comparison</i> .....	125
<b>Appendix B</b> .....	<b>127</b>
<b>Appendix C</b> .....	<b>143</b>
<b>Appendix D</b> .....	<b>149</b>
<b>Bibliography</b> .....	<b>154</b>
<b>Vita</b> .....	<b>156</b>

## List of Figures

Figure 1: First Mode Shape of a Cantilever Beam .....	9
Figure 2: 0/90/90/0 Laminate Thickness Definition .....	15
Figure 3: 2024-T3 Aluminum Beam Length and Width .....	17
Figure 4: 2024-T3 Aluminum Beam Thickness .....	17
Figure 5: 2024-T3 Aluminum Beam Young's Modulus and Poisson's Ratio .....	18
Figure 6: 2024-T3 Aluminum Beam Density .....	18
Figure 7: 2024-T3 Aluminum Beam 1 <sup>st</sup> Bending Mode ABAQUS Eigenvector – Isometric View .....	19
Figure 8: 2024-T3 Aluminum Beam 1 <sup>st</sup> Bending Mode ABAQUS Eigenvector – Side View .....	19
Figure 9: T300/5208 Length and Width .....	20
Figure 10: T300/5208 Thickness and Orientation Angle .....	20
Figure 11: T300/5208 Mechanical Properties .....	21
Figure 12: T300/5208 Mechanical Properties .....	21
Figure 13: T300/5208 Beam 1 <sup>st</sup> Bending Mode Abaqus Eigenvector – Isometric View .....	22
Figure 14: Laser Measurement and Reference Beams .....	23
Figure 15: Michelson Interferometer .....	24
Figure 16: Laser Doppler Vibrometer Schematic .....	25
Figure 17: SolidWorks Drawing – Aluminum Beam .....	28
Figure 18: SolidWorks Drawing – Lower Half of Aluminum Clamp .....	29
Figure 19: SolidWorks Drawing – Upper Half of Aluminum Clamp .....	30
Figure 20: SolidWorks Assembly – Beam & Clamp Configuration .....	30
Figure 21: Isometric View of Beam/Clamp/Shaker Configuration .....	32
Figure 22: Top View of Beam/Clamp/Shaker Configuration .....	33
Figure 23: PCB Power Amplifier – Rear View .....	35
Figure 24: PCB Power Amplifier – Front View .....	35
Figure 25: Tektronix Oscilloscope .....	36
Figure 26: Test Stands, Spotlights, and Ruler Setup for High Speed Testing .....	37
Figure 27: Right, Center, and Left PSV-400 Scanning Heads .....	40
Figure 28: Right, Center, and Left PSV-400 Scanning Heads .....	41
Figure 29: Polytec OF V-5000 Vibrometric Controller .....	42
Figure 30: Polytec Test Console .....	43
Figure 31: Uncoated Carbon-Epoxy Beam .....	44
Figure 32: White Coating on Carbon-Epoxy Beam .....	44
Figure 33: 3-D Alignment Coordinate Axes .....	45
Figure 34: 3-D Alignment Remote Control .....	45
Figure 35: Photron FASTCAM Positioned Vertically Above Beam .....	48
Figure 36: Photron FASTCAM Positioned Vertically Above Beam .....	49
Figure 37: Optical Test Setup .....	50
Figure 38: Photron FASTCAM Viewer Software .....	51
Figure 39: Photron Motions Tools Analysis Software .....	53
Figure 40: Photron Motion Analysis Data Sheet .....	53
Figure 41: 3-D Asymmetric Aluminum Beam Configuration – Horizontally Affixed to Shaker .....	55
Figure 42: 3-D Asymmetric Aluminum Beam Configuration – Frequency Spectrum .....	57
Figure 43: 3-D Asymmetric Aluminum Beam Configuration – Log-Scale Frequency Spectrum .....	57
Figure 44: 3-D Asymmetric Aluminum Beam Configuration – 20 Hz FastScan Mode Shape .....	58
Figure 45: Vibration Velocity Approaching 10 m/s Limit .....	59
Figure 46: 3-D Asymmetric Carbon-Epoxy Beam Configuration – 20 Hz FastScan Mode Shape .....	60
Figure 47: 3-D Asymmetric Carbon-Epoxy Beam Configuration – Frequency Spectrum .....	61
Figure 48: 3-D Asymmetric Carbon-Epoxy Beam Configuration – 31 Hz FastScan Eigenvectors .....	62
Figure 49: 3-D Laser Vibrometer Issues with Large Deflecting Beam .....	63
Figure 50: 1-D Asymmetric Aluminum Beam Configuration – Vibrometer Scan Grid .....	65
Figure 51: 1-D Asymmetric Aluminum Beam Configuration – Acquisition General Settings .....	65
Figure 52: 1-D Asymmetric Aluminum Beam Configuration – Acquisition Channel Settings .....	66
Figure 53: 1-D Asymmetric Aluminum Beam Configuration – Acquisition Frequency Settings .....	67
Figure 54: 1-D Asymmetric Aluminum Beam Configuration – Acquisition Window Settings .....	67

Figure 55: 1-D Asymmetric Aluminum Beam Configuration – Acquisition Generator Settings.....	68
Figure 56: 1-D Asymmetric Aluminum Beam Configuration – Frequency Spectrum .....	69
Figure 57: 1-D Asymmetric Aluminum Beam Configuration – Eigenvector.....	70
Figure 58: 1-D Symmetric Aluminum Beam Configuration – Vibrometer Scan Grid .....	71
Figure 59: 1-D Symmetric Aluminum Beam Configuration – Generator Settings.....	71
Figure 60: 1-D Symmetric Aluminum Beam Configuration – Frequency Spectrum .....	72
Figure 61: 1-D Symmetric Aluminum Beam Configuration – Problematic Eigenvector.....	73
Figure 62: 1-D Asymmetric Carbon-Epoxy Beam Configuration – Affixed to Shaker .....	74
Figure 63: 1-D Asymmetric Carbon-Epoxy Beam Configuration – Frequency Spectrum.....	75
Figure 64: 1-D Asymmetric Carbon-Epoxy Beam Configuration – Eigenvector Torque .....	76
Figure 65: Respective Softening/Hardening Nonlinearity in Frequency Response.....	77
Figure 66: 1-D Symmetric Carbon-Epoxy Beam FFT Configuration – General Settings.....	79
Figure 67: 1-D Symmetric Carbon-Epoxy Beam FFT Configuration – Frequency Settings.....	79
Figure 68: 1-D Symmetric Carbon-Epoxy Beam FFT Configuration – Vibrometer Settings.....	80
Figure 69: 1-D Symmetric Carbon-Epoxy Beam FFT Configuration – Generator Settings .....	80
Figure 70: 1-D Symmetric Carbon-Epoxy Beam Configuration – Frequency Spectrum.....	81
Figure 71: 1-D Symmetric Carbon-Epoxy Beam Configuration – Eigenvector.....	81
Figure 72: 1-D Symmetric Carbon-Epoxy 29.5-30.5 Hz Zoom-FFT Config. – General Settings.....	82
Figure 73: 1-D Symmetric Carbon-Epoxy 29.5-30.5 Hz Zoom-FFT Config. – Channel Settings .....	83
Figure 74: 1-D Symmetric Carbon-Epoxy 29.5-30.5 Hz Zoom-FFT Config. – Frequency Settings.....	83
Figure 75: 1-D Symmetric Carbon-Epoxy 29.5-30.5 Hz Zoom-FFT Config. – SE Settings.....	84
Figure 76: 1-D Symmetric Carbon-Epoxy 29.5-30.5 Hz Zoom-FFT Config. – Vibrometer Settings.....	84
Figure 77: 1-D Symmetric Carbon-Epoxy 29.5-30.5 Hz Zoom-FFT Config. – Generator Settings .....	85
Figure 78: Displacement Transfer Function of Carbon Epoxy Beam Tip – 1 Hz Bandwidth.....	87
Figure 79: Displacement Frequency Spectrum of Carbon Epoxy Beam Tip – 1 Hz Bandwidth.....	87
Figure 80: 1-D Symmetric Carbon-Epoxy Beam 25-35 Hz Zoom-FFT Config. – Frequency Settings .....	88
Figure 81: 1-D Symmetric Carbon-Epoxy Beam 25-35 Hz Zoom-FFT Config. – Generator Settings .....	89
Figure 82: 1-D Symmetric Carbon-Epoxy Beam – Tip 9.0g Velocity Illustration.....	90
Figure 83: Displacement Transfer Function of Carbon Epoxy Beam Tip – 10 Hz Bandwidth.....	91
Figure 84: Displacement Frequency Spectrum of Carbon Epoxy Beam Tip – 10 Hz Bandwidth.....	92
Figure 85: Velocity Transfer Function Phase Shift - 0.2g-3.0g Tests of Carbon Epoxy Beam Tip .....	93
Figure 86: Velocity Transfer Function Phase Shift - 3.0g-9.0g Tests of Carbon Epoxy Beam Tip .....	94
Figure 87: Displacement Transfer Function of Carbon Epoxy Beam Tip – 5 Hz Bandwidth.....	95
Figure 88: Displacement Frequency Spectrum of Carbon Epoxy Beam Tip – 5 Hz Bandwidth.....	96
Figure 89: 1-D Symmetric Carbon-Epoxy Beam – Midpoint 9.0g Velocity Illustration .....	97
Figure 90: Velocity Transfer Function Phase Shift– 0.2g-3.0g Tests of Carbon Epoxy Beam Midpoint ...	98
Figure 91: Velocity Transfer Function Phase Shift – 3.0g-9.0g Tests of Carbon Epoxy Beam Midpoint ...	99
Figure 92: Displacement Transfer Function of Carbon Epoxy Beam Midpoint – 5 Hz Bandwidth.....	100
Figure 93: Displacement Frequency Spectrum of Carbon Epoxy Beam Midpoint – 5 Hz Bandwidth .....	101
Figure 94: Placement of Accelerometer on Clamp for Method Validation.....	102
Figure 95: Placement of Accelerometer on Beam Tip for Method Validation.....	102
Figure 96: Connection of Signal Leads into Junction Box .....	103
Figure 97: SignalCalc Software Methods During 1g Comparison Testing .....	105
Figure 98: Transfer Function Comparison of Vibrometer and Accelerometer Methods.....	106
Figure 99: Example Frame of the High Speed Camera Carbon Epoxy Testing .....	107
Figure 100: Symmetric Carbon-Epoxy Peak-to-Peak H.S. Camera Tip Displacement vs. Frequency.....	109
Figure 101: Matlab Aluminum Beam Length Result .....	115
Figure 102: Matlab Carbon-Epoxy Beam Length Result .....	119
Figure 103: ABAQUS Part Creation Tool.....	127
Figure 104: ABAQUS Part Drawing.....	128
Figure 105: ABAQUS Material Density Editor .....	129
Figure 106: ABAQUS Material Elastic Properties Editor .....	130
Figure 107: ABAQUS Section Creation.....	130
Figure 108: ABAQUS Section Editor .....	131
Figure 109: ABAQUS Section Assignment Tool.....	132
Figure 110: ABAQUS Instance Creation .....	133

Figure 111: ABAQUS Step Creation .....	134
Figure 112: ABAQUS Step Editor .....	135
Figure 113: ABAQUS Boundary Condition Creation .....	135
Figure 114: ABAQUS Boundary Condition Editor.....	136
Figure 115: ABAQUS Boundary Condition Designation .....	136
Figure 116: ABAQUS Global Seed Control .....	137
Figure 117: ABAQUS Assign Element Type.....	137
Figure 118: ABAQUS Element Type Editor.....	138
Figure 119: ABAQUS Mesh Part Instance.....	138
Figure 120: ABAQUS Create Job Toolbox.....	139
Figure 121: ABAQUS Job Manager .....	139
Figure 122: ABAQUS Relative Displacement Plot of 1 <sup>st</sup> Bending Mode .....	140
Figure 123: ABAQUS Field Creator .....	140
Figure 124: ABAQUS Field Editor.....	141
Figure 125: ABAQUS Stress Contour Plot .....	142
Figure 126: Acquisition General Settings.....	149
Figure 127: Acquisition Channel Settings.....	150
Figure 128: Acquisition Frequency Settings .....	152
Figure 129: Acquisition Signal Enhancement Settings .....	152
Figure 130: Acquisition Vibrometer Settings.....	153
Figure 131: Acquisition Generator Settings .....	153

## List of Tables

Table 1: MAV Design Requirements .....	3
Table 2: Comparison of 1 <sup>st</sup> Mode Beam Length.....	10
Table 3: Mechanical Properties of IM7/5250-4.....	12
Table 4: Comparison of 1 <sup>st</sup> Mode IM7/5250-4 Beam Length .....	16
Table 5: Comparison of 1 <sup>st</sup> Mode 4-ply T300/5208 Beam Length.....	22
Table 6: Beams Fabricated for Experimental Analysis .....	22
Table 7: PSV-400-3D General System Specifications .....	38

# **I Introduction**

## **1.1 Motivation**

Flapping wing micro air vehicles (MAVs) have become a topic of interest for several research institutions over the past decade. Other literature sources may use the following terminology when referring to flapping wing MAVs; bird flight machines are also known as ornithopters and robotic insects are also known as entomopters (11:1). Entomopters have the ability to achieve abnormally high lift with rapidly flapping wings, thereby allowing the fuselage to move slowly in relation to the ground (4:1). When vibration deformations are large, linear vibration theory will not always be suitable. This is the case with the flapping wing MAVs. Linear vibration problems are governed by linear differential equations, while nonlinear vibration problems can be described by nonlinear differential equations, causing lengthy if not impossible computational efforts. One focus of this research involves investigating this nonlinear vibration of a beam, allowing these methods to eventually be applied to a MAV wing.

Due to the complexity of a three-dimensional wing structure, there are only two desirable techniques to conduct a nonlinear vibration study. First, a finite element analysis program may be used and depending upon the quality of the program, solutions to highly complex nonlinear vibration problems may be found. A finite element analysis program is derived from theory and is not perfect, so in an attempt to validate these results another method is necessary. This second method involves conducting experiments to analyze the characteristics of the nonlinear vibration problem. Experimentation is the primary interest for this research.

The MAV wing's non-linear vibration characteristics were analyzed through the use of three different experiments. The first option involves using a three-dimensional scanning laser vibrometer to capture the velocities and displacements of the entire surface of the wing structure in three dimensions. For the second, a high speed camera is used to take pictures of the vibrating wing, and from these pictures displacements and velocities along the leading and/or trailing edges can be determined. The third method used the scanning laser vibrometer in a one-dimensional configuration.

## **1.2 Relevance to the USAF**

The United States military would benefit from operational flapping wing micro air vehicles. Potential applications that exist would likely involve urban reconnaissance, which would generate a multitude of confined space scenarios. A successfully proven flapping wing MAV could mimic the capabilities of nature's insects and birds. When paired with video or audio devices, this technology could become a formidable tool in urban combat reconnaissance. The Air Force Research Laboratory is promoting the research of flapping wing micro air vehicles. The following are three areas of study currently being investigated (18:25):

- Experimental Validation of Nonlinear Structural Dynamic Models
- Computational Modeling Technologies for MAVs
- Determination of Aeroelastic Effects of Flexible Wings on Low Reynolds Number Aerodynamics

This research effort has specifically been carried out in an attempt to address the first of these three research thrusts.

### 1.3 Micro Air Vehicle Background

Recently, numerous research institutes have undertaken the challenge of low Reynolds number aerodynamics. Due to highly complex flow within this flight envelope, effectively designing a vehicle to operate at low Reynolds numbers may go against conventional aeronautical engineering practices. Micro air vehicles are to have wingspans no greater than six inches according to requirements from the Defense Advanced Research Projects Agency (DARPA) MAV program and generally are to be within the design requirements of Table 1, (15:292,298).

**Table 1: MAV Design Requirements**

<b>Specification</b>	<b>Requirements</b>	<b>Details</b>
Size	<6 in	Maximum dimension
Weight	~100 g	Objective GTOW
Range	1 to 10 km	Operational range
Endurance	60 min	Loiter time on station
Altitude	<150 m	Operational ceiling
Speed	15 m/s	Maximum flight speed
Payload	20 g	Mission dependent
Cost	\$1500	Maximum Cost

Conceivably, one could develop a MAV using conventional propulsion designs.

According to two experts, a fixed wing conventionally propelled MAV is not an ideal choice for the following reasons:

Fixed wing solutions are immediately discounted because they require either high forward speed, large wings, or a method for creating circulation over the wings in the absence of fuselage translation.

High speed is not conducive to indoor operations because it results in reduced reaction time, especially when autonomously navigating through unbriefed corridors or amid obstacles. When indoors, slower is better.

If, on the other hand, the wings are enlarged to decrease wing loading to accommodate slower flight, the vehicle soon loses its distinction as a “micro” air vehicle. (11:2)



One could think of more limitations of a fixed wing MAV configuration not mentioned in the previous quotation. For example, when used in a military application, the person initially launching the vehicle into flight would prefer to minimize the launch and recovery distance requirements. A fixed wing vehicle would require a runway, or a comparable flat surface from which to takeoff and land. So why not create a rotorcraft MAV? Michelson and Reece were able to answer this question in the following quotation:

A significant advantage of a flapping wing over a rotor is the rigidity of the wider chord wing relative to the high aspect ratio of a narrow rotor blade, and the fact that it can be fixed relative to the fuselage (e.g., nonflapping glide) to reclaim potential energy more efficiently than an autorotating rotor.

There is also a stealth advantage of a flapping implementation over a comparably sized rotor design in that the acoustic signature will be less because the average audible energy imparted to the surrounding air by the beating wing is much less than that of a rotor. The amplitude of vortices shed from the tips of the beating wing grows, and then diminishes to zero as the wing goes through its cyclical beat, whereas the rotor tip vortices (which are the primary high frequency sound generator) are constant and of higher local energy. The sound spectrum of a flapping wing will be distributed over a wider frequency band with less energy occurring at any particular frequency, thereby making it less noticeable to the human ear. All the energy of the rotor spectrum will be concentrated in a narrow band that is proportional to the constant rotor tip velocity.

As the diameter of a rotor system decreases with the size of the air vehicle design, it will become less efficient since the velocity at the tips will decrease while the useless center portion becomes a larger percentage of the entire rotor disk.  
(11:2-3)

Due to the challenges present in designing a MAV, many more research opportunities exist. This is especially true when considering the design of an effective flapping wing MAV. Not only are there aerodynamic challenges, many design and technology challenges must also be overcome with wing design, thrust and lift generation, energy storage, motor/gear assemblies, power conversion, propulsion, and avionics (6:3-6).

## **II Problem Formulation**

### **2.1 Beam Theory and Analysis of Methods**

For this experimental research, beams are used to simulate a flapping wing. There are a few assumptions from Euler-Bernoulli theory that define beams. A beam must be prismatic and straight, but the cross sectional shape has no restrictions; the loading and bending moments are applied in a plane of one of the principle moments of inertia; plane sections of the beam remain plane during bending and all shearing stresses are uniformly distributed across the beam width (19:354).

The vibration of a beam's first bending mode resembles basic flapping motion of a wing. Euler-Bernoulli linear beam theory assumes that rotation of differential elements are negligible compared to the translation. This theory is valid for beams with a length to depth ratio  $>10$  (10:384). It should be noted that Euler-Bernoulli theory was not intended to account for the nonlinearity present in flapping.

Several beam support choices exist when considering beam vibration. One may choose from a combination of clamped/fixed ends, pinned ends, or free ends. A perfect clamp would allow zero rotation at the root of the beam, creating a bending moment at the root. A pinned end would allow for rotation and therefore not have a moment at the root; rather a shearing force would exist. A free end boundary condition would have neither bending moments nor shearing forces. Other unique conditions could be used as well; one in particular, two symmetric beams representing a complete vehicle span, will be addressed subsequently. Considering all of these boundary condition options, which method or methods is best suited for this research effort?

A free-free beam would not have support structure factors to interfere with the vibration results. However, the experimental design requirements involved with getting a free-free beam to undergo large flapping deflections presents a major challenge when considering the vibration measurement options at present. Two primary methods of measurement are being evaluated: high speed camera and laser vibrometry. It will be shown in a later section the critical importance of the laser vibrometer in determining the frequency response information for the beam. Accurate use of the laser vibrometer requires that the test object be somewhat fixed and not rotating three dimensionally. A free-free condition by its nature is not fixed in any way. The high speed camera would have no trouble recording the movement of a free-free vibrating beam; however, scaling issues would arise. Due to potentially large three dimensional movements, the camera analysis would be unable to accurately determine true beam deflections and velocities. This will become more apparent when the camera method is thoroughly described in Section 3.3.6.

A cantilever beam has one clamped or fixed end and one free end. This method allows for the large “flapping” movement, and also presents an arrangement suitable to the available data acquisition tools. From this point on, only cantilever beam theory will be addressed. Additionally, since the beam tip displacements will be large when compared to the thickness, the beam will no longer be best approximated by linear theory. Due to the experimental nature of this research, there will not be an attempt to formulate nonlinear differential equations of motion for a rotating beam. Beam nonlinearity will be shown only as a result of experimental analysis.

With the beam boundary conditions determined, the next step is to determine what method of excitation should be used. Steady-state vibration is important to guarantee repeatable and accurate experimental results. While a beam may be excited by an instantaneous force, this method will not sustain steady-state vibration. Rather, vibration decay will exist as a result of the instantaneous force method. Another method of excitation of a cantilever beam involves the use of an acoustic horn placed at the tip of the beam. While this method is an excellent choice for exciting the beam at lower amplitudes, when larger deflections are generated the horn method can not be used. The acoustic amplitudes will decay as the beam deflects away from the horn, and will increase as the beam deflects toward the horn, causing unsteady excitation. A third option exists, and that is base excitation of a cantilever beam. This method can guarantee steady state vibration. The equipment used to create this base excitation, a shaker table, is discussed in detail in the next chapter.

While it is theoretically possible to determine the vibration characteristics of any sized beam, there certainly are experimental limitations. In addition, this study has been an attempt to address “flapping” as it would apply to a micro air vehicle. A perfect flapping wing MAV would be capable of mimicking the flight of insects and/or birds. Depending upon their size, insects and birds have a very large range of wing beat frequencies. For birds, flapping frequency can be estimated by Equation 2.1:

$$f = 1.08(m^{1/3}g^{1/2}b^{-1}S^{-1/4}\rho^{-1/3}) \quad (2.1)$$

where  $m$  is the bird's body mass,  $g$  is the acceleration due to gravity,  $b$  is the wing span,  $S$  is the wing area and  $\rho$  is the air density (14:171-185). A large hummingbird which can have a wingspan of up to eight inches, for example, would have a wing flapping

frequency range of 18-28 Hz (3:1). For beam sizing, the first bending mode bandwidth of 20-30 Hz was chosen due to the comparable size and wingbeat frequency with those species already existing in nature. A MAV must have a wingspan of no greater than six inches, or a halfspan no greater than three inches. Due to structural limitations explained in Section 2.2, six inches was the minimum dimension used throughout this project for the beam length, representing a wing halfspan of twice the MAV required length.

## 2.2 Beam Sizing

### 2.2.1 Matlab Eigenvalue Determinations

A study was carried out to establish the most appropriate, affordable, and available materials to be used for the beams. Since the testing involves steady state vibration with the beam tip undergoing large deflection, the beam material must be able to withstand repetitive testing at high amplitudes. The beam must not break, crack, or plastically deform in any way during testing. The first bending mode of a cantilever beam has the following shape:

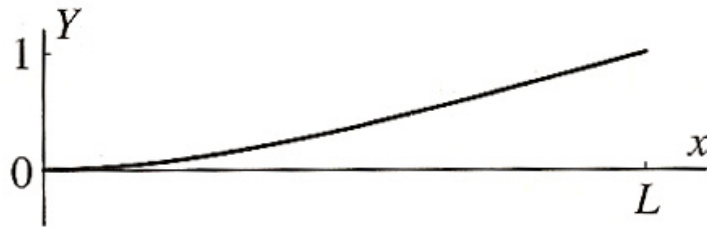


**Figure 1: First Mode Shape of a Cantilever Beam**

As Figure 1 displays, the beam is fixed at  $x = 0$  and free at  $x = L$ . The undamped natural frequency of a cantilever beam can be solved by

$$\omega_n = \zeta_n^4 \sqrt{\frac{EI}{mAL^4}} \quad (2.2)$$

where “n” is the mode number, or in this case 1,  $\zeta_1^2 = 1.875104$ , “E” is the modulus of elasticity, “I” is the moment of inertia of the beam cross section, “m” is the mass density, “A” is the area of the beam cross section, and “L” is the beam length (1:99).

As a review, moment of inertia of a beam is found by the equation:

$$I = \frac{b \times h^3}{12} \quad (2.3)$$

A program was written in Matlab that used Eqn. 2.2 to solve for beam length for a given frequency. Appendix A includes the Matlab code created during this research to solve for length of a beam with a first mode natural frequency of 20 Hz. It should be noted that this equation is only valid for homogeneous beams. The following table shows the Matlab generated comparison between aluminum alloy and steel beams:

**Table 2: Comparison of 1<sup>st</sup> Mode Beam Length**

<b>2024-T3 Aluminum Alloy Beam</b>			<b>Steel Beam</b>		
Frequency	h = Thickness (in)	Length (in)	Frequency	h = Thickness (in)	Length (in)
20 Hz	1/4	20.19	20 Hz	1/4	20.23
30 Hz	1/4	16.49	30 Hz	1/4	16.52
Frequency	h = Thickness (in)	Length (in)	Frequency	h = Thickness (in)	Length (in)
20 Hz	1/8	14.28	20 Hz	1/8	14.31
30 Hz	1/8	11.66	30 Hz	1/8	11.68
Frequency	h = Thickness (in)	Length (in)	Frequency	h = Thickness (in)	Length (in)
20 Hz	1/16	10.10	20 Hz	1/16	10.12
30 hz	1/16	8.24	30 hz	1/16	8.26
<i>Material Properties</i>			<i>Material Properties</i>		
Density: 2780 kg/m <sup>3</sup>			Density: 7810 kg/m <sup>3</sup>		
Young's Modulus: 73.1 Gpa			Young's Modulus: 207 Gpa		

It is shown here that no significant difference occurs between length of aluminum and steel at the 1<sup>st</sup> mode of the undamped natural frequency. Three different thickness

examples are shown, and one can see the effect on beam length of a constant 1<sup>st</sup> mode undamped frequency beam as thickness is decreased. Theoretically, for an aluminum beam to meet the MAV halfspan requirement of under three inches and have a 1<sup>st</sup> mode undamped natural frequency of 20 Hz, it would have to be no greater than 1/180 inch thick, which is only five times the thickness of aluminum foil! While manufacturability of this beam may be possible, any beam of this thickness will not have the capacity to resist bending during flapping due to the extremely small moment of inertia; resulting in plastic deformation.

In another attempt to decrease the beam length, other materials were investigated. Brief studies have discovered that while other homogeneous materials, such as inexpensive polymers, could succeed in reducing the beam length and maintaining a reasonable thickness, they would be structurally inadequate; meaning they would not be capable of withstanding repetitious movements without fracture. A compromise was found through the use of carbon-epoxy composite material. To solve for the natural frequencies of a composite beam using Matlab, a more extensive look is required into composite materials. One carbon-epoxy material that is available to the Air Force Institute of Technology through the Air Force Research Lab Materials Division (AFRL/ML) is IM7/5250-4. This material is described by the following material properties table:



**Table 3: Mechanical Properties of IM7/5250-4 (7:2011)**

	<b>Symbol (Units)</b>	<b>IM7/5250-4</b>
Longitudinal normal modulus	$E_{11}$ (GPa)	176.79
Transverse normal modulus	$E_{22}$ (GPa)	10.2
Transverse normal modulus	$E_{33}$ (GPa)	10.2
Shear modulus	$G_{12}$ (GPa)	6.29
Shear modulus	$G_{13}$ (GPa)	6.29
Shear modulus	$G_{23}$ (GPa)	4
Poisson's ratio	$\nu_{12}$	.277
Poisson's ratio	$\nu_{13}$	.277
Poisson's ratio	$\nu_{23}$	0.33

The task of solving the eigensystem of a carbon beam using Matlab requires a study of the theory of composite materials. Carbon-epoxy material, unlike homogeneous aluminum, has mechanical properties that are entirely dependent upon the material's fiber orientation. A 4-ply material with a  $0^\circ/90^\circ/90^\circ/0^\circ$  orientation will have the material properties shown in Table 3. It was mentioned previously that the natural frequencies of

a beam could be solved using Equation 2.2,  $\omega_n = \zeta_n^4 \sqrt{\frac{EI}{mAL^4}}$ . However, as one can see by referencing Table 3, when considering composite carbon fiber materials, there is not just simply one elastic modulus, E. Additionally, the moment of inertia value can not be solved by Eqn. 2.3 as it was for homogeneous materials. There is another option, and that is to solve for the product of E and I by using composite theory detailed in the book *Mechanics of Fibrous Composites*, which is Reference 5.

This theory is the basis for the composite beam's natural frequency Matlab solver that was created as a part of this study and is located in Appendix A. It is first necessary to calculate the reduced stiffness coefficients of the beam. These can be found by using Young's modulus and Poisson's ratio, as shown in the following equations (5:81).

$$Q_{11} = \frac{E_1}{1 - \nu_{12}\nu_{21}} \quad (2.4)$$

$$Q_{12} = \frac{\nu_{21}E_1}{1 - \nu_{12}\nu_{21}} \quad (2.5)$$

$$Q_{22} = \frac{E_2}{1 - \nu_{12}\nu_{21}} \quad (2.6)$$

$$Q_{22} = \frac{E_2}{1 - \nu_{12}\nu_{21}} \quad (2.7)$$

$$Q_{66} = G_{12} \quad (2.8)$$

The plane stress transformed reduced stiffness matrix “ $\bar{Q}$ ” is needed to eventually account for all differing orientations of any given carbon-fiber lamina, however, each  $\bar{Q}$  only represents one layer of laminate material. This transformed matrix is generated by using Eqns. 2.4 – 2.8 as well as the sine and cosine values of the fiber orientation angle “ $\theta$ ” as follows:

$$m = \cos \theta \quad (2.9)$$

$$n = \sin \theta \quad (2.10)$$

The next set of equations defines the individual terms of  $\bar{Q}$  (5:85).

$$\bar{Q}_{11} = Q_{11}m^4 + 2(Q_{12} + 2Q_{66})m^2n^2 + Q_{22}n^4 \quad (2.11)$$

$$\bar{Q}_{12} = (Q_{11} + Q_{22} - 4Q_{66})m^2n^2 + Q_{12}(n^4 + m^4) \quad (2.12)$$

$$\bar{Q}_{22} = Q_{11}n^4 + 2(Q_{12} + 2Q_{66})m^2n^2 + Q_{22}m^4 \quad (2.13)$$

$$\bar{Q}_{16} = (Q_{11} - Q_{22} - 2Q_{66})m^3n + (Q_{12} - Q_{22} + 2Q_{66})n^3m \quad (2.14)$$

$$\bar{Q}_{26} = (Q_{11} - Q_{12} - 2Q_{66})mn^3 + (Q_{12} - Q_{22} + 2Q_{66})nm^3 \quad (2.15)$$

$$\bar{Q}_{66} = (Q_{11} + Q_{22} - 2Q_{12} - 2Q_{66})m^2n^2 + Q_{66}(n^4 + m^4) \quad (2.16)$$

Now having established the reduced stiffness matrix for one layer, it is now possible to solve for  $\bar{Q}$  for each respective layer of the composite material. The remaining steps are derived from quasi-isotropic laminate theory.

All symmetric laminates with  $2N$  equal-thickness layers ( $N \geq 3$ ) and  $N$  equal angles between fiber orientations are quasi-isotropic. (5:127)

This is indeed the case for a  $0^\circ/90^\circ/90^\circ/0^\circ$  laminate. A new matrix “ $A_{ij}$ ” appears in the following derivation:

$$A_{ij} = \sum_{k=1}^{2N} \bar{Q}_{ij}^k t_k \quad (2.17)$$

where “ $t_k$ ”, represents the  $k^{\text{th}}$  layer thickness.

For a symmetric cross-ply laminate, such as the one previously discussed, “ $A_{ij}$ ” is solved by the following equation (5:134):

$$[A] = \sum_{k=1}^N [\bar{Q}]^k (z_k - z_{k-1}) \quad (2.18)$$

The  $z$  terms represent layer thickness and are solved according to Figure 2 as follows:

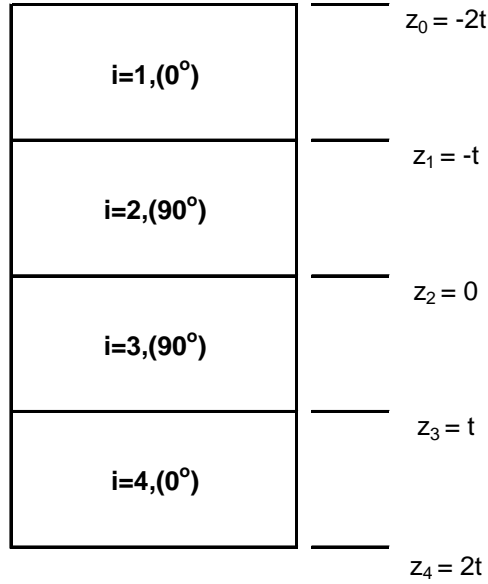


**Figure 2: 0/90/90/0 Laminate Thickness Definition (5:134)**

When Eqn. 2.18 has been solved, all layers of the laminate material are represented. One final matrix equation must be defined and solved before the EI product can be determined. This new matrix “[D]” is found by (5:135):

$$[D] = \frac{1}{3} \sum_{k=1}^N [\bar{Q}]^k (z_k^3 - z_{k-1}^3) \quad (2.19)$$

Finally, the product of Young’s Modulus and moment of inertia can be found by:

$$EI = b * D_{11} \quad (2.20)$$

where “b” represents the beam width. Once Eqn. 2.20 has been calculated, one can refer back to Eqn. 2.2 to solve for a composite beam’s natural frequency. In the case of this work, a natural frequency was initially provided and Eqn 2.2 was rearranged to solve for the corresponding beam’s length.

Since the frequency range of 20-30 Hz had already been determined, it was decided, for the 4-ply 0°/90°/90°/0° IM7/5250-4 beam, to solve for the beam length

resulting in a 30 Hz 1<sup>st</sup> mode natural frequency. This will allow for the smallest possible dimension that meets this research project's cost and schedule constraints. According to the Matlab solver, this length was 6.5", as seen in Table 4.

**Table 4: Comparison of 1<sup>st</sup> Mode IM7/5250-4 Beam Length**

<b>IM7/5250-4 0/90/90/0 Carbon-Epoxy Beam</b>		
Frequency	Thickness (in)	Length (in)
20 hz	0.02	8.0
30 hz	0.02	6.5

### **2.2.2 ABAQUS Finite Element Analysis**

A second method available to analytically determine the natural frequency of a beam is through the use of the finite element analysis software, ABAQUS. Appendix B carefully steps through the entire process of creating and analyzing a composite beam in ABAQUS. Similar to the Matlab work in the previous section, this FEM analysis is carried out to solve for the length of an aluminum beam having a 1<sup>st</sup> mode natural frequency of approximately 20 Hz. ABAQUS requires that the material initially be defined based only upon its dimensionality and material properties. Therefore, to determine a length from the known 1<sup>st</sup> mode natural frequency, several length cases would need to be tried until the correct 20 Hz frequency is found. Since the Matlab step was conducted prior to the ABAQUS verification, the initial length guess was almost perfect. Figures 3-6 show the 20 Hz aluminum beam's dimensionality and material properties:

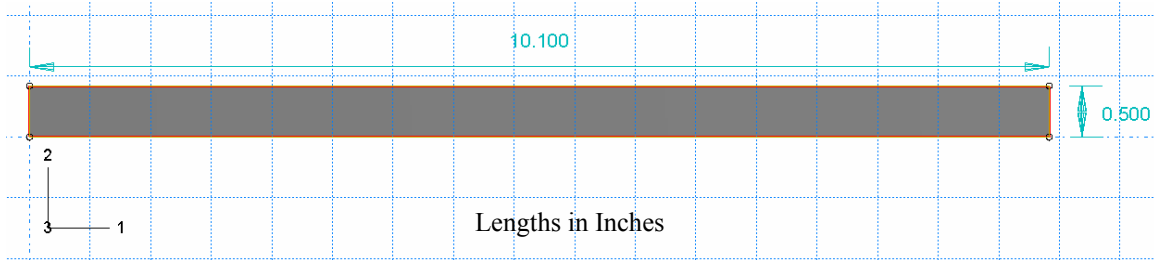


**Figure 3: 2024-T3 Aluminum Beam Length and Width**

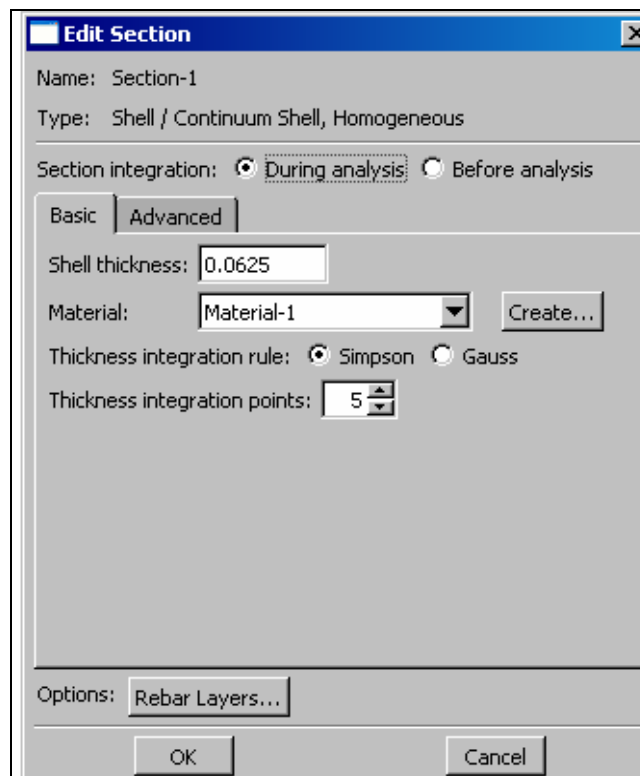


**Figure 4: 2024-T3 Aluminum Beam Thickness**

**Edit Material**

Name: Material-1

**Material Behaviors**

Density

Elastic

General Mechanical Thermal Other

**Elastic**

Type: Isotropic

☐ Use temperature-dependent data

Number of field variables: 0

Moduli time scale (for viscoelasticity): Long-term

**Data**

	Young's Modulus	Poisson's Ratio
1	1.06E+007	0.33

Figure 5: 2024-T3 Aluminum Beam Young's Modulus and Poisson's Ratio

**Edit Material**

Name: Material-1

**Material Behaviors**

Density

Elastic

General Mechanical Thermal Other

**Density**

☐ Use temperature-dependent data

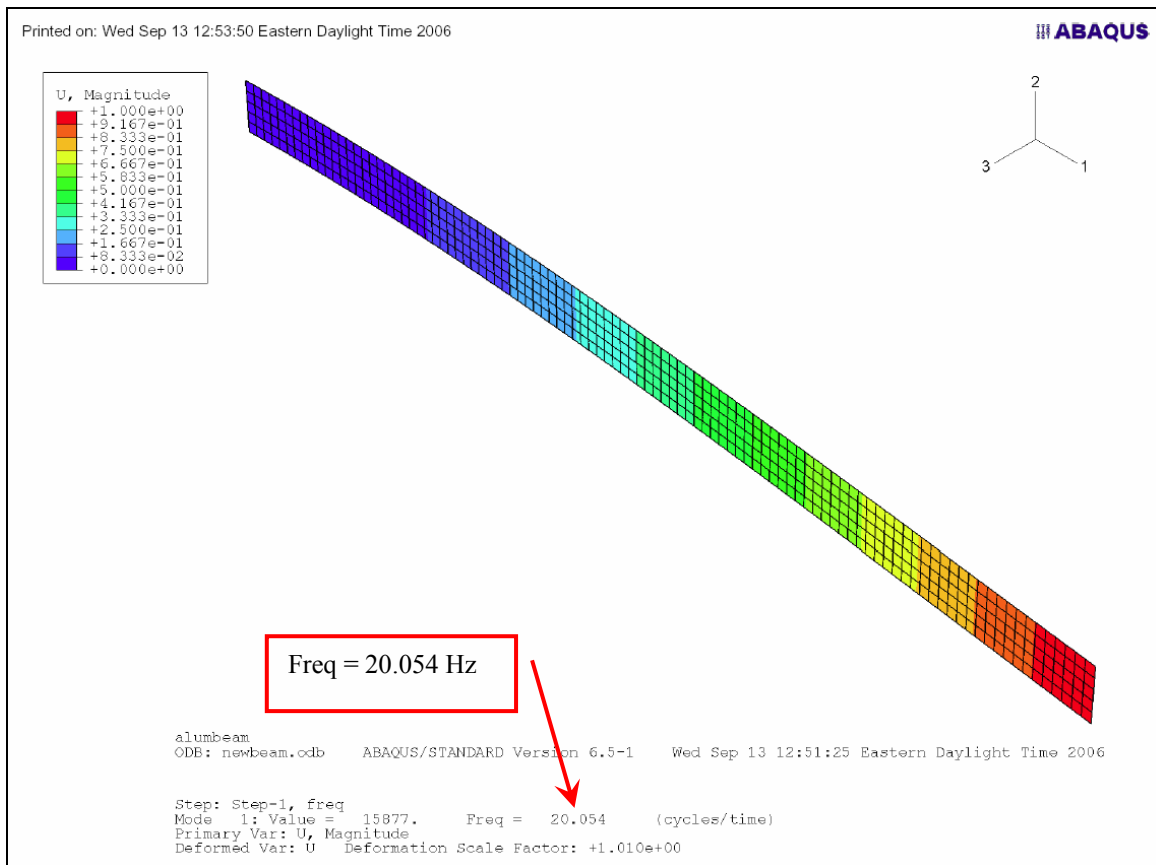
Number of field variables: 0

**Data**

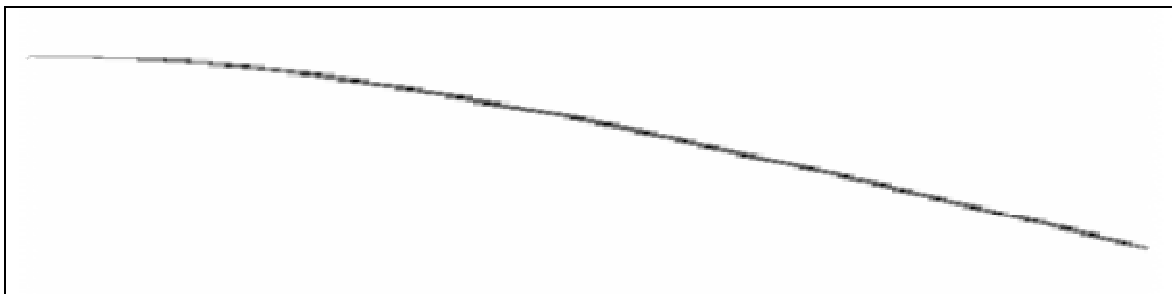
	Mass Density
1	0.00026

Figure 6: 2024-T3 Aluminum Beam Density

It should be noted that all input variables in ABAQUS are in English units, and all lengths are in inches. One must be careful to ensure units are consistent because ABAQUS will indiscriminately make an attempt to solve for any real combination of inputs. After completing the procedures described in Appendix B, except for those parts specific to composite materials, the beam's bending vibration modes can be found. Figures 7 and 8 provide the result of a successful ABAQUS finite element analysis:



**Figure 7: 2024-T3 Aluminum Beam 1<sup>st</sup> Bending Mode ABAQUS Eigenvector – Isometric View**



**Figure 8: 2024-T3 Aluminum Beam 1<sup>st</sup> Bending Mode ABAQUS Eigenvector – Side View**



An ABAQUS finite element analysis was also conducted for a T300/5208  $0^\circ/90^\circ/90^\circ/0^\circ$  composite beam. This ABAQUS analysis was completed using T300 at both 20 Hz and 30 Hz, and it should be noted that the composite material made available for testing at a later date was IM7/5250-4. The Matlab study documented in Section 2.2.1 was performed at a later time using IM7/5250-4 properties. For this preliminary sizing effort, the Appendix B process was strictly followed. The following figures represent the ABAQUS 20 Hz beam dimensionality and material property definitions, again using English units and lengths in inches:

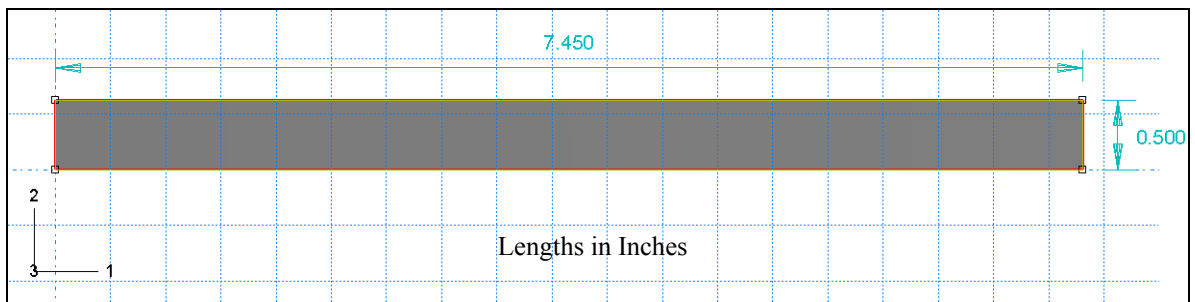


**Figure 9: T300/5208 Length and Width**

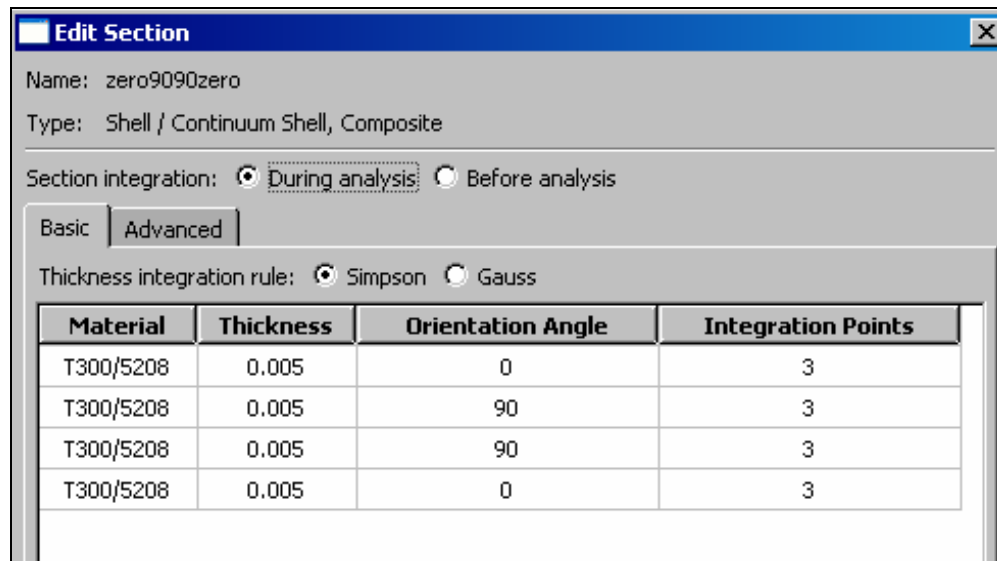


**Figure 10: T300/5208 Thickness and Orientation Angle**

Name: T300/5208

**Material Behaviors**

Density

Elastic

General Mechanical Thermal Other Delete

**Elastic**

Type: Lamina Suboptions

☐ Use temperature-dependent data

Number of field variables: 0

Moduli time scale (for viscoelasticity): Long-term

**Data**

	E1	E2	Nu12	G12	G13	G23
1	1.92E+007	1.56E+006	0.24	820000	820000	490000

Figure 11: T300/5208 Mechanical Properties

Name: T300/5208

**Material Behaviors**

Density

Elastic

General Mechanical Thermal Other Delete

**Density**

☐ Use temperature-dependent data

Number of field variables: 0

**Data**

	Mass Density
1	0.000145

Figure 12: T300/5208 Mechanical Properties

The final step was to calculate the beam's modal information. The 7.45" beam length analysis provided the 20 Hz 1<sup>st</sup> bending mode result described by Figure 12. The side view eigenvector shape for this beam is identical to that shown by the Figure 8 aluminum results, and so it has not been repeated.



**Figure 13: T300/5208 Beam 1<sup>st</sup> Bending Mode Abaqus Eigenvector – Isometric View**

The following table shows the 20 Hz and 30 Hz length comparisons provided by the ABAQUS analysis.

**Table 5: Comparison of 1<sup>st</sup> Mode 4-ply T300/5208 Beam Length**

<b>T300/5208 0/90/90/0 Carbon-Epoxy Beam</b>		
Frequency	Thickness (in)	Length (in)
20 hz	0.02	7.5
30 hz	0.02	6.0

As a result of this analytical investigation, the 20 Hz and 30 Hz respective sizing of the aluminum and carbon-epoxy materials were determined. Based upon the preceding conclusions the following beams were fabricated:

**Table 6: Beams Fabricated for Experimental Analysis**

<b>2024-T3 Aluminum Alloy Beam - 20 hz</b>			<b>IM7/5250-4 0/90/90/0 Carbon-Epoxy Beam 30 hz</b>		
Length (in)	Width (in)	Thickness (in)	Length (in)	Width (in)	Thickness (in)
10.1	0.5	0.0625	6.0	0.5	0.02

### III Experimental Investigation

#### 3.1 Laser Vibrometry Theory

A laser emits photons to produce light that has a single wavelength. The laser used for the PSV-400 Doppler vibrometer is a helium neon laser. This laser produces a visible red laser beam. Helium neon gas lasers create a very low-noise visible laser, which is perfect for structural vibrometry.

A laser Doppler vibrometer, such as the PSV-400 used in this research, detects the Doppler shift of laser light that is reflected from a test specimen. Figure 14 illustrates how a single frequency laser is sent to an object and the same laser signal returns at a changed wavelength.

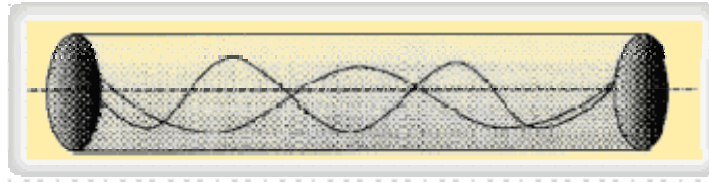


**Figure 14: Laser Measurement and Reference Beams (8:1)**

The Doppler shift is used to measure the component of velocity which lies along the axis of the laser beam. Since laser light has a very high frequency, a direct measurement of the reflected beam is not possible. An optical interferometer must be used to mix the scattered light with a reference beam. Next, a photo detector measures the intensity of the mixed light whose frequency is equal to the difference frequency between the reference and the measurement beam. This setup is known as a Michelson interferometer as shown in Figure 15 (21:1):

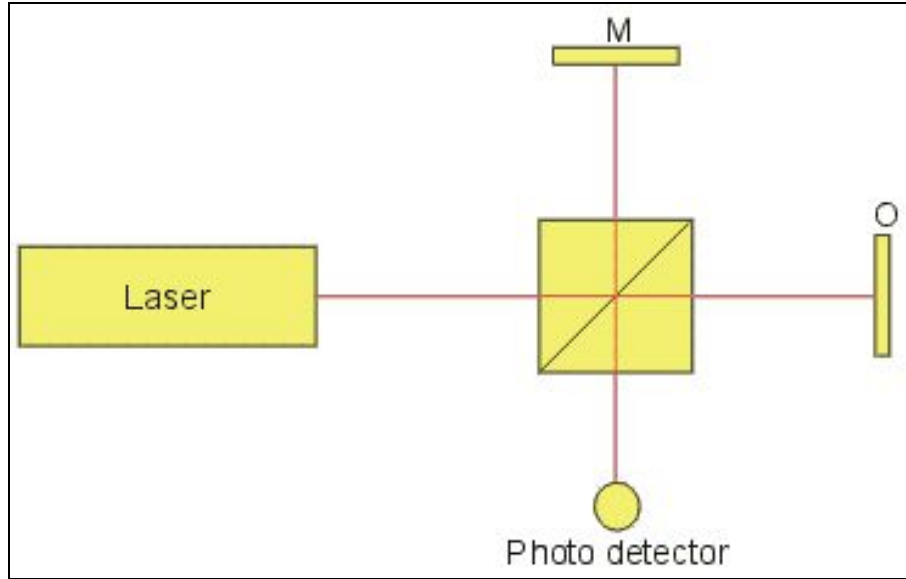


**Figure 15: Michelson Interferometer (21:1)**

The interferometer does this by splitting the light into a reference beam and a measurement beam. The vibrating specimen scatters the light from the measurement beam. Differences in frequency and phase can be detected from the reflecting laser light. These differences correspond to the velocity and displacement of the object. Comparison of this measurement beam with the original reference beam creates a modulated detector output signal which reveals the Doppler shift in frequency. The rate of change of phase is proportional to the rate of change of position. This leads to the velocity of the surface by using the formula for the Doppler frequency shift where  $\lambda$  is the wavelength of the laser and  $u(t)$  is the velocity of the tested specimen:

$$\Delta f(t) = \frac{4u(t)}{\lambda} \quad (3.1)$$

A decoder in the vibrometer generates a voltage proportional to the velocity of the vibration and parallel to the measurement beam. This voltage is digitized and processed as the vibrometer signal (21:1).

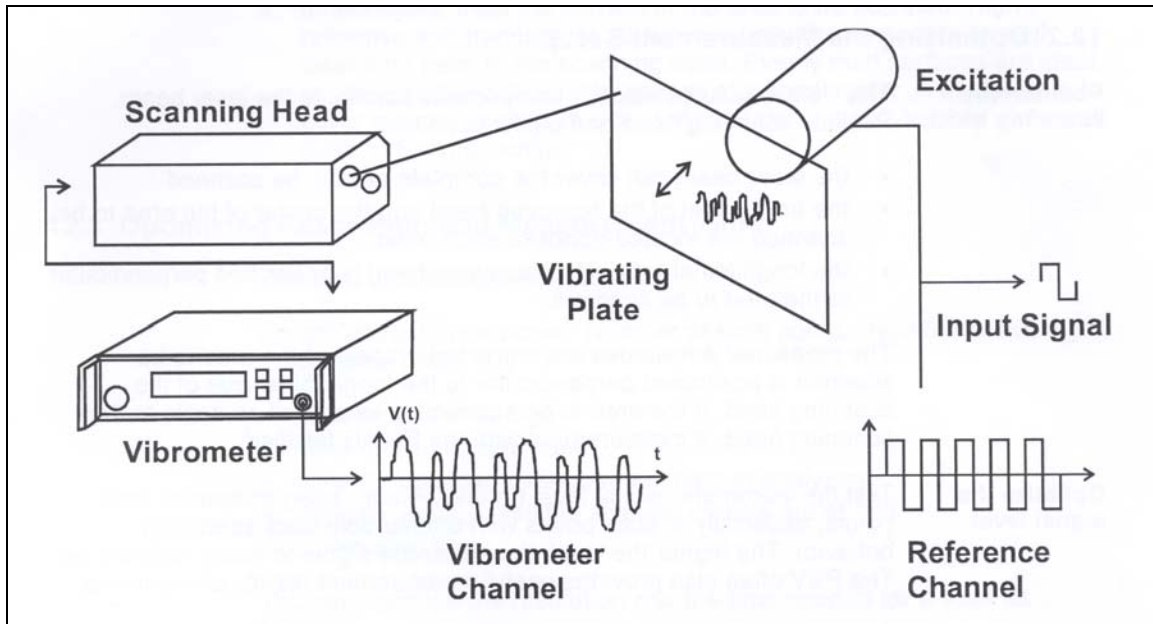


Figure 16: Laser Doppler Vibrometer Schematic (17:Ch 12)

Figure 16, from the Polytec Theory Manual, shows the complexity involved in laser vibrometer testing. Reference the Polytec Theory Manual (17:Ch 12) for a more thorough explanation of the theory behind laser Doppler vibrometry.

### 3.2 High Speed Camera Methodology

The second experimental choice selected to assist with the analysis of flapping is image analysis. Image analysis is the extraction of useful information from 2-D images; mainly from digital images by means of digital image processing techniques. Another relatively common term relating to image analysis is photogrammetry. With present technology, high speed digital cameras are often the choice for image analysis.

Several factors come into play when looking into using a high speed camera. The camera must have a frame rate capable of imaging the test object. In addition, the image must have a resolution or quality that is satisfactory to obtain the testing objectives. The camera should interface with a system that allows for quick and inexpensive access to the

images. For example, non-digital high speed film is expensive, requires developing, and the analysis can be extremely labor intensive; all factors that are unattractive for low cost and reduced schedule testing. An additional factor is size and mobility. The camera must be relatively small and equipped with a tripod or similar mounting system that allows for generous camera angle manipulations, and must have communication cables of sufficient length. Light level is very significant when conducting high speed tests. The higher frame rates require added illumination so that the sensitive camera is able to properly image the object. The Air Force Institute of Technology (AFIT) engineering laboratory had a PHOTRON FASTCAM 512 PCI camera. This high speed imaging system is able to achieve frame rates of up to 2,000 frames per second, while maintaining 512 x 512 pixel resolution, which meets the experimental objectives of this study. The camera is capable of higher frame rates, up to 16,000 fps; however, beyond 2,000 fps the pixel window size decreases from 512 x 512, and may not be suitable for capturing the entirety of beam movement.

### **3.3 Experimental Equipment**

The first chapter introduced the subject of flapping wing MAVs and the methods available to investigate the vibration characteristics of these flapping wings, or in this case beams. The second chapter involved a theoretical vibrational analysis of beams to determine the sizing for the remaining experimental tests. This analysis down-selected to two beams, one comprised of aluminum alloy and one of carbon-epoxy composite. To make this experimental research possible, these beams would have to be fabricated along with a tool that will securely clamp them to maintain a true cantilever “fixed-free”

condition. This section covers the design and setup of the experimental flapping beam analysis.

### **3.3.1 Aluminum Beam Design**

The dimensionality for the aluminum beam was shown in Table 6. For this beam to have a 1<sup>st</sup> bending mode natural frequency of 20 Hz, it required a 10.1” length and 0.0625” thickness. According to beam theory, beam width is arbitrary and does not affect the result of the modal frequencies, so a width of 0.5” was selected. Since the theoretical size has been determined, the beam dimensionality must be placed into engineering drawings for fabrication. These drawings were completed using the SolidWorks three dimensional computer aided design (CAD) software. Figure 17 shows the CAD drawing of the aluminum beam. It can be seen on this drawing that the beam is not simply 10.1” in length; it actually extends for a total of 13.2”. It was mentioned previously that a shaker is the choice to create the beam’s vibratory response. This shaker has an armature that is the focal point of vibration, while the rest of the shaker’s vibration is damped. Therefore, the beam must be attached to the shaker. A clamp was designed to secure the beam to the shaker’s armature. This design required the additional 3.1” in beam length, as seen in Figure 17. Two holes are machined into the beam. The outermost hole is used to secure the beam to the shaker armature, while the innermost hole gets secured by the clamp.



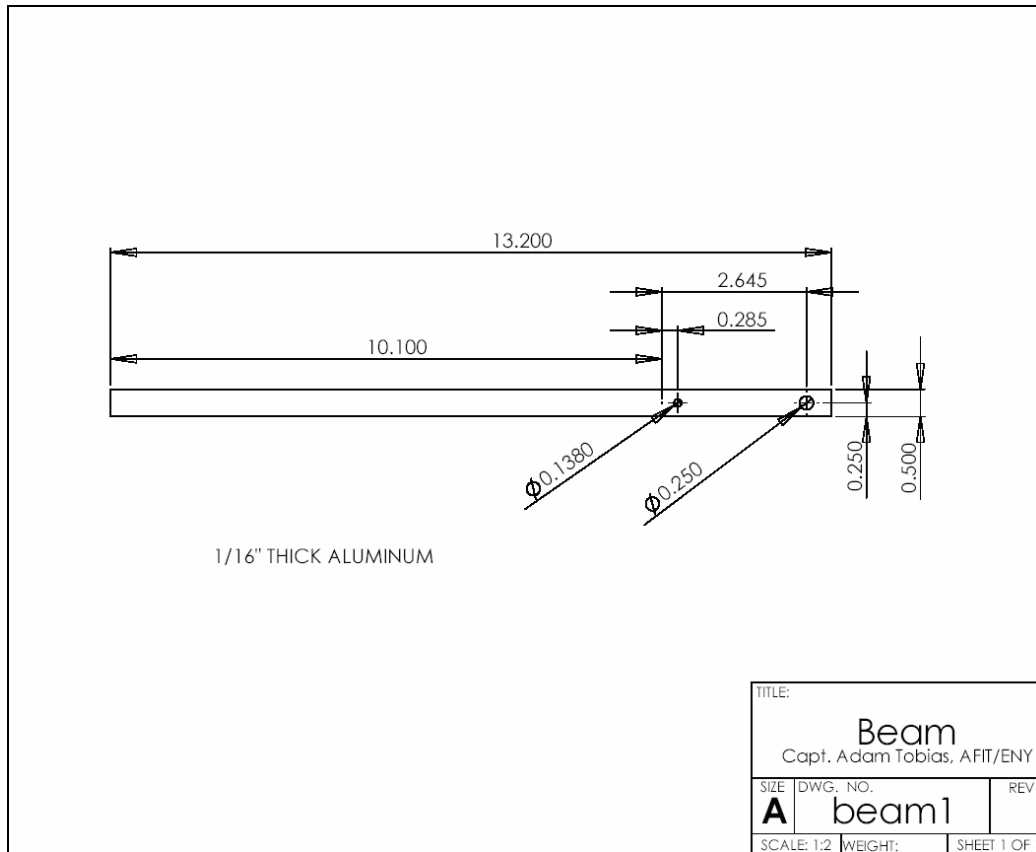


**Figure 17: SolidWorks Drawing – Aluminum Beam**

### 3.3.2 Carbon-Epoxy Beam Design

The 4-ply carbon-epoxy beam had a drawing identical to Figure 17, the only exceptions being in the 4-ply's thickness (0.02") and unclamped length (6.0"). This beam was designed to be tested using the same shaker as the aluminum beam, and therefore a separate clamp was not necessary. In the machining of the carbon-epoxy beam, two holes indicated in Figure 17 were drilled through the carbon fibers. The possibility exists for this modification to have introduced slight changes to the beam's vibration characteristics, compared to that which would be found by using an undrilled configuration. These differences could contribute to minor changes in the beam's natural

frequency; however, due to time constraints, other clamped configurations were not analyzed to document this difference.

### 3.3.3 Aluminum Clamp Design

When it comes to creating an effective clamp, many considerations must be taken into account. By clamping the beam, one desires to force all clamped degrees-of-freedom to zero. The beam can not have any movement at the clamped end; otherwise the vibration results will not be comparable to those from the computation analysis. In an attempt to properly fix the beam with the clamp, the following design, shown in Figures 18-20, is illustrated:

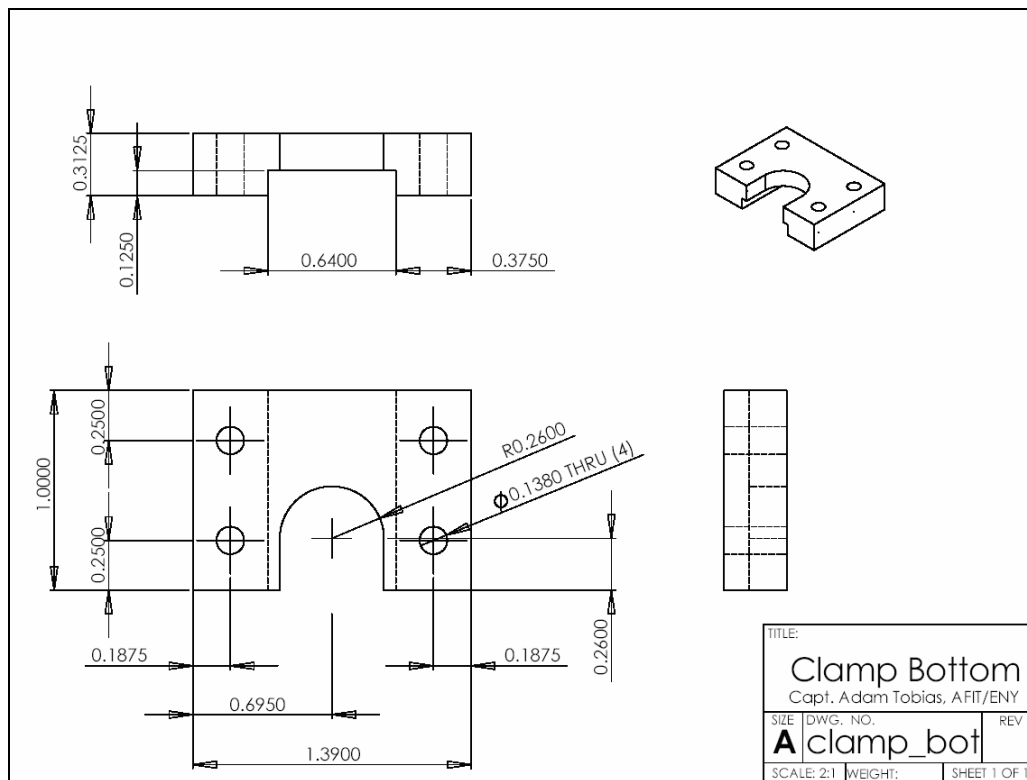
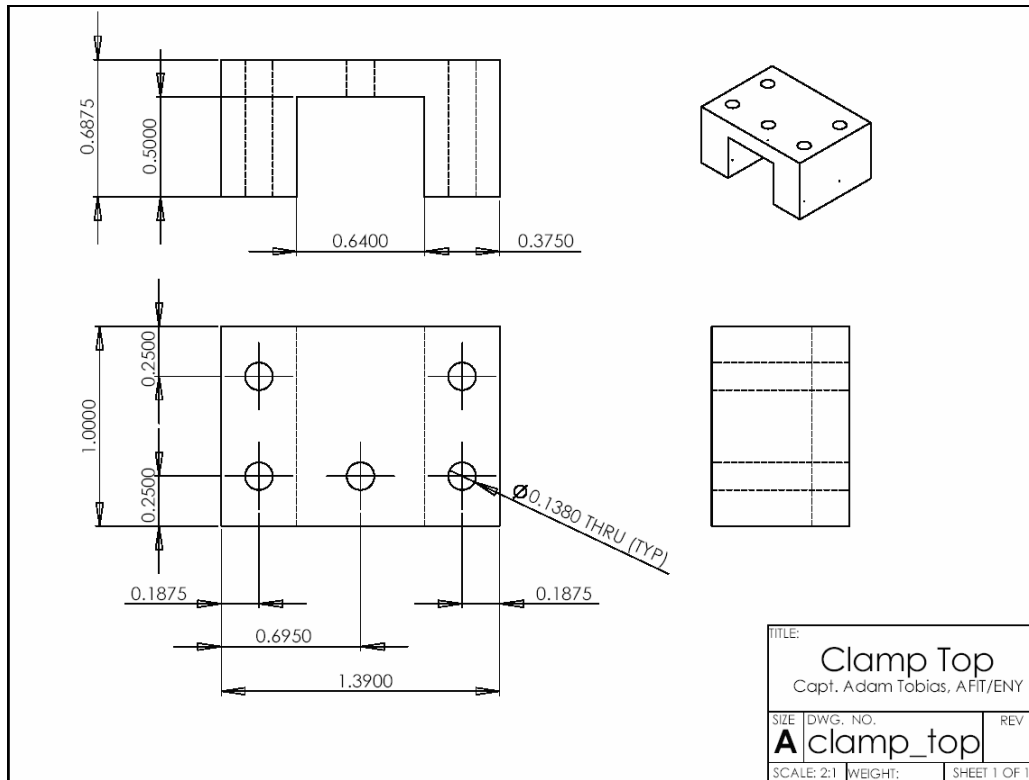
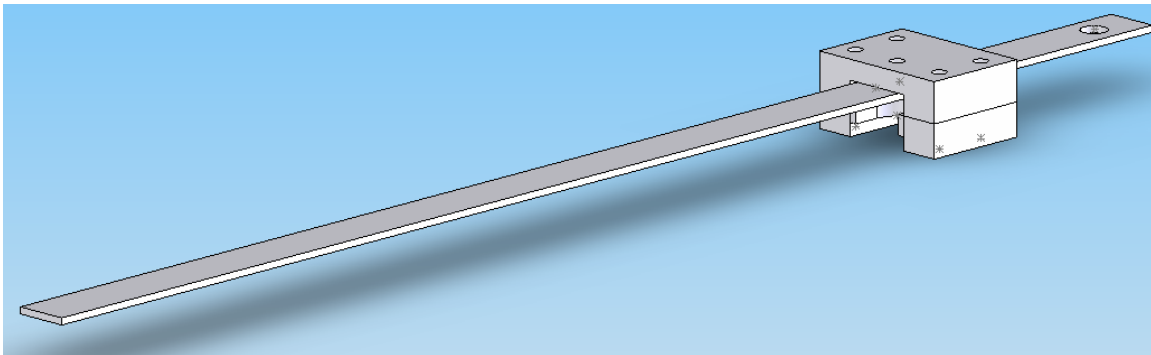


Figure 18: SolidWorks Drawing – Lower Half of Aluminum Clamp



**Figure 19: SolidWorks Drawing – Upper Half of Aluminum Clamp**



**Figure 20: SolidWorks Assembly – Beam & Clamp Configuration**

The beam rests between the upper half of the clamp and the armature of the shaker, while the lower half is positioned on the other side of the armature. A machine screw is used to first secure the beam to the clamp's upper half center hole. Care is taken to ensure the beam is fastened to the clamp's center hole in a perfect 90 degree alignment. Next the beam and clamp are to be placed onto the shaker, and the clamp's upper and lower halves

are secured together using machine screws. Finally, one last machine screw fastens the beam to the midpoint of the shaker armature.

### **3.3.4 Laboratory Test Support Equipment**

Up to this point, the laser vibrometer, the high speed camera, the beams, and the clamp have been mentioned. To make the vibration experiments possible, much more laboratory support equipment was needed. One of the most important items was the system that generated controlled vibration, the shaker. The APS Dynamics ELECTRO-SEIS long stroke shaker was ideal for generating input forces great enough to get the beam's first vibration mode to mimic a flapping wing. The following features quoted from APS Dynamics webpage describe the capabilities of these long stroke shakers (12:1):

- Generate sinewave, swept sinewave, random or impulse force waveforms, fully adjustable at source.
- Test set-up flexibility - operate in fixed body, free body, and free armature - reaction mass modes.
- Optimized to deliver power to resonant load with minimum shaker weight and drive power.
- Adjustable armature re-centering for horizontal and vertical operation or other required pre-loads.
- Rugged armature with linear guidance system carries full weight of body.
- One or two man portability.
- Optional Air Bearings, Lightweight Armature and Extended Stroke.

This particular shaker is rated to 200 Hz, limiting the nonlinear investigation to only the first natural frequency mode. Due to the excellent vibration control features and its compatible size, the APS shaker was the best available fit for these flapping beam

experiments. It also should be mentioned that during testing, the shaker was tested for modal interference in the range of 20-30 Hz. The shaker exhibited no interference for this range of frequencies. The beam/clamp/shaker configuration is shown in Figures 21 and 22.

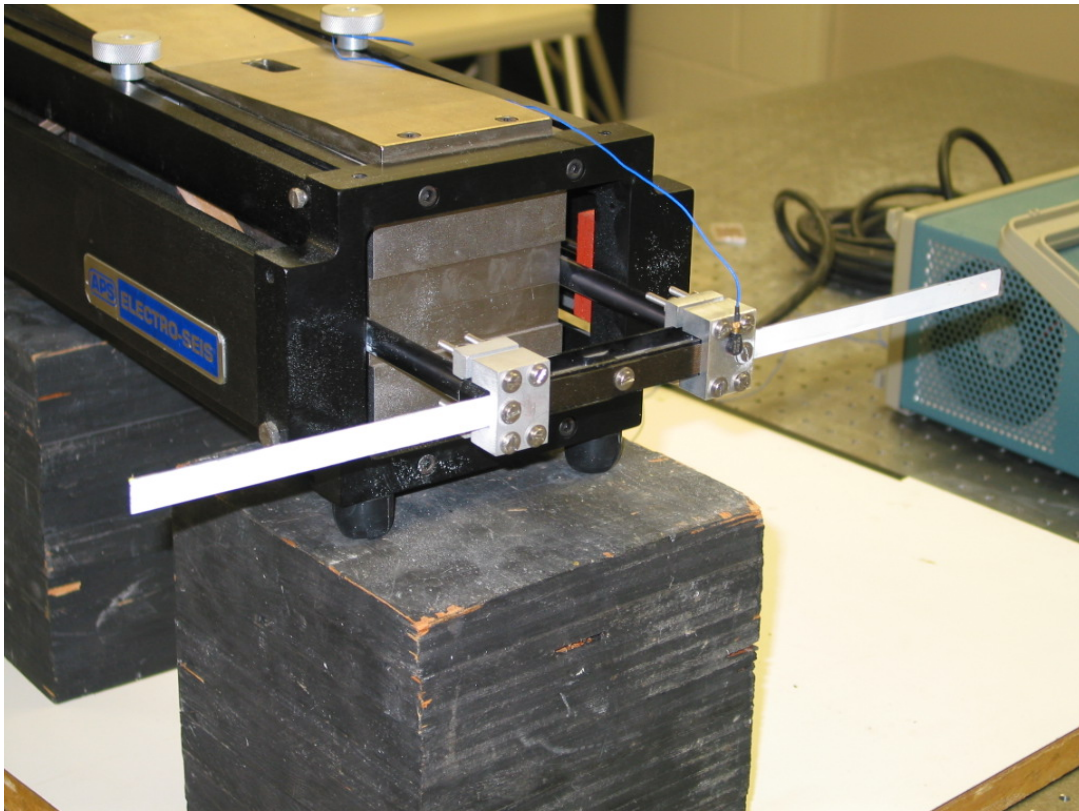


**Figure 21: Isometric View of Beam/Clamp/Shaker Configuration**

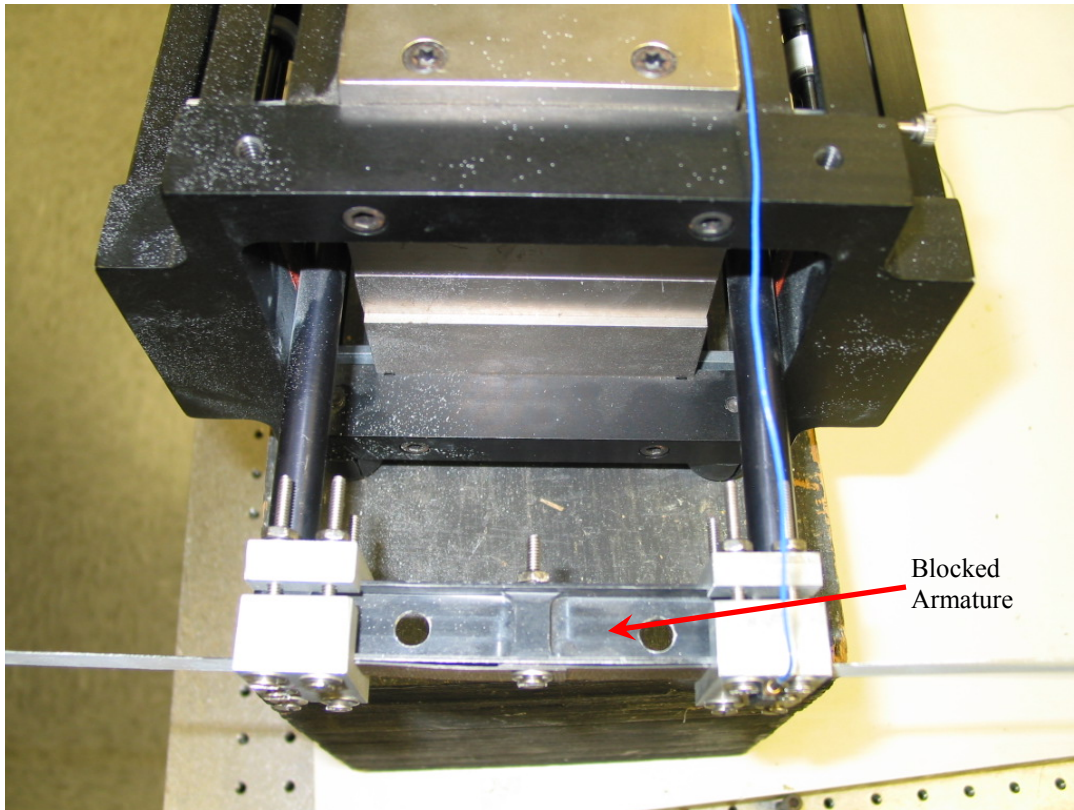


**Figure 22: Top View of Beam/Clamp/Shaker Configuration**

The shaker requires a voltage input fed from a matching amplifier. This amplifier, the APS 124, is designed specifically to provide drive power for the APS electrodynamic shakers. The features of the amplifiers make them uniquely suited for studying the dynamic characteristics of structures. These features are (2:1):

- Voltage or current mode operation allows constant shaker force
- Current Monitor signal proportional to instantaneous output
- Protection circuitry - short-to-ground detection and overload shutdown
- Forced air cooling for continuous operation at maximum output
- Delivers rated current to shaker with blocked armature (seen in Figure 22), resonant loads and reactive loads
- High reliability operation - proven circuitry and components

This particular APS amplifier has a rated frequency range of 0-2000 Hz, which makes it able to handle the testing around 20 Hz and 30 Hz for the two respective beams.

Other items used for these experiments were PCB Piezotronics miniature accelerometers. This accelerometer's very small size minimized mass contribution issues with the majority of experiments which used only one accelerometer fixed to the clamp with wax. It will be shown at a later time where an additional set of testing was carried out with an accelerometer placed at the tip of the beam as well. The accelerometer was connected to a PCB power amplifier with a lightweight cable, as seen in Figure 23. The accelerometer signal was read directly off of an oscilloscope and average peak-to-peak amplitude in millivolts was recorded. Each accelerometer has a conversion of approximately 10 mV/g, allowing the oscilloscope amplitude to be converted directly to peak-to-peak g-force by simply dividing the oscilloscope result by the conversion factor.

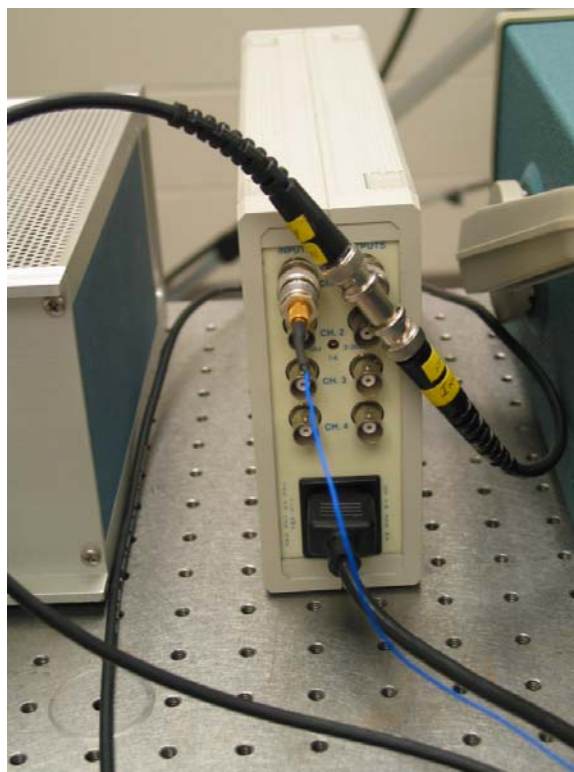


**Figure 23: PCB Power Amplifier – Rear View**



**Figure 24: PCB Power Amplifier – Front View**



The equipment used was a Tektronix TDS-420A oscilloscope (see Figure 25). The amplified voltage signal from the PCB Power Amplifier was sent to this oscilloscope, where peak-to-peak voltage could be documented. It will be shown later how this voltage is converted to peak-to-peak acceleration in g's.

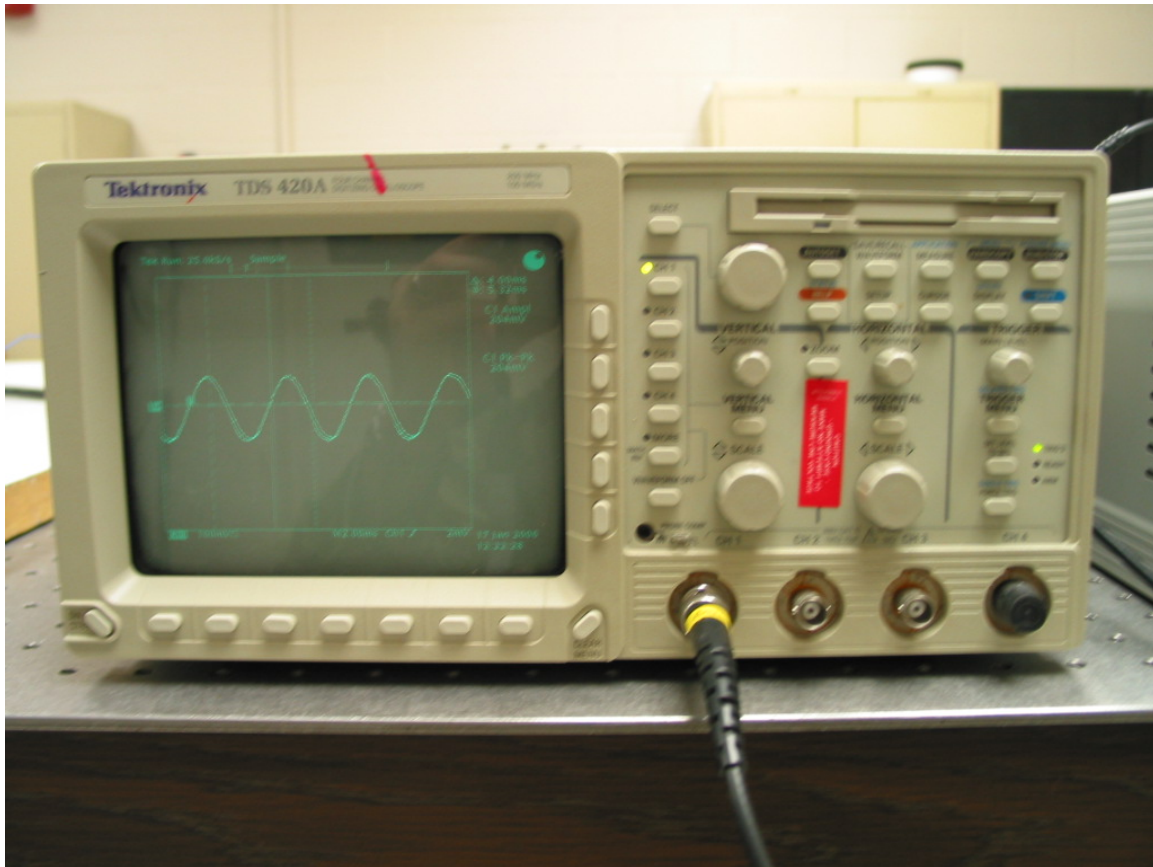


**Figure 25: Tektronix Oscilloscope**

Another valuable piece of equipment in the lab for this testing was the stainless steel Newport Research Corporation Model 45 cylindrical test stand affixed to a Newport Research Corporation Model 100 magnetic base. Two of these test stands were used to hold spotlights for high speed camera test illumination. One of the stands was also used to hold a clamp which positioned a ruler in the camera's field of view in the high speed

camera testing, to be discussed subsequently. The photograph provided in Figure 26 shows this setup:



**Figure 26: Test Stands, Spotlights, and Ruler Setup for High Speed Testing**

### **3.3.5 Laser Vibrometer Setup and Procedure**

It has been mentioned that a laser vibrometer is one of two experimental methods used for this flapping investigation. AFIT is equipped with a Polytec PSV-400-3D scanning laser vibrometer. The particular version, 3-D, means that three scanning heads are available for testing. Each scanning head is equipped with its own laser and video camera. The use of these three lasers rather than one allows for a very accurate 3-D depiction of a given object's vibration activity. The following are some additional features of the PSV-400-3D system (20:1):

- Short setup time
- Fast, precise, non-contact 3-dimensional measuring technique
- Complete acquisition of the optically accessible 3-dimensional vibration vectors
- Use of either predefined (after importing geometry data) or interactively created scan mesh
- Simultaneous measurement using 3 linear independently oriented sensor heads
- High spatial resolution
- Simple calibration of the sensor heads position in the moving object's coordinate system
- Intuitive presentation of the measurement results in 3D animation
- Clear separation of the Out-of-Plane and In-Plane components in 3D animation
- Export of data in UFF- and other formats for processing in Modal Analysis Systems

Some general system specifications for the PSV-400 are:

**Table 7: PSV-400-3D General System Specifications (20:1)**

<b>Frequency range</b>	<b>0 – 80 kHz</b>
<b>Velocity range</b>	<b>0 - 10 m/s</b>
<b>Working distance</b>	<b>Greater than 0.4 m</b>
<b>Laser wavelength</b>	<b>633 nm (red)</b>
<b>Laser protection class</b>	<b>Class II He-Ne laser, 1 mW per sensor, eye-safe</b>
<b>Pointing accuracy of the single sensor head (angular resolution)</b>	<b>± 0.002°</b>
<b>Sample size</b>	<b>Several mm<sup>2</sup> up to m<sup>2</sup> range</b>

Three important points jump out of this Polytec table. First, the velocity range of 0-10 m/s is a limitation built into the laser hardware. It should be noted that an increase in maximum measurable velocity capability exists, of up to 30 m/s with a hardware upgrade and associated velocity decoder upgrades. Second, the frequency range of 0-80 kHz makes this vibrometer more than capable of handling 20-30 Hz testing. Finally, the

working distance of greater than 0.4 m is taken into account in the initial test setup. It is a requirement that the front of the scanning heads is at a distance greater than 0.4 meters from the surface of the beam being tested.

Initially, only 3-D testing was planned for these beam experiments. However, it will be pointed out that eventually 1-D testing became more suited for measuring the vibration of a beam undergoing very large bending deflection. For the purposes of detailing test setup, the 3-D method will be covered in this section since it is all-inclusive. Appendix C includes thorough step-by-step instructions detailing the procedures one would follow to conduct vibration testing using PSV-400 scanning laser vibrometer, this section will provide an overview of the 3-D procedures. The 1-D setup is identical to the 3-D up to the completion of a 2-D alignment, as detailed in Appendix C. If running 1-D tests, when the basic 2-D alignment is complete one may proceed to the actual testing. For the 3-D process, once finished with the 2-D alignment, one must complete the 3-D alignment and the remaining steps outlined in Appendix C. The total 3-D setup time is nearly doubled when compared to the 1-D setup as a result of the additional steps necessary to properly perform the 3-D alignment.

The first requirement is to establish the specimen to be tested, and the method to input forces onto that specimen. Beams and their supporting clamp, along with a long-stroke shaker fulfill that objective. The PSV computer and its three control boxes must have their power “on” to begin testing. The scanning heads, shown in Figure 28, are connected to a Polytec OF V-5000 Vibrometric Controller, displayed in Figure 29. The amplifier’s signal input receptacle was connected to the SIGNAL 1 output on the PSV Junction Box with a signal cable. This same signal was initially also connected to an

input channel of the PSV Junction Box as a reference. Later it will be shown how an accelerometer's signal connected directly into the Junction Box reference input provided much more accurate FRF results. The output on the back of the APS amplifier was connected to the shaker. Figure 27 provides a connecting diagram of the 3-D vibrometer test setup. This is identical to the 1-D setup, with the exception that the left and right vibrometer scanning heads are not used.

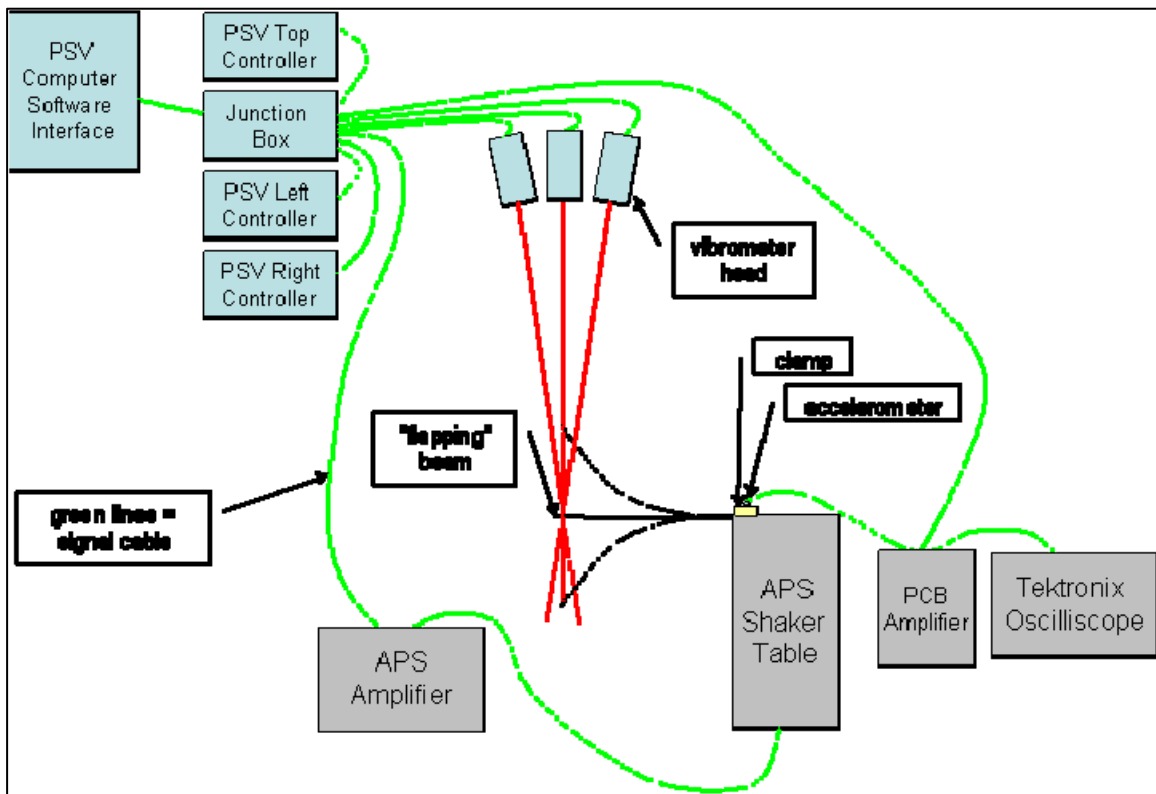


Figure 27: Right, Center, and Left PSV-400 Scanning Heads





**Figure 28: Right, Center, and Left PSV-400 Scanning Heads**

It is recommended that the scanning head's control boxes be turned on at least 30 minutes prior to the experiment for warm-up. The PSV software is then initiated and the scanning head shutters may be opened. If performing a 1-D test, one must adjust the scanning heads tripods so that they are approximately level and perpendicular to the beam; a 3-D test does not have this same requirement. The PSV 8.4 program has tilt, zoom, and auto-focus features for the top scanning head's camera. One can use tilt to carefully adjust the camera until it is centered on the object. The top scanning head's laser also needs to be positioned in the center of the specimen. When both of these are accomplished, the camera should be zoomed-in and auto-focused as appropriate. The left and right scanning heads must be manually adjusted, and their cameras are not needed for this

testing. At this point, hardware manipulations are complete. It is imperative that once the tripods and scanning heads are configured and set, that they are not disturbed until testing is complete. Any minor disturbance will require repeating the hardware setup as well as the software setup procedures that follow.

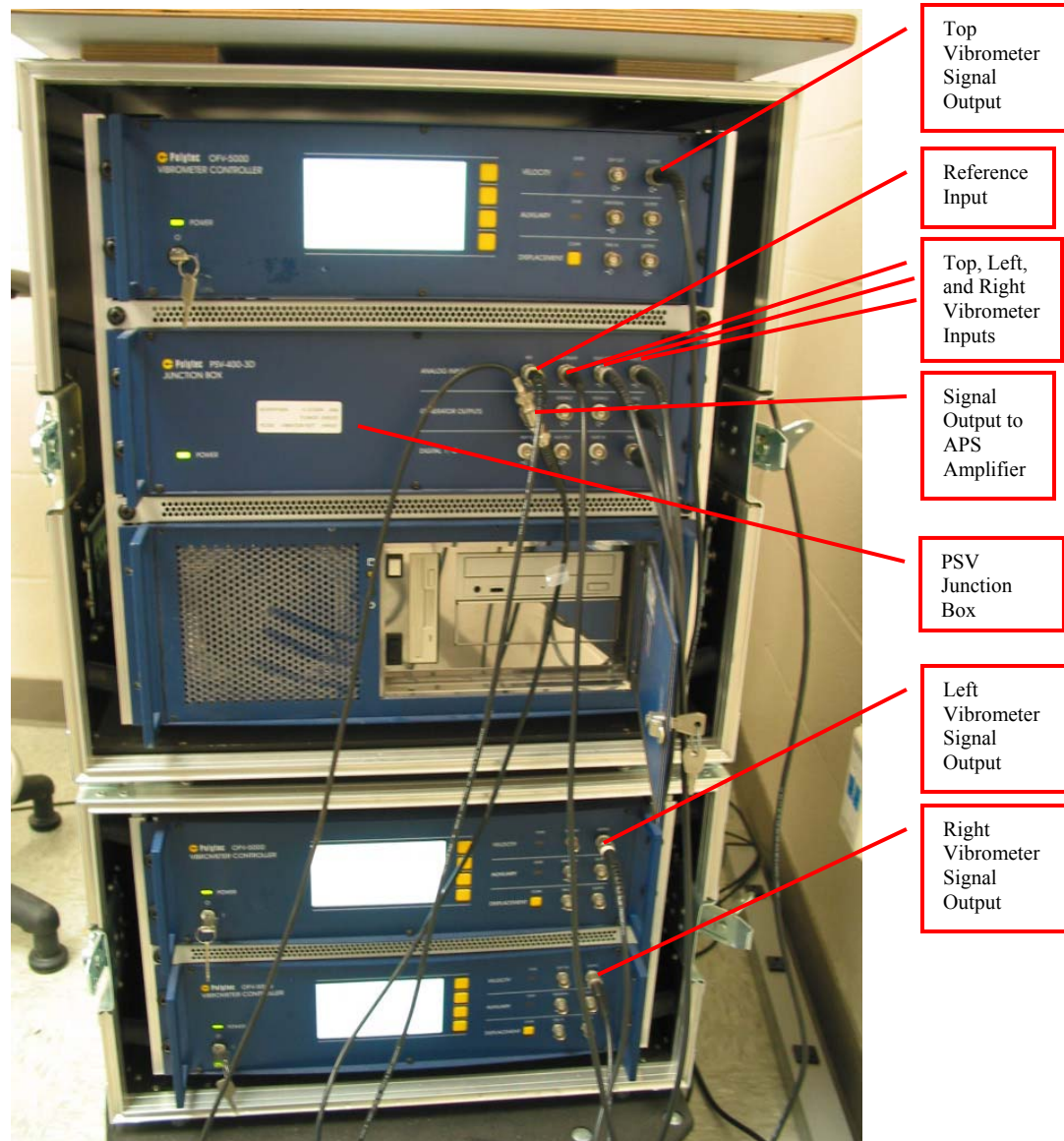


**Figure 29: Polytec OF V-5000 Vibrometric Controller**

The PSV 8.4 software consists of two major functions: acquisition mode and presentation mode. Figure 30 shows the Polytec computer system while in acquisition mode.

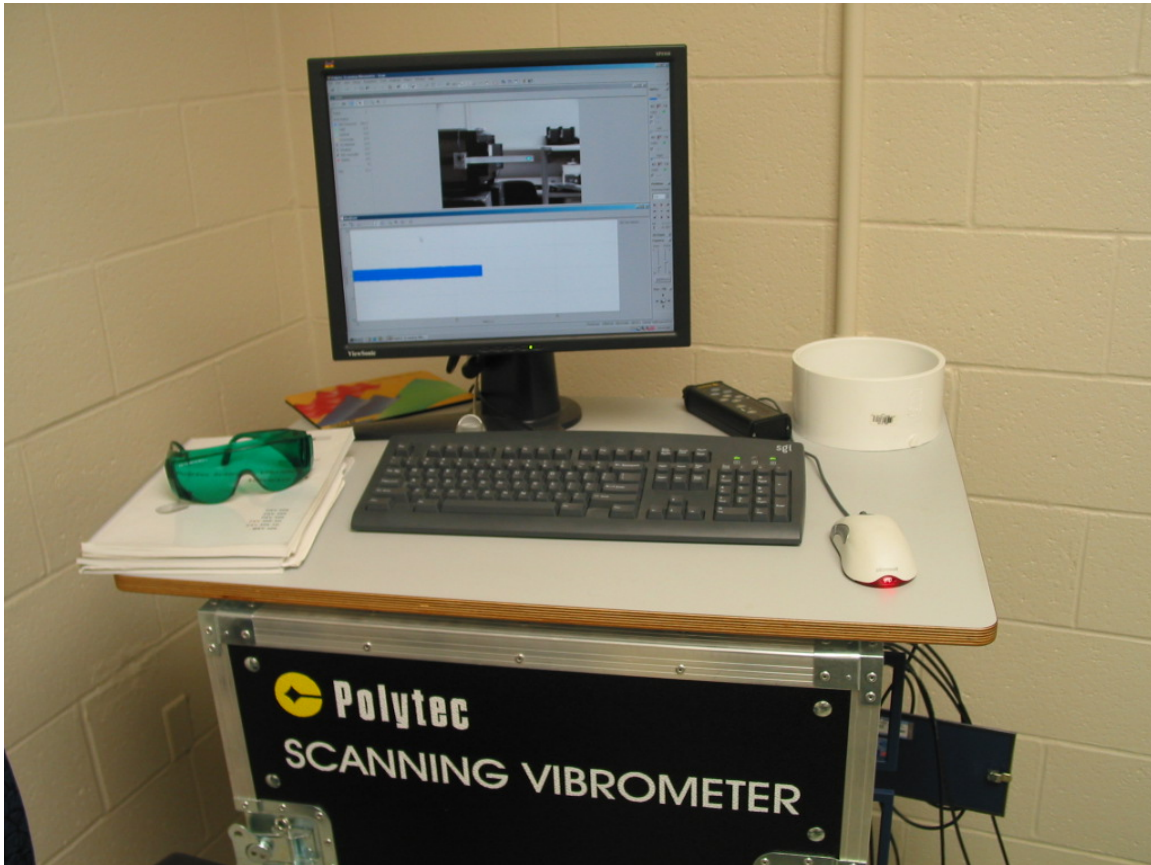


**Figure 30: Polytec Test Console**

Acquisition mode is where all testing is completed, and presentation mode is where one analyzes the test results. When conducting 3-D testing, all three lasers must be checked “on” in the software in three places. There are check boxes within the optics tool boxes, within the acquisition settings (A/D) the system must be set to 3-D testing mode, and also within A/D all three laser head must be checked on. All lasers must initially be auto-focused to create a concentrated laser beam upon the desired location, and one can check all three respective signal qualities after the auto-focus is complete. Some materials



absorb the laser light enough to significantly reduce the reflected light, causing a poor or non-existent signal. This was the case with the black carbon-fiber beams. In this event a white powder aerosol spray, SpotCheck SKD-S2, may be used to lightly coat the surface of the object being tested thereby improving the laser signal quality. This coating is shown by the difference between Figure 31 and Figure 32. This powder is specifically designed for vibration testing and it does not introduce a damping effect as other surface coating materials may.

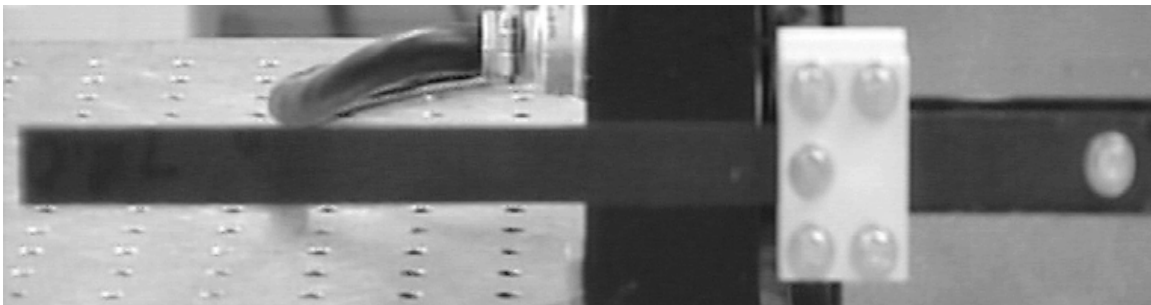


**Figure 31: Uncoated Carbon-Epoxy Beam**

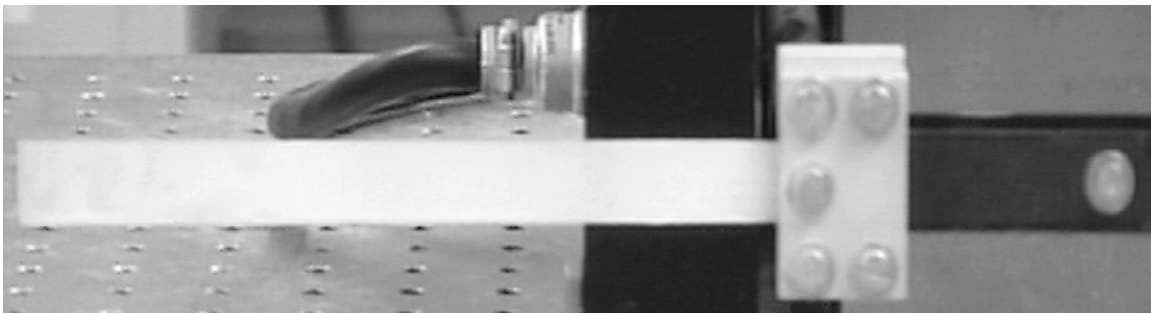


**Figure 32: White Coating on Carbon-Epoxy Beam**

When the laser signal quality is at an acceptable level, one can proceed with the next step, performing a 2-D alignment. 2-D alignment is required for all tests when using the PSV system. When only one scanning head is used, as will be the case for most of the latter testing, only a 2-D alignment is necessary. For all 3-D tests, once a 2-D alignment is completed, one must also complete a 3-D alignment as well. A 2-D alignment establishes the 2-D boundaries and surface of the object being tested. A

minimum of four alignment points is necessary; however it is recommended for more complex surface geometry that at least ten points be used. The details of the 2-D alignment procedure are provided in Appendix C.

The 3-D alignment must be also carried out. This step will define the most desirable three-dimensional coordinate system. Figure 33 displays the convention used throughout the experiments conducted in this research project.

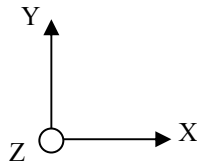


**Figure 33: 3-D Alignment Coordinate Axes**

To establish this coordinate system, the origin and two other axis points must be defined in the 3-D alignment. After these three points have been set, four more alignment points may be defined. The process of creating each and every alignment point involves positioning all three lasers in approximately the same spot; auto-focusing the lasers; and then manually move the lasers so that they are positioned at exactly the same spot. This last step requires the use of Helium Neon filter goggles, shown in Figure 30, as well as a hand-held remote for repositioning the laser beams, given in Figure 34.



**Figure 34: 3-D Alignment Remote Control**

Similar to the 2-D alignment, the number of alignment points chosen depends upon the complexity of the object being tested. Appendix C carefully addresses all of the 3-D alignment procedures.

The next step required is to create a grid which represents the object's surface. This grid is made up of multiple grid points which are equivalent to the nodes of a finite element analysis program. The grid tool establishes the grid points across the entire shape of your object. This tool creates common shapes in methods similar to those used by Microsoft Office drawing toolboxes. In the 3-D laser scan, all points that have been defined will be used. More grid points will create lengthy test scans with more accurate results. After the grid has been defined, a *Geometry Scan* must be performed. This step records the precise distances from each grid point and the three scanning heads. Using this geometry, a very detailed depiction of the objects surface can be mapped with the PSV software. The user has the option to create a memory record of the appropriate laser beam focus setting for each and every grid point, or to create an average focus setting for the tests. This is accomplished using the *Assign Focus Best* and *Assign Focus Fast* commands. Objects having a surface with basic 2-D geometry, such as a beam, will only require use of the fast focus method. This significantly reduces the length of time required for a 3-D test setup.

Before testing can begin, one must select the appropriate acquisition board settings. This step requires a background in the fields of structural dynamics as well as vibration testing and control. This preparation concerns the general settings, channels used, filtering, frequency ranges, vibrometer specifications and generator settings. For a

detailed Polytec Software Manual aided explanation of the available settings, please refer to Appendix D.

With the appropriate acquisition settings set the next step is to initiate the vibration test. Two major measurement options exist: single point and scan measurements.

With a single shot, the software makes a single measurement and then ends data acquisition. A scan is a sequence of single point measurements. The order in which the software approaches the scan points is determined by an internal algorithm. For every scan point, the software carries out the following steps:

- Position the laser beam at the scan point.
- Set the optics of the scanning head to the focus value of the scan point.
- Wait for the end of the settling time of the scanner mirrors.
- Make a single shot.
- Assign scan point status.
- Save measurement data.

After a scan, the software can automatically remeasure certain scan points or you can start remeasuring manually. You can also mark single scan points in presentation mode to be remeasured and then remeasure this file in acquisition mode. (16:Ch 6)

Both single shot and scan were used extensively throughout the course of testing for this project. A scan of multiple grid points spread across the beam may be used to generate a graphical display of the beam's mode shapes. A single shot collects data for one grid point; therefore creating eigenvectors representative of the entire shape is not possible with this method. Single shots, however, are used extensively throughout this testing. To determine displacement of a specific point, such as the beam tip, only a single shot is necessary. Test time is greatly reduced by eliminating the data acquisition of numerous unneeded grid points.

When a scan was completed, the measurement was saved to a file that would be available for further post-processing. The analysis, or post-processing, of the vibration

data obtained in the acquisition step will be completed by using the presentation mode of the PSV software and in some cases, Matlab programs. The vibrometer experimentation sections will address all features of the Polytec 8.4 presentation mode applicable to this project.

### 3.3.6 High Speed Camera Setup and Procedure

The experimental setup of the high speed camera consisted of positioning the Photron FASTCAM camera in a location that best enabled the imaging of the vibrating movements of the beam. It was determined that the beam movement would be best captured by positioning the camera directly above the beam. The camera's arrangement when setup for testing is shown by Figure 35.

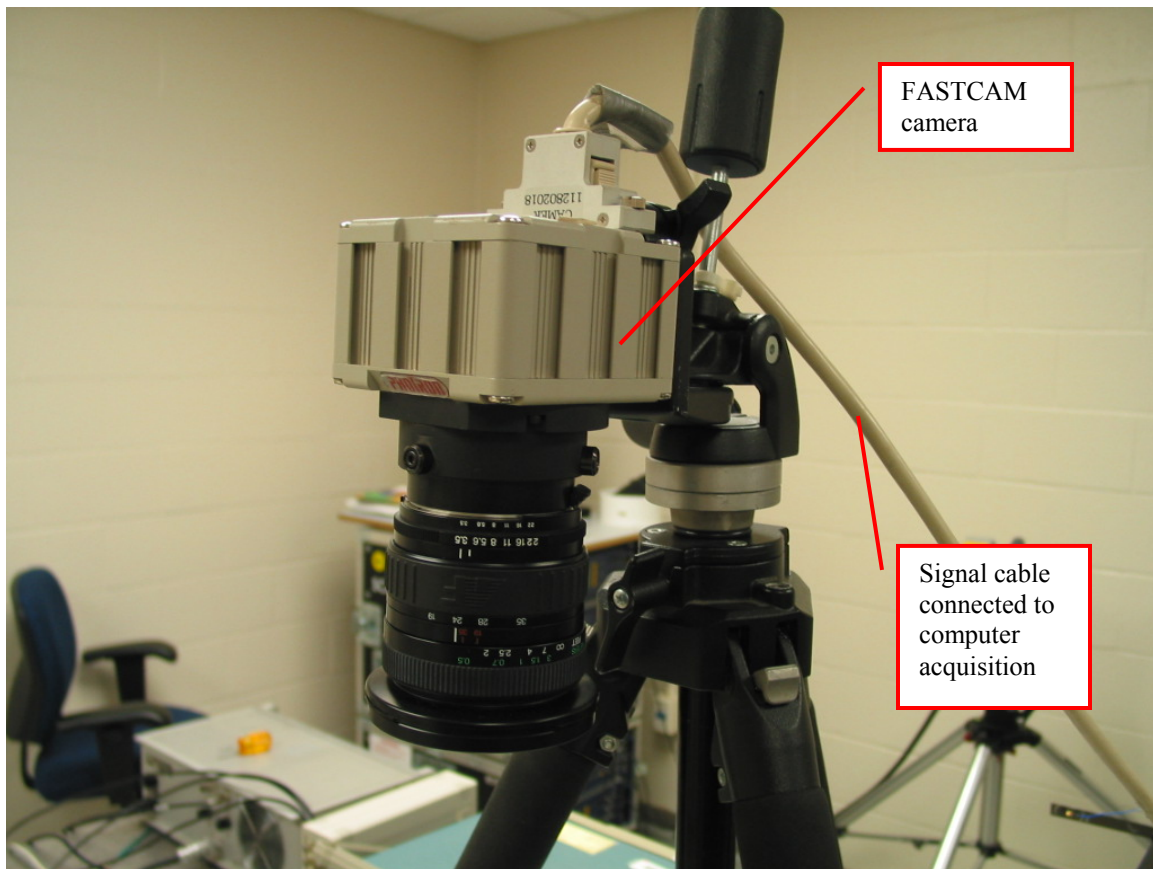


**Figure 35: Photron FASTCAM Positioned Vertically Above Beam**

The Photron FASTCAM camera has no ability to measure displacements or velocities; it behaves as any non-scientific purposed video camera would. This fact brought about the need to create some method to make these measurements possible. The FASTCAM Motion Tools analysis software was equipped with a pixel to unit conversion tool. The solution chosen was to place a ruler beside the tip of the beam directly in the camera's field of view. This would allow all video and still pictures to always have a measurement scale aligned with the beam's primary direction of vibration. Figure 36 provides an illustration of the ruler positioning in relation to the beam.

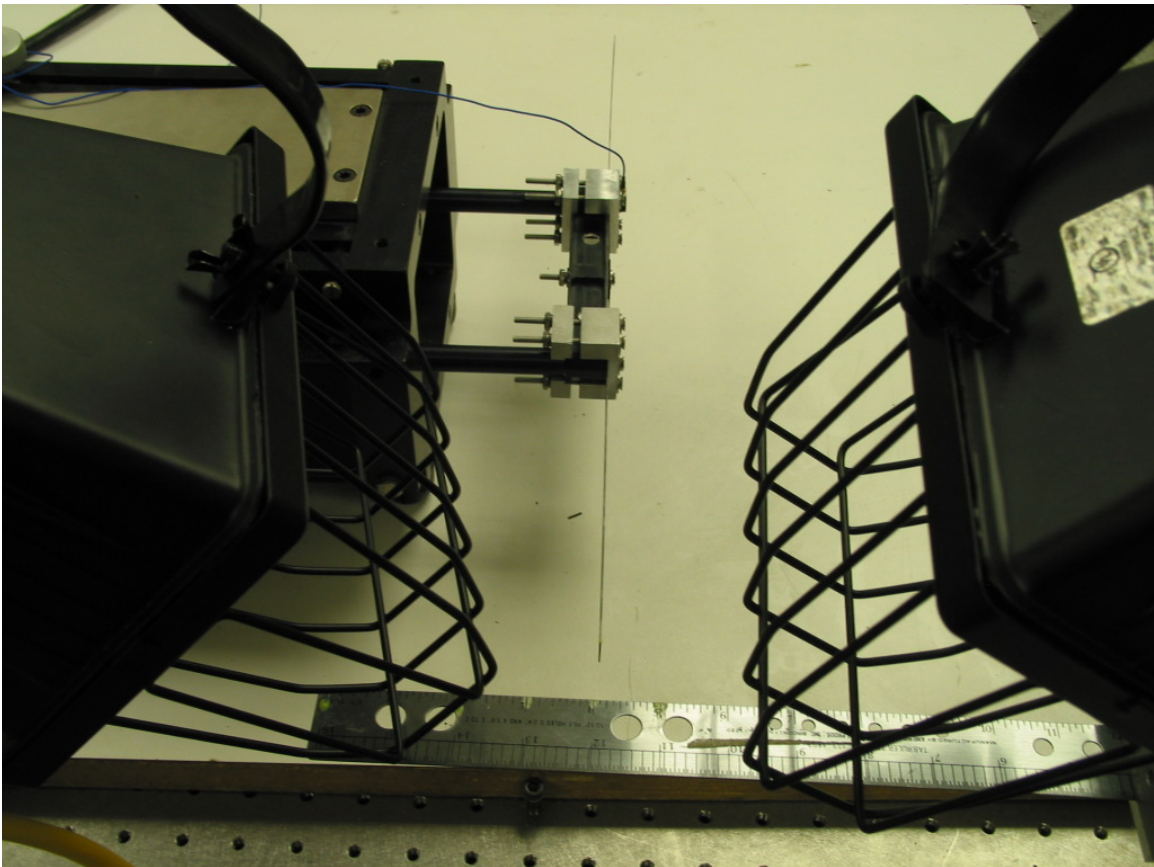


**Figure 36: Photron FASTCAM Positioned Vertically Above Beam**

Section 3.2 discussed the importance of light levels as frame rate is increased. While this particular camera was capable of 16,000 frames per second (fps), the



spotlights shown in Figures 36 and 37 were only able to create enough illumination to allow for 1,000 fps during the testing. Any film or photos above 1,000 fps were too dark to be of any use. In addition to the spotlights, “glow-in-the-dark” paint was used to better illuminate the beam tip as well as each inch on the ruler. This allowed for better recognition of these most important spots during post-processing of the videos. Another photograph showing the overall setup of the clamped beam, shaker, lights, and ruler is included in Figure 37. It should be reemphasized that during testing, the high speed camera was positioned on a tripod directly above and perpendicular to the beam tip to accurately capture the entire tip movement. It has not been in Figure 37 due to the obstruction to view caused by the tripod.



**Figure 37: Optical Test Setup**

All post-processing was performed on a desktop computer equipped with a PCI card (attached to the camera) and a software package consisting of viewer and analysis programs. The Photron FASTCAM Viewer, pictured in Figure 38, is where initial setup and image capture took place. Within the FASTCAM Viewer, the user had the ability to specify desired frame rate, resolution, shutter speed, and light sensitivity settings. Additionally, the format to save the data, whether .jpg picture files or .mpg movie files, was determined with this Viewer.

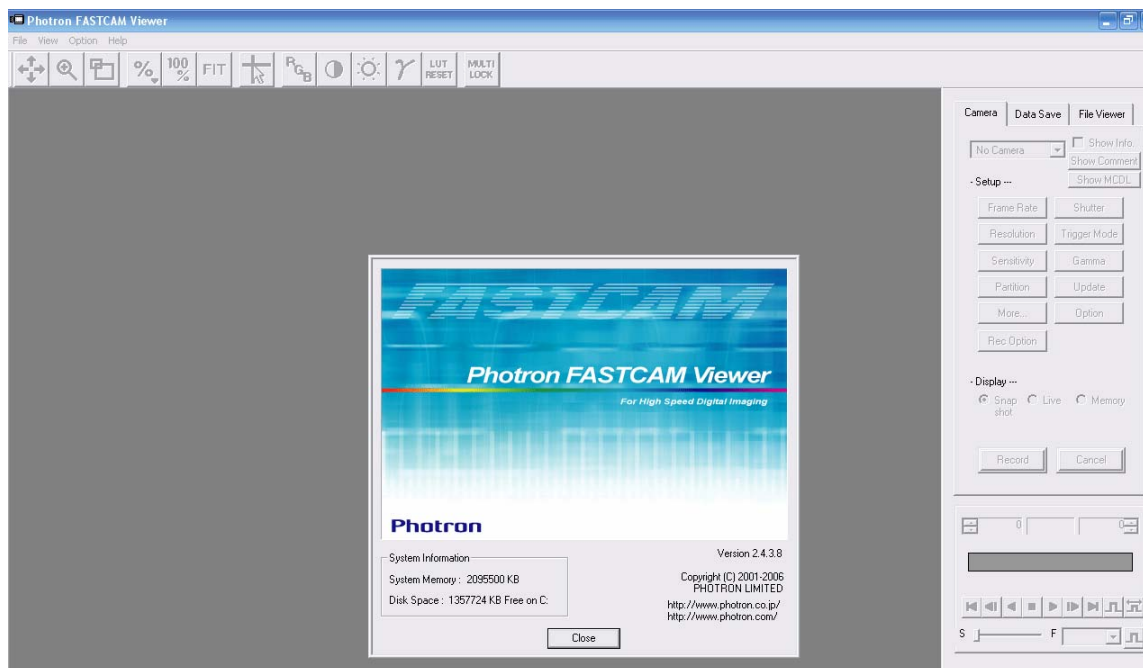


**Figure 38: Photron FASTCAM Viewer Software**

Once the picture frames or videos were saved, the Motion Tools analysis software, pictured in Figure 39, allowed the user to perform pixel-inch conversion and make precise beam deflection measurements. These measurements were carried out by using the Motion Tools "Analysis" toolbox. The user would create a point on two desired known measurement locations, such as a two inch distance on a ruler, and choose



to define the unit conversion scaling. The example calibration shown in Figure 40 states that 84.5 pixels/inch existed in this particular conversion.

After this was achieved, the video was played until the desired frame was on the screen. Analysis points were created to mark the tip location of the beam at its initial non-deflected state, and then a second point marked the maximum deflected location. Peak-to-peak displacement amplitude, in inches, was generated by subtracting out the rigid body motion occurring at each respective maximum beam tip positions. It is similarly possible to determine velocity. Each analysis point corresponds to a specific camera frame. Each frame is separated by the reciprocal of the amount of time established by the frame rate chosen. For example, 1000 fps would generate 1000 individual pictures in one second, and each picture is separated by 1/1000 of a second. Velocity would be the previously calculated peak-to-peak displacement divided by the time difference between the frames of the two specified track points. Figure 40 shows an example of the net displacement determination between respective root and tip points.

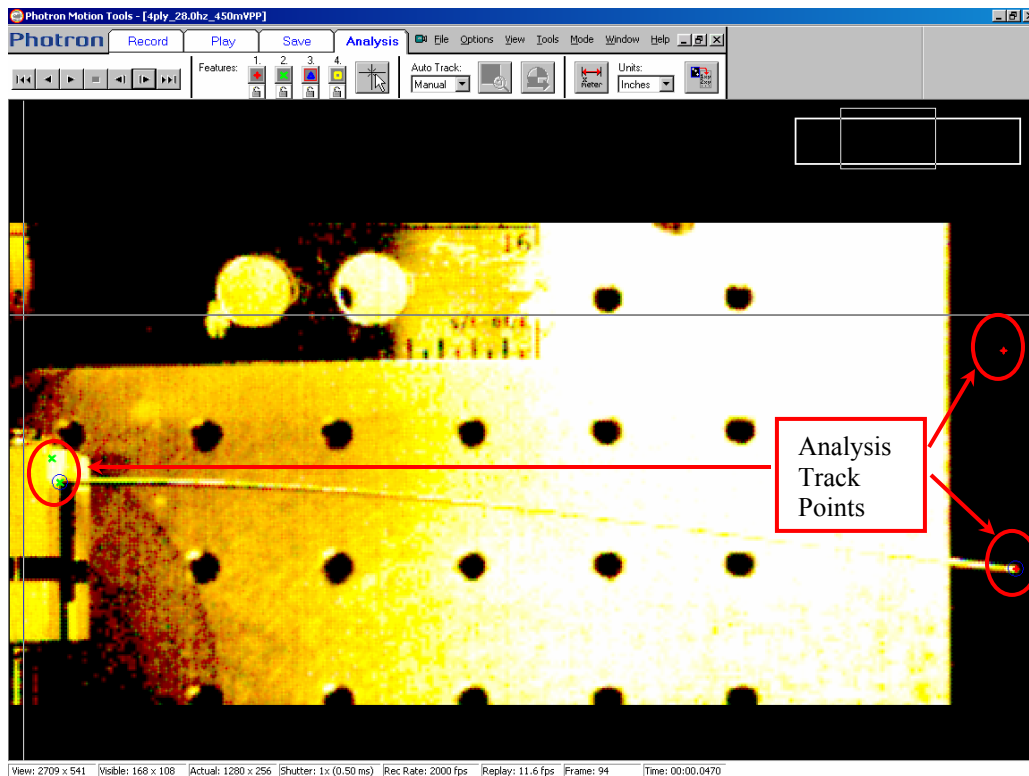


Figure 39: Photron Motions Tools Analysis Software

PHOTRON				Motion Analysis Data Sheet			
<b>Motion Tools</b>							
the power to stop motion							
<b>Test Data</b>							
Date:	10/6/2006						
Time:	11:03:45 AM						
File Name:	4ply_27.0hz_450mVPP						
<b>Calibration</b>							
Calibration	84.5	Pixels / Inch					
Tilt:	0	Degrees					
Export Uni	Inches						
<b>Tracking Data</b>							
Frame	Time	Track Point 1		Track Point 2		Net Displacement Change: Root to Tip	
		x	y	x	y	x	y
81	0.0405	9.278107	0.95858	3.325444	1.467456	5.952663	-0.50888
118	0.059	9.337278	2.011834	3.372781	1.621302	5.964497	0.390533

Figure 40: Photron Motion Analysis Data Sheet

### **3.4 Three Dimensional Laser Vibrometer Experimentation**

An initial focus of the experimental research involved using the Polytec 3-D scanning laser vibrometer. As it was previously discussed, the 3-D feature requires the use of all three scanning heads and their respective lasers. This laser vibrometer system, while very capable, involved considerable instruction, trial, and error. This is especially true due to the nature of the work of this project, large deflecting beams. A majority of the efforts to conduct 3-D experimentation of both aluminum and carbon fiber beams were met by vibrometer hardware limitations. The details of all 3-D experimentation as well as the accompanying successes and challenges are the purpose of this section.

The first beam acquired was a 10.1” 2024-T3 aluminum beam. This beam was fabricated in the AFIT machine shop according to the drafting specifications provided earlier in this document. It was decided that this experimentation would document the best methods available to AFIT to conduct vibration testing on a beam stimulated to mimic a flapping wing at frequency ranges of 20 Hz to 30 Hz. These experimental methods must also be suitable for documenting non-linear vibration occurring at various force input amplitudes. The computational efforts already had shown that the aluminum beam met the 20 Hz 1<sup>st</sup> mode natural frequency requirement. The experimental methods now had to be proven out in the laboratory.

### 3.4.1 Aluminum Beam - Asymmetric Shaker Configuration

The procedures documented in Section 3.3.5 and Appendix C were followed for each and every 3-D test. Figure 41 shows the original setup of the aluminum beam mounted to the long-stroke shaker in a horizontally mounted orientation.

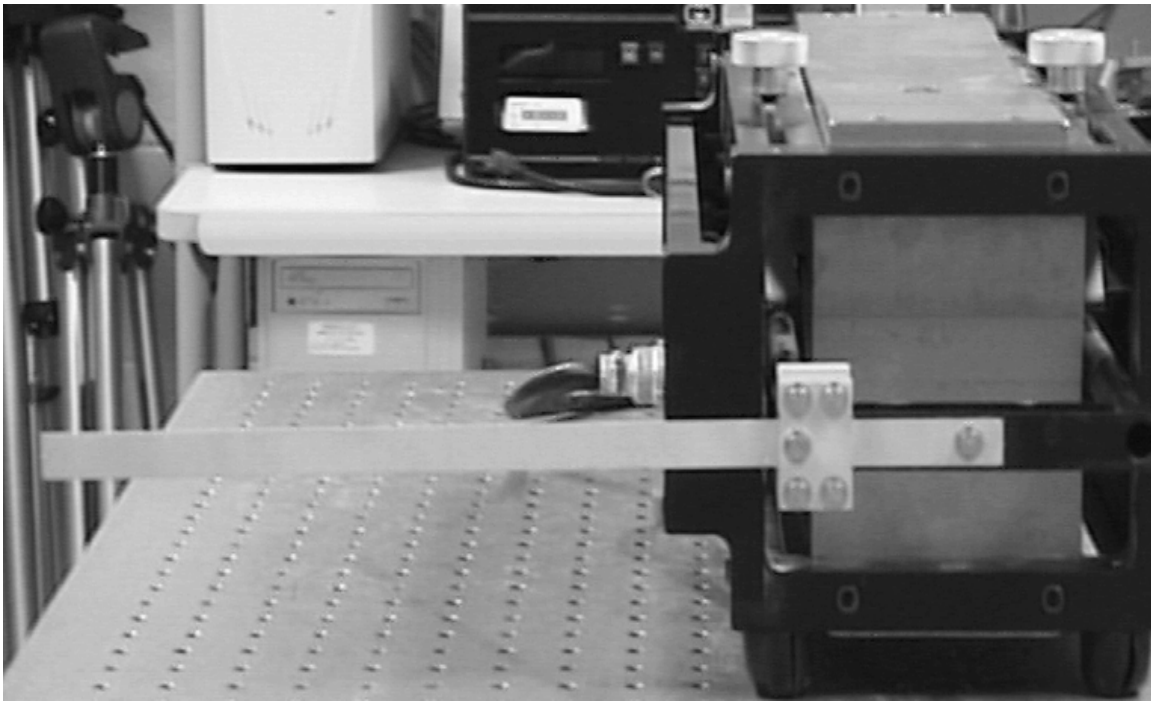


**Figure 41: 3-D Asymmetric Aluminum Beam Configuration – Horizontally Affixed to Shaker**

The purpose of the first set of testing with a single aluminum beam using the three dimensionally configured laser vibrometer was to show that experimentally the beam's 1<sup>st</sup> mode natural frequency did match the computational result from Table 2. This first set of tests, at 20 Hz, used a line of grid points positioned across the length of the beam, as to accurately capture a range of deflections for the entire beam. These tests were conducted at relatively low amplitudes causing little visible movement of the beam tip. The first experiments were Fast Fourier Transform (FFT) sine sweep scan tests over a frequency range from 0.125 Hz to 100 Hz, using multiple grid points. The 0.125 Hz to 100 Hz sweep range defines what frequencies will be sent to the shaker. Figure 42

provides a rough example of the resulting arbitrary magnitudes occurring throughout the sweep from 0.125-100 Hz. Since the preceding analytical methods had provided good initial approximations of the aluminum beam's first mode natural frequency, the initial testing was carried out relatively quickly just to verify this frequency. Options such as complex averaging and high numbers of FFT lines resulting in longer sample times were not exercised for these preliminary experiments. This is the reason for the "false peaks" shown in Figures 42 and 43. As the research narrows to methods that are proven to be most desirable for measuring flapping, test sample times will be drastically increased, resulting in smoother spectrum plots. One other note of importance, while the natural frequencies provided in all proceeding spectrum plots are accurate, new methods were uncovered and utilized beginning in the experiments of Section 3.5.4 to accurately display the magnitude information. Precise magnitudes, whether given as velocity or displacement, should not be used for analytical comparison until Section 3.5.4.

The result of Figure 42 indicates that perhaps a logarithmic scale on the horizontal axis would be more suitable for displaying the magnitude plots. An example of the same single beam test result represented by a logarithmic magnitude plot is shown in Figure 43. This figure provides a more suitable method of plotting the resulting magnitudes of the vibrometer FFT scans. This logarithmic scale standard will be maintained throughout the remainder of laboratory testing.

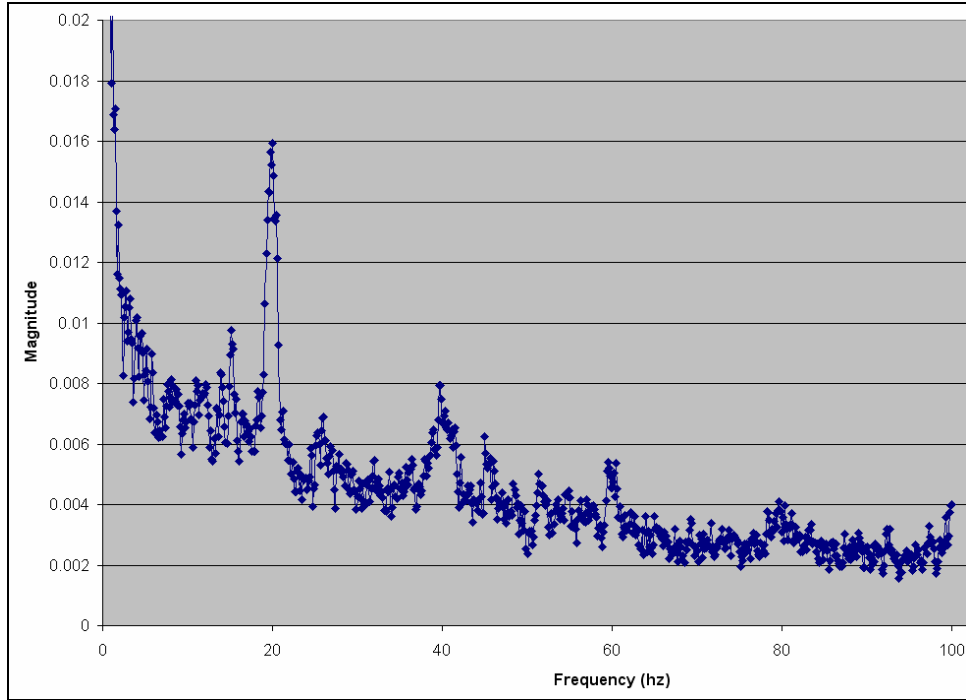


**Figure 42: 3-D Asymmetric Aluminum Beam Configuration – Frequency Spectrum**

The experiments were repeated to confirm the accuracy of the theoretical result for the 1<sup>st</sup> mode bending frequency. The 1<sup>st</sup> mode was recorded to be 20 Hz for this single 10.1” beam, which matches the expectation from the computational analysis.

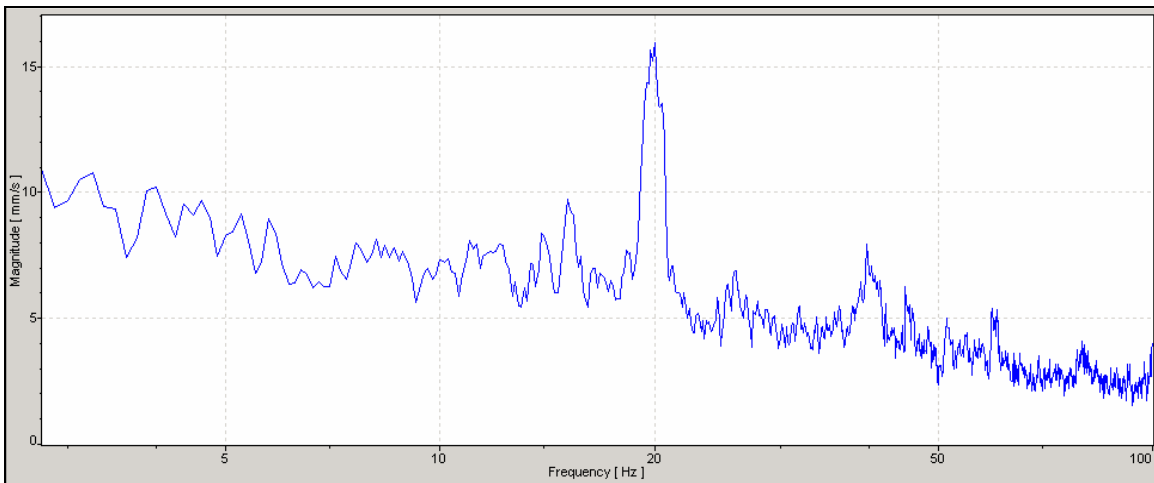


**Figure 43: 3-D Asymmetric Aluminum Beam Configuration – Log-Scale Frequency Spectrum**

After completing the FFT sweep, it is possible to take a closer look at the eigenvectors occurring at the 20 Hz 1<sup>st</sup> bending mode. The original methods followed

during the vibrometer testing were to conduct an FFT sweep followed by a FastScan (described in Appendix C) at the frequency of interest. It will be shown later the effectiveness of a Zoom-FFT sweep, which centers the test on the frequency of interest. The FastScan tests only measure one specific constant frequency. This can be very useful if the user desires to use a greater number of grid points to complete a more thorough vibration analysis of the structure's respective modal frequencies, generating smoother eigenvectors. A FastScan can be completed in just a fraction of the time when compared to both the FFT and Zoom-FFT methods. The resulting 1<sup>st</sup> mode eigenvector, or mode shape, of the combined grid points is shown in Figure 44. This mode shape begins exactly as one would expect for a beam's first bending mode, but changes slightly toward the tip, displaying a slight kink. This same effect is present throughout the carbon fiber tests as well; by visual inspection, both beams coincidentally were slightly distorted at the location of this kink.

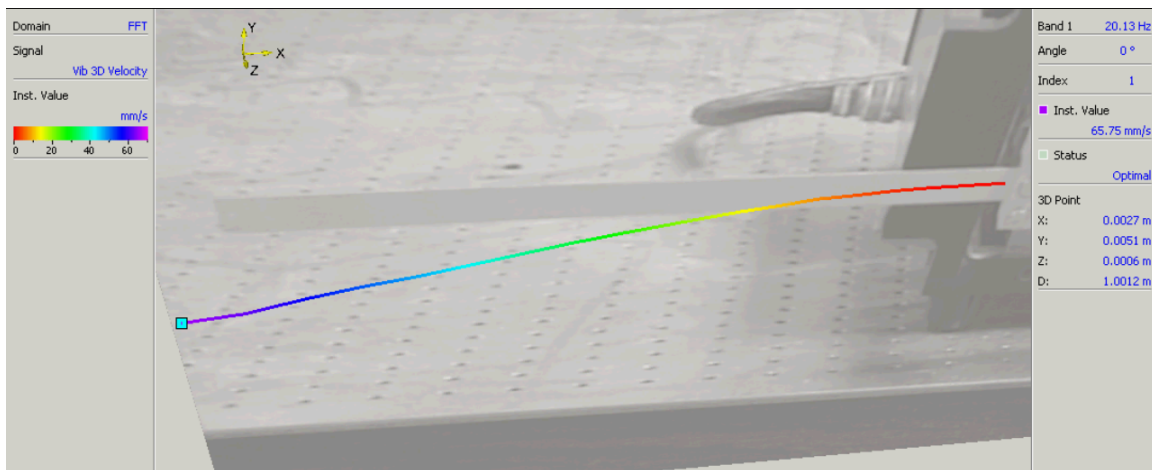


**Figure 44: 3-D Asymmetric Aluminum Beam Configuration – 20 Hz FastScan Mode Shape**

As the input amplitude was increased for these tests to levels that one could visually observe a flapping-type of motion, it became readily apparent that the large tip deflections occurring for the 10.1" beam would not be a very close comparison with the

scale of flapping magnitudes that a micro air vehicle would likely experience. For example, a 45 degree peak-to-peak rotation would generate an approximate displacement magnitude of 7.73". MAV's are to have a halfspan no greater than 3".

Also when running the 3-D testing, issues were beginning to surface with velocities *overranging* the 10 m/s capability of the vibrometer system with scan points close to the tip of the beam. Figure 45 shows an example of the display present during acquisition mode during testing. This default magnitude is the beam's real-time velocity as recorded by the laser vibrometer.

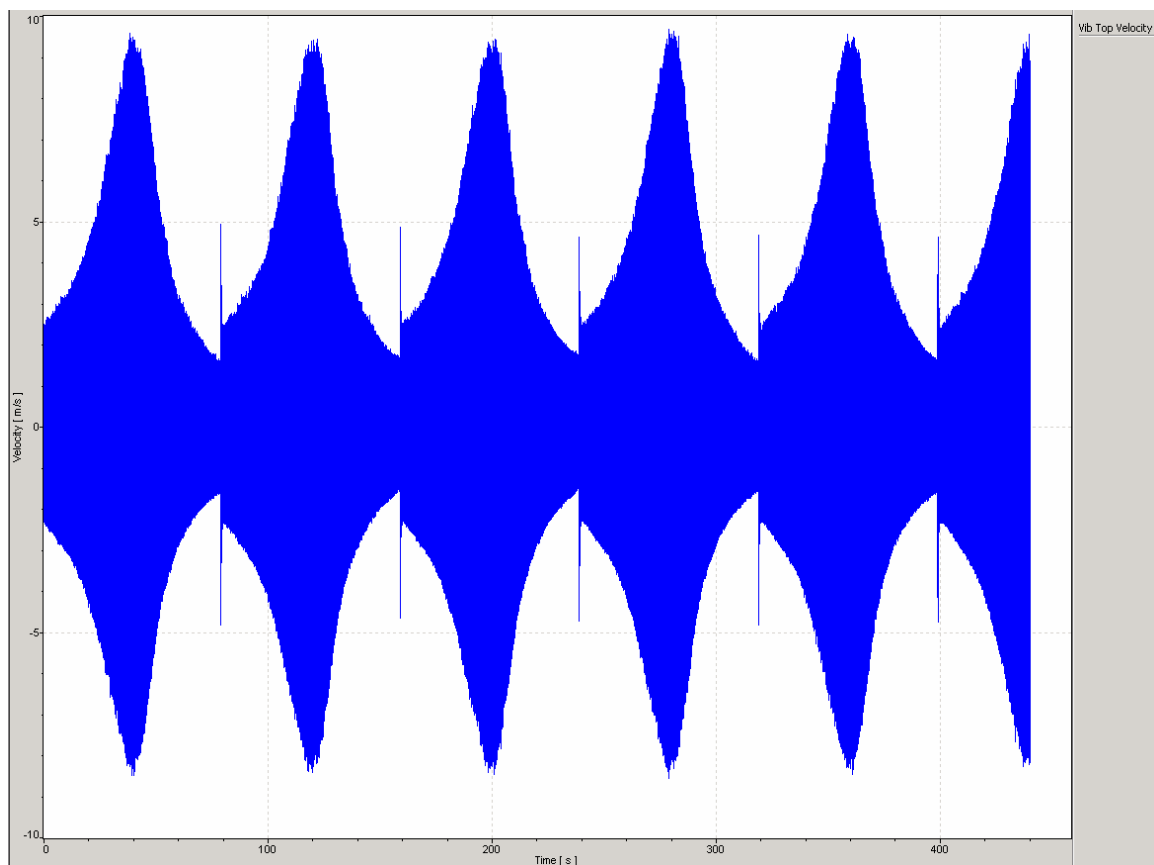


**Figure 45: Vibration Velocity Approaching 10 m/s Limit**

Anytime an overrange occurred, tests at the amplitude causing the overrange were no longer valid. The difficulty was that this overrange error was presenting itself at very



small velocities according to the real-time acquisition display in the PSV program. So in an attempt to downsize the beam to something more relatable to a MAV, and due to this overrange error, the four ply IM7/5250-4 carbon-fiber-epoxy beam discussed in earlier sections was put through these same sequences of tests.

### **3.4.2 IM7/5250-4 Carbon-Epoxy Beam - Asymmetric Shaker Configuration**

It was shown previously that the frequency of the 1<sup>st</sup> bending mode for a 6” IM7/5250-4 beam would be approximately 30 Hz. To again provide an experimental comparison with the analytical result, an FFT scan was again attempted. For this set of testing, a grid of scan points was created over the surface of the beam. The aluminum beam test results were primarily from a line of grid points placed through the center of the beam. Creating a grid for this carbon-epoxy beam was an attempt to generate better graphic images of the eigenvector results. Figure 46 shows the grid setup for this set of testing.

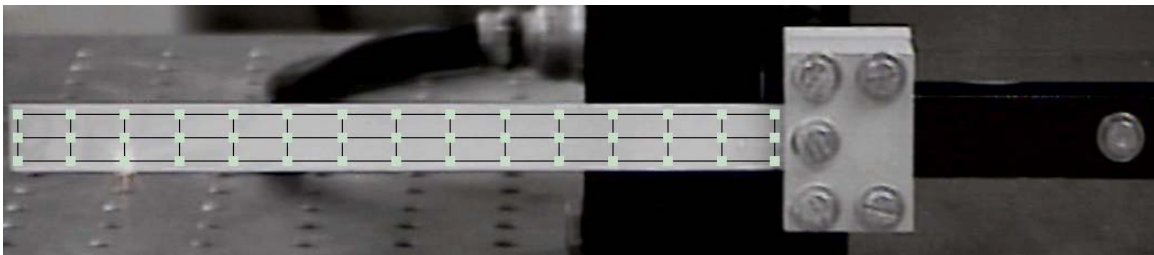


**Figure 46: 3-D Asymmetric Carbon-Epoxy Beam Configuration – 20 Hz FastScan Mode Shape**

Again the shaker forcing inputs were kept to small amplitudes. Similar to with the aluminum beam, the reason for this lower amplitude testing was to provide a comparison of the linear 1<sup>st</sup> bending mode natural frequency of this beam to the linear analytical results. If higher amplitudes would have been used, the resonant frequency may change due to damping or material nonlinearity. The first test again was a FFT scan with a sine

sweep ranging from 1 Hz to 100 Hz. In Figure 47 the velocity spectrum results in a first mode at approximately 31 Hz.

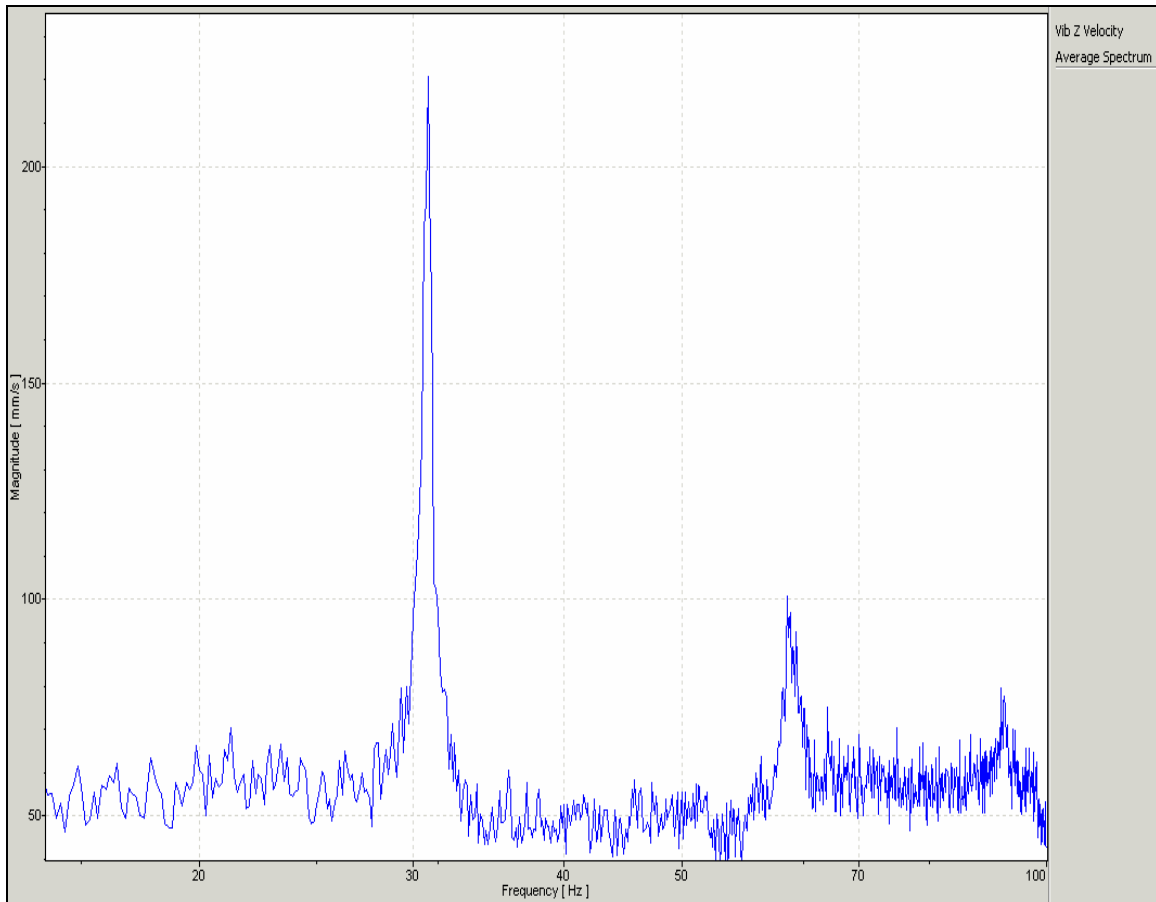


**Figure 47: 3-D Asymmetric Carbon-Epoxy Beam Configuration – Frequency Spectrum**

A FastScan was completed for this beam at 31 Hz. The conclusions of the FastScan provide the eigenvectors for this 31 Hz mode and are shown in Figure 48. Notice the shape that the beam takes when represented by the eigenvectors of this mode does not resemble very closely what one would expect from a true first bending mode of a beam, as seen in Figure 1. The grid generated over the surface of the beam provides a 3-D result that indicates an undesirable torque or twisting effect occurring at resonance. Keep in mind that these tests were completed at low amplitudes; the precision of the vibrometer was able to easily capture this torque motion.

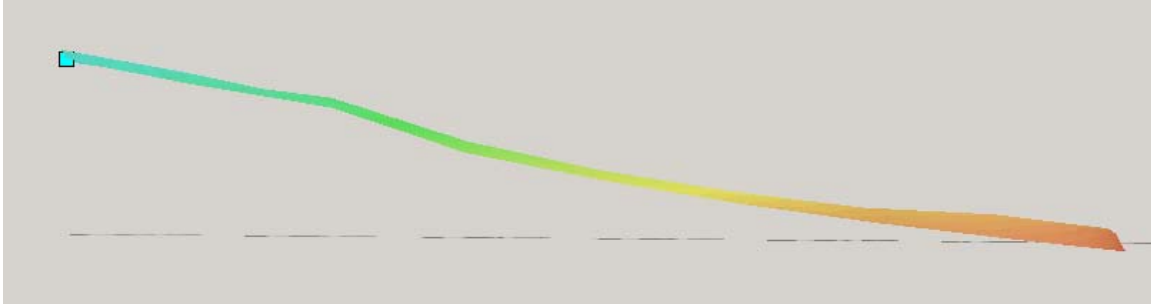


**Figure 48: 3-D Asymmetric Carbon-Epoxy Beam Configuration – 31 Hz FastScan Eigenvectors**

When the amplitude was increased, again the velocity overrange issue began occurring for scan points close to the tip of the beam. Now two issues have been pointed out as a result of these preliminary experiments using the three dimensional laser vibrometer configuration tests of a single beam.

- The 3-D laser vibrometer tests experience overrange warnings when tip deflection is increased to experience large movement
- Twisting has been shown by 2-D grid laser vibrometry of the carbon-fiber beam

By both visual inspection from the high speed camera testing, which are shown later, and also the Figure 48 mode shape showing a twisted beam, some changes to the testing are necessary. It was determined from these inspections that an out-of-plane motion was being generated from an asymmetric placement of a single beam off one end of the shaker armature. This out-of-plane movement is enough to invalidate the experimental results for comparison with analytical methods. As a result of this find, a symmetric orientation was established through the fabrication of another beam and clamp which are to attach to the opposite side of the shaker armature.

The second issue was the overrange errors occurring during the 3-D laser testing. While conducting the 3-D experiments at gradually increasing beam deflections,

something interesting was realized. The left and right lasers would actually miss the beam completely due to the amount of deflection. This problematic effect is shown by Figure 49.

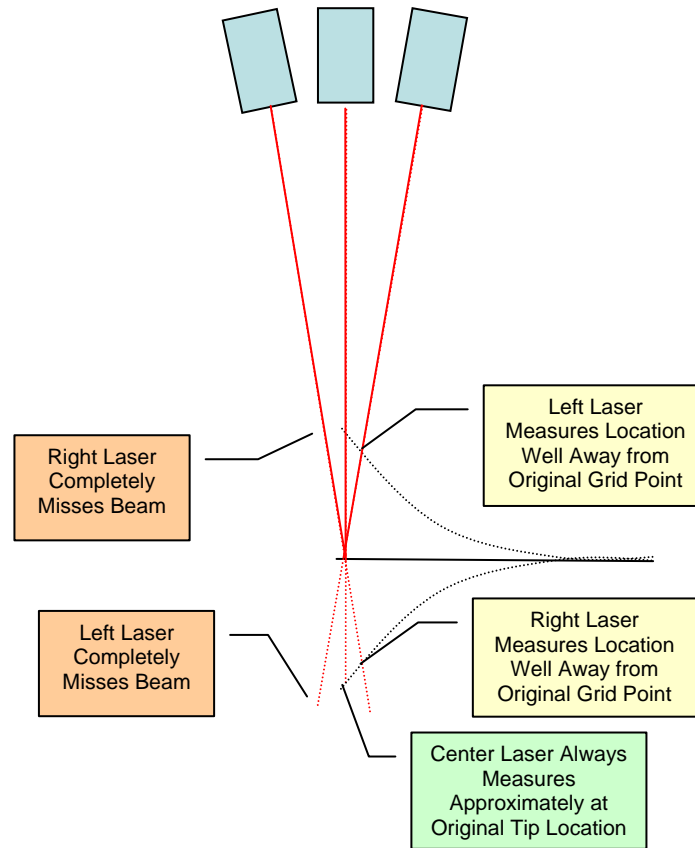


**Figure 49: 3-D Laser Vibrometer Issues with Large Deflecting Beam**

The laser beam must maintain a position close to or at the original grid point location on the beam. When the left scanning head misses the beam entirely while the right scanning head records measurements at a position significantly closer to the root of the beam from its original grid point, the data from the tests will be invalid, causing an overrange error. If the data is invalid, further attempts to document non-linear vibrations would be futile. Since the Polytec scanning laser vibrometer heads can not be placed any closer together than the position from their original position in these tests, the only options that remain

are to use only the center scanning head in a one dimensional configuration or longer range testing. The choice selected in this research was to continue using only a single scanning head.

### **3.5 One Dimensional Laser Vibrometer Experimentation**

For this specific beam setup, the three dimensional configuration was proven to be incapable of accurately capturing the vibration of a beam undergoing large deflections. The remainder of the vibrometry conducted in this project was in a one dimensional configuration. Both beams were again examined, first in the single beam asymmetric orientation, and then using both beams in a symmetric orientation. An accelerometer affixed to the clamp was added to these tests. This accelerometer provides the exact input amplitude in  $g$  ( $m/s^2$ ) for each test for comparison with theoretical results or future testing inside a vacuum chamber. One other very significant use of the accelerometer took place in Section 3.5.4. To remove the rigid body motion occurring at the clamp, the clamp-affixed accelerometer signal was input into the PSV Junction Box, to be used as the reference input for generation of the transfer functions. This allows for reliable and accurate transfer functions and eventual displacement frequency spectrums. The transfer function and displacement frequency spectrum plots of Section 3.5.4 may be compared with analytical methods or other experiments such as vacuum testing.

### 3.5.1 Aluminum Beam - Asymmetric Shaker Configuration

Examining the aluminum beam was the starting point for these 1-D experiments. A 3x15 grid was created to capture the averaged movement of the entire surface of the beam.

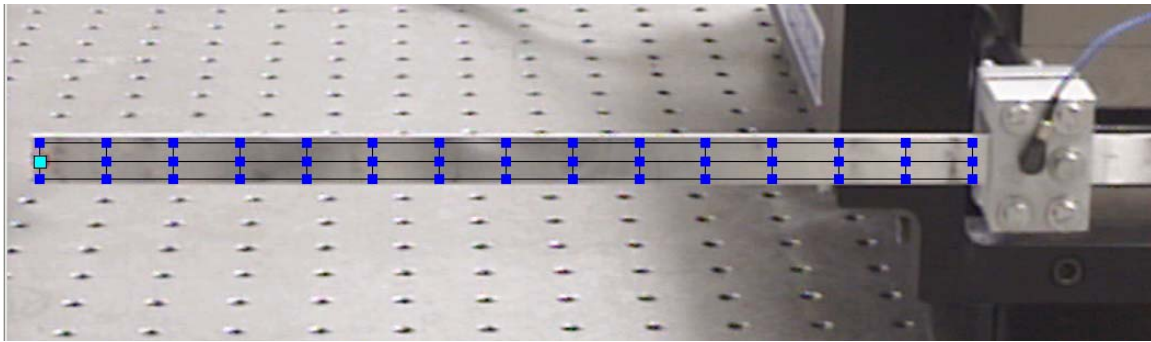


**Figure 50: 1-D Asymmetric Aluminum Beam Configuration – Vibrometer Scan Grid**

An FFT sweep was initially performed to capture the eigenvalues and eigenvectors of the beam over a range of 0-100 Hz. As was mentioned in the experimental methods section, one has many options when choosing the acquisition settings for a test using the PSV 8.4 software. To provide a closer look at the choices selected for the 1-D FFT sweep of the single aluminum beam, Figures 51-55 are included.

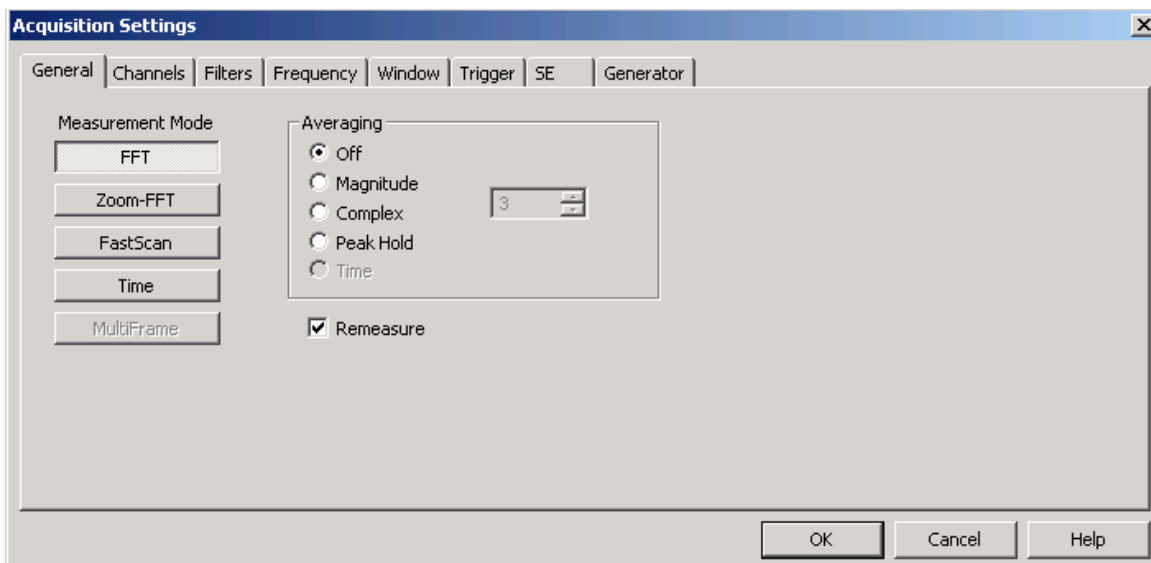


**Figure 51: 1-D Asymmetric Aluminum Beam Configuration – Acquisition General Settings**

Since the first mode natural frequencies for the previous small amplitude testing of the three dimensional configuration agreed with the computational finite element analysis and Matlab results, it was decided that the initial FFT scan would not use any averaging. This was a timesaving decision made during this preliminary testing.

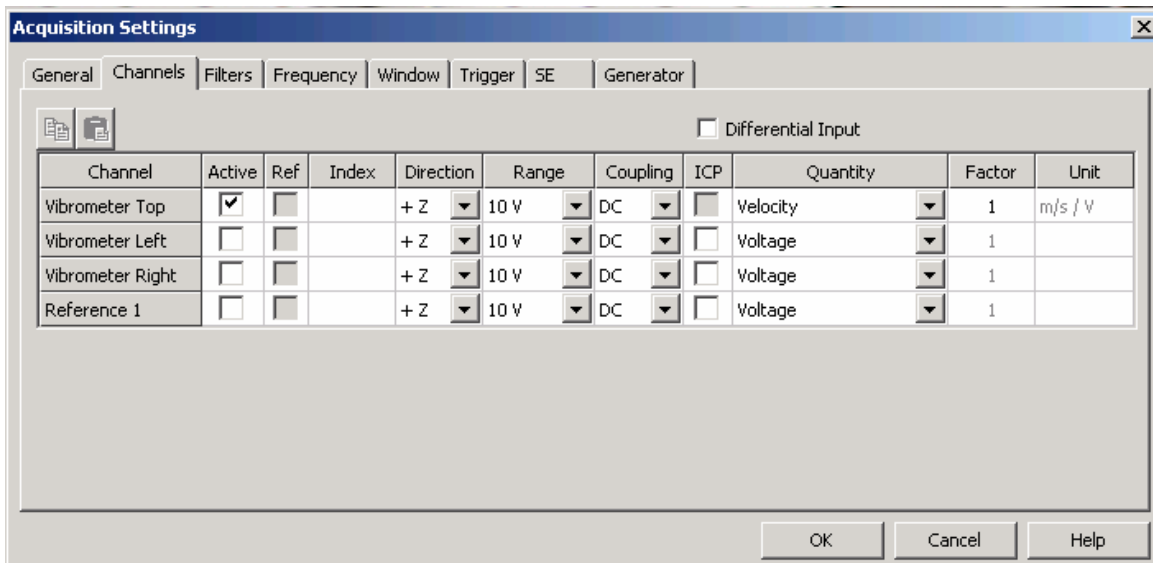


**Figure 52: 1-D Asymmetric Aluminum Beam Configuration – Acquisition Channel Settings**

Only the Top Vibrometer channel was initially selected for the first FFT sweep and is shown in Figure 52. However, this lesson was learned during testing, and at that time the Reference 1 channel was also turned on to allow for calculation of a frequency response function.

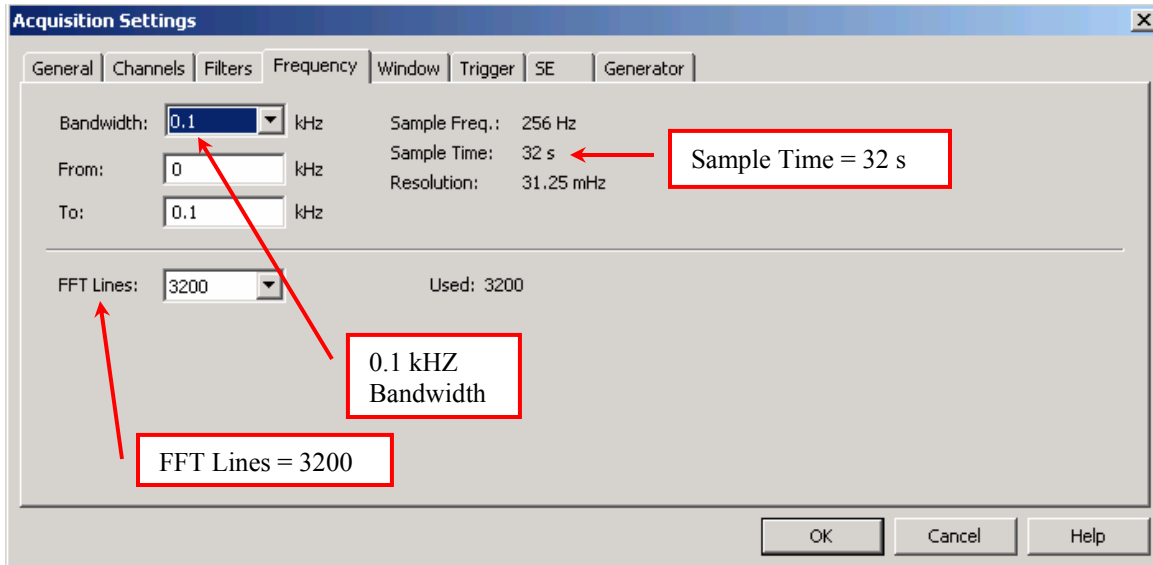


**Figure 53: 1-D Asymmetric Aluminum Beam Configuration – Acquisition Frequency Settings**

A bandwidth of 100 Hz was selected with the initial frequency of the bandwidth set to 0 Hz. The sample time of the test, shown in Figure 53, is equal to the number of FFT lines divided by the bandwidth. This sample time is the time it takes for each grid point to be tested, assuming no overlap.

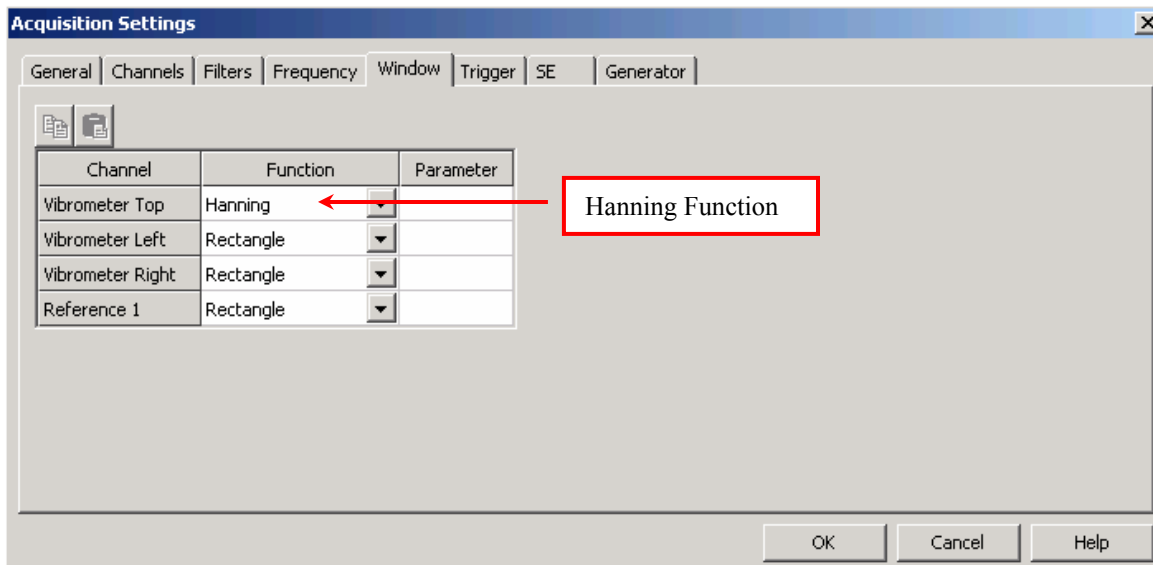


**Figure 54: 1-D Asymmetric Aluminum Beam Configuration – Acquisition Window Settings**



There are several choices for windowing function. The Hanning function, shown in Figure 54, was selected for this experiment; however, for all remaining experiments the windowing was left at the default Rectangle function.

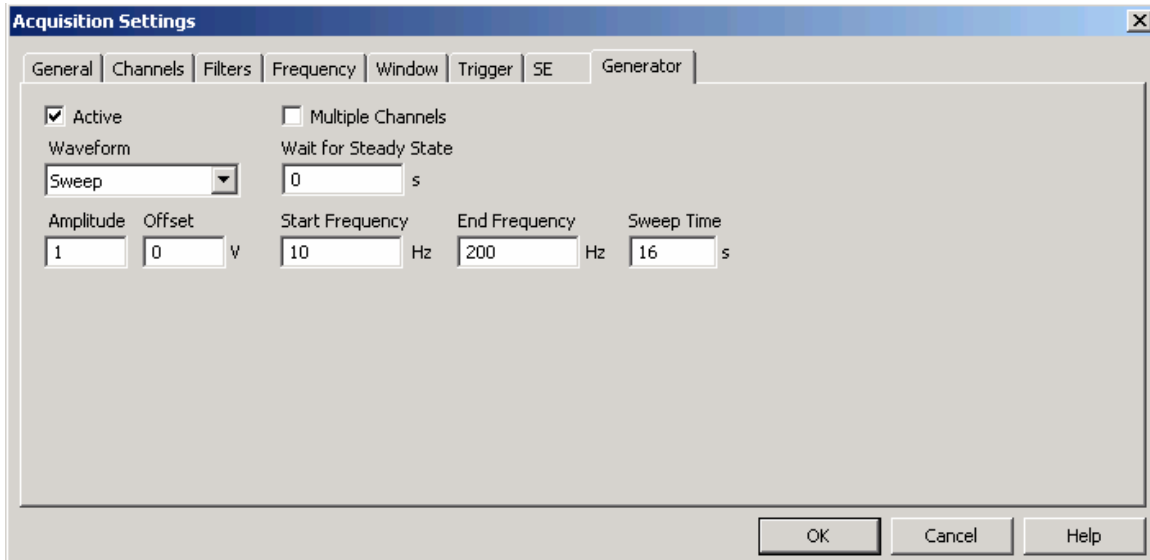


**Figure 55: 1-D Asymmetric Aluminum Beam Configuration – Acquisition Generator Settings**

Similar to the 1-D experiments, again a sweep waveform (seen in Figure 55) was used for this FFT test. The amplitude was set to 1V output from the PSV Junction Box; however an analog dial on the power amplifier had the ability to magnify this voltage as necessary. This analog dial introduced the chance that an input setting would be incorrectly documented. So while the acquisition settings may be set to 1V in multiple tests, very different input accelerations could really exist. Therefore in the Section 3.5.4 nonlinear vibration investigations, the accelerometer and oscilloscope were used to document the accurate peak-to-peak acceleration input. The sweep time in this test is simply the time it takes to get from the start frequency of 10 Hz to the end frequency of 200 Hz. The magnitude plot of a 1-D FFT sweep for the single aluminum beam configuration is included as Figure 56. The amplitude of input acceleration for this initial FFT was small.

As it was explained previously, a low amplitude and therefore small beam tip deflection is required if one is to compare the natural frequency results with those found using computational methods based in linear vibration theory. Figure 56 was generated using three complex averages, resulting in a smoother spectrum plot than was seen in Figures 42, 43, and 47.

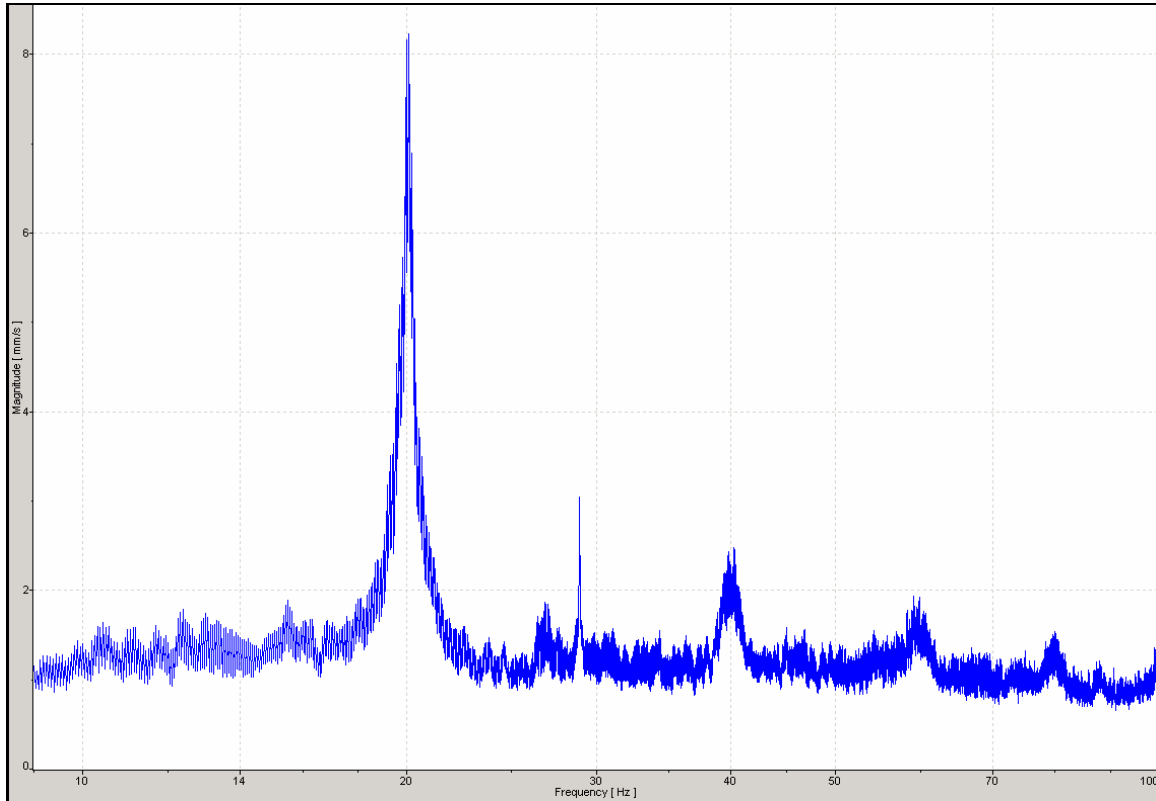


**Figure 56: 1-D Asymmetric Aluminum Beam Configuration – Frequency Spectrum**

Using the contour plot option in the PSV 8.4 presentation mode, the mode shape for this beam has been generated and is shown in Figure 57. From the root boundary condition up to mid-length, the mode shape for this asymmetric aluminum beam resembles a beam's correct first bending mode shape. From the mid-length location and out to the beam tip, the mode shape does not match what is shown in Figure 1. It has been shown that an asymmetric beam setup on the shaker generates out-of-plane motion. This

configuration along with the previously mentioned beam structural warping are potentially contributing factors to the tip-kinked mode shape result shown in Figure 57.

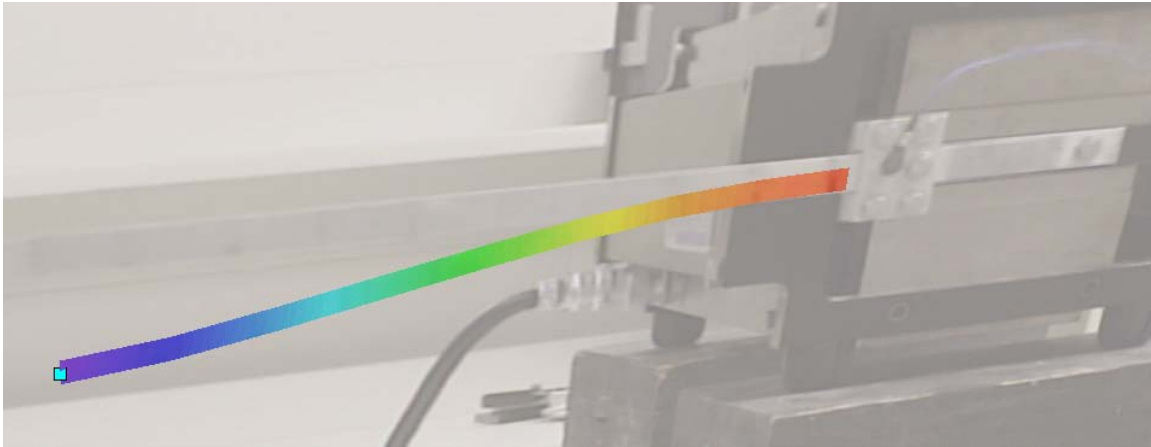


**Figure 57: 1-D Asymmetric Aluminum Beam Configuration – Eigenvector**

### **3.5.2 Aluminum Beam - Symmetric Shaker Configuration**

The final aluminum beam testing will be for the symmetric two beam configuration. Up to this point two major experimental investigations have taken place: the first being the three dimensional laser vibrometer configuration which tested both the asymmetric aluminum and carbon fiber beams; the second being the one dimensional laser vibrometer configuration measuring vibration characteristics for the symmetric aluminum beam. None of these have generated data sufficient and reliable enough to allow for a choice to use these methods further in a non-linear vibration study. The FFT sweep of the symmetric two beam configuration had acquisition settings again very similar to methods previously discussed. Again a grid of scan points was placed over the entire surface of the beam, as shown in Figure 58.

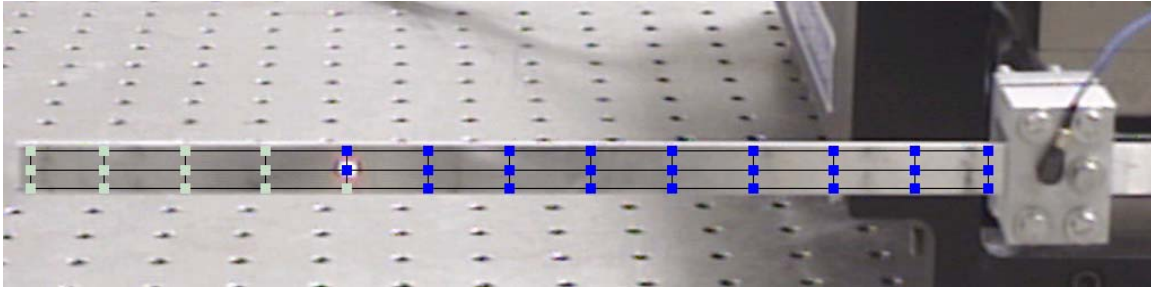


**Figure 58: 1-D Symmetric Aluminum Beam Configuration – Vibrometer Scan Grid**

The acquisition settings for this FFT test were very similar to those previously shown, however the start and end frequencies in the sweep now ranged from 10 Hz to 70 Hz. Figure 59 is included to document this change. Again, a small input causing no visible movement was generated for this initial test.

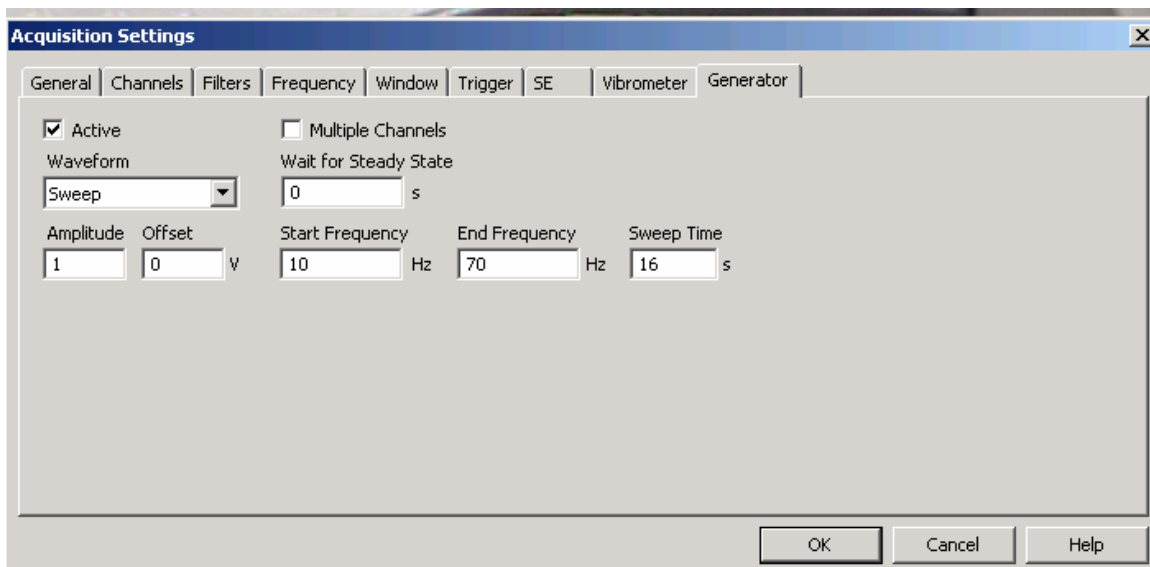


**Figure 59: 1-D Symmetric Aluminum Beam Configuration – Generator Settings**

The resulting displacement frequency spectrum plot from the FFT sweep did not resemble those of any of the previous testing, and is shown in Figure 60. Keep in mind that at this point the frequency spectrum magnitudes have not been calculated in a method to remove rigid body motion, and so while the natural frequencies are still accurate, the resulting amplitude values are incorrect. Section 3.5.4 corrects this issue.

The plot shown in Figure 60 is displacement frequency spectrum while the others have been of velocity frequency spectrum. Figure 60 was the best plot available for the following coupling example, and therefore it is included.

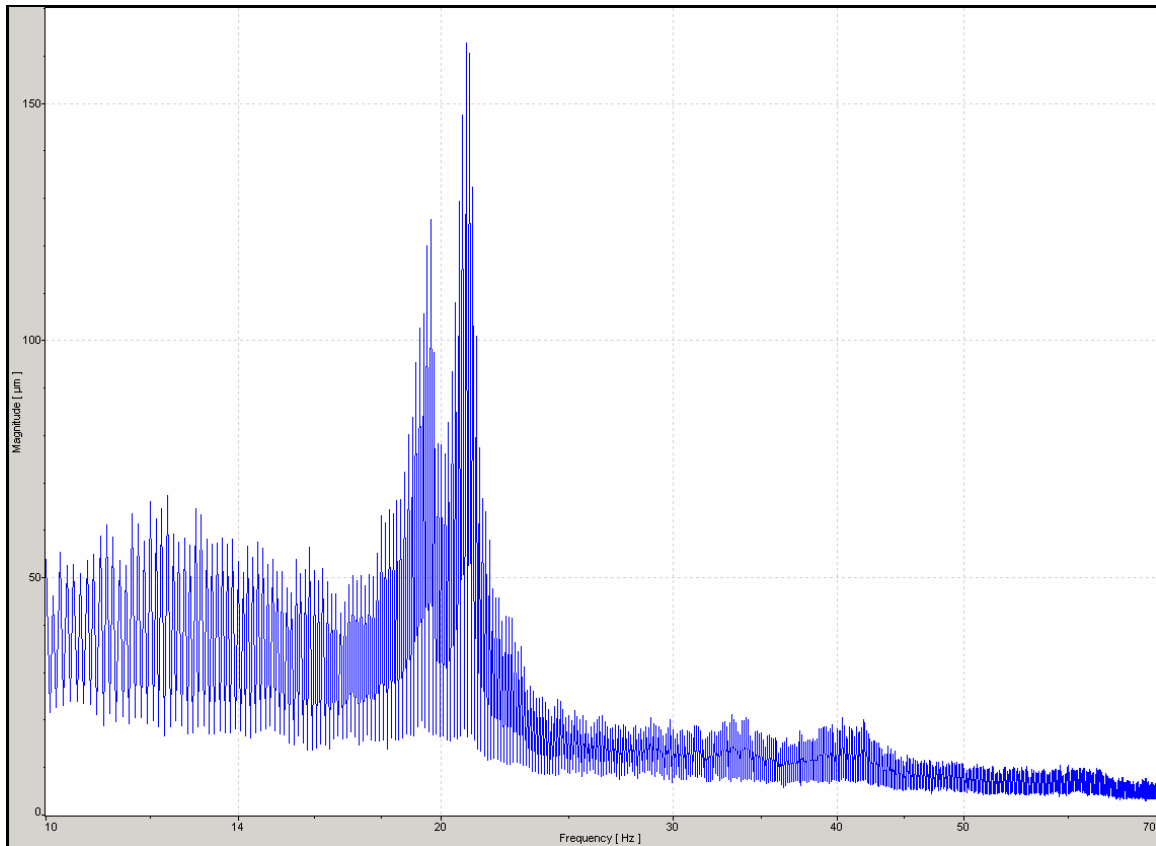


**Figure 60: 1-D Symmetric Aluminum Beam Configuration – Frequency Spectrum**

An unexpected phenomenon of frequency coupling has occurred in this symmetric aluminum beam configuration, causing the single first mode frequency spike to be split into side-by-side spikes. During the frequency sweep, resonance was observed to be at a slightly different frequency for each of the respective “symmetric” beams. This indicates that while the intent was to create a symmetric vibration test free of out-of-plane motion caused by an unbalanced moment on the shaker armature, a new problem was introduced. The two aluminum beams, both with 0.0625” thickness and 10.1” length were not experiencing the same resonant frequency. Upon closer inspection of the beams

and of their clamped boundary condition, it was realized that the beams were not exactly the same. Their small thickness had brought about twisting deformations during either the manufacturing process or in test setup. These defects could have caused a shift in at least one of the beams' natural frequencies, thereby creating the interference and ensuing coupling phenomenon. Figure 61 displays the resulting eigenvector contour created at 20 Hz. As one can see this eigenvector is not one that would be used to accurately portray a beam's first mode shape.

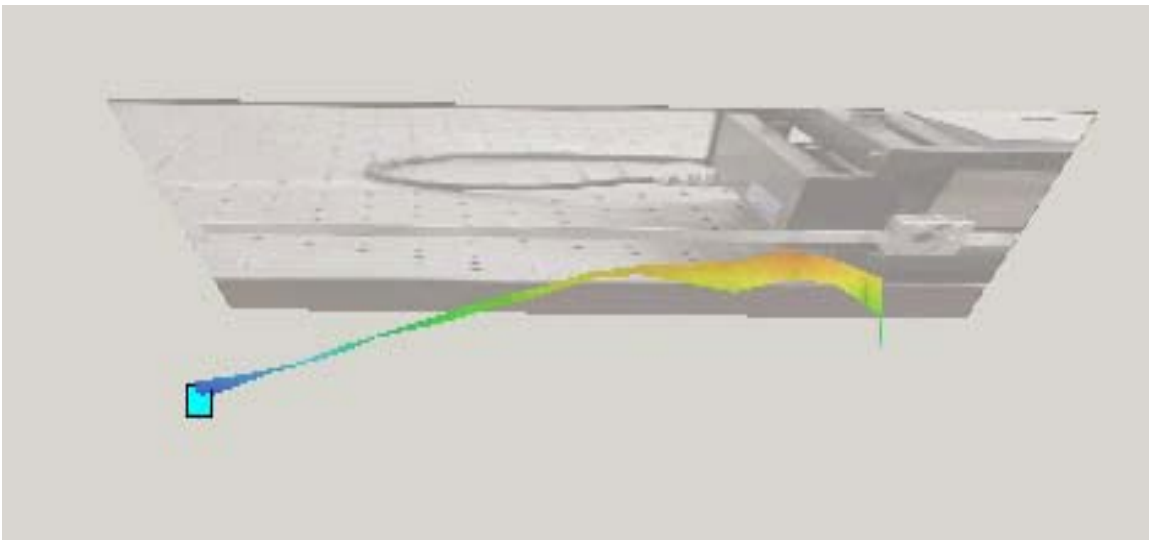


**Figure 61: 1-D Symmetric Aluminum Beam Configuration – Problematic Eigenvector**

As a result of the continued challenges of this work shown by these tests, the next step was to investigate the carbon-fiber beam vibration characteristics using the 1-D PSV setup.

### **3.5.3 IM7/5250-4 Carbon-Epoxy Beam - Asymmetric Shaker Configuration**

A brief experimental study was conducted for the IM7/5250-4 beam using only a single beam clamped to the shaker, in the original asymmetric configuration using the 1-D laser vibrometer. The purpose of this study was to validate the previous findings that

document a torque moment being applied to the beam through the out-of-plane motion of the shaker armature.

After having securely clamped only one beam on the shaker armature as shown in Figure 62, the PSV software was again arranged for a FFT sweep. Average peak-to-peak input amplitude of 0.2g was applied for this experimentation. This acceleration value was determined by sending a signal from the accelerometer shown in Figure 62 to an oscilloscope, where peak-to-peak voltage was read and then converted to g-force. This method for determining input g's will be repeated for the remainder of this experimentation.

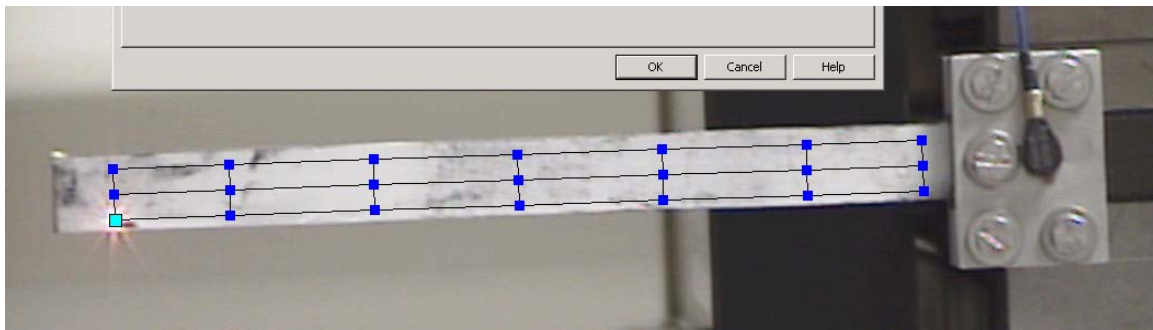


**Figure 62: 1-D Asymmetric Carbon-Epoxy Beam Configuration – Affixed to Shaker**

The resulting FFT sweep shows a 1<sup>st</sup> mode natural frequency occurring at 30.88 Hz, which is approximately the same result as was found in Section 3.4.2. This velocity frequency spectrum is shown in Figure 63.

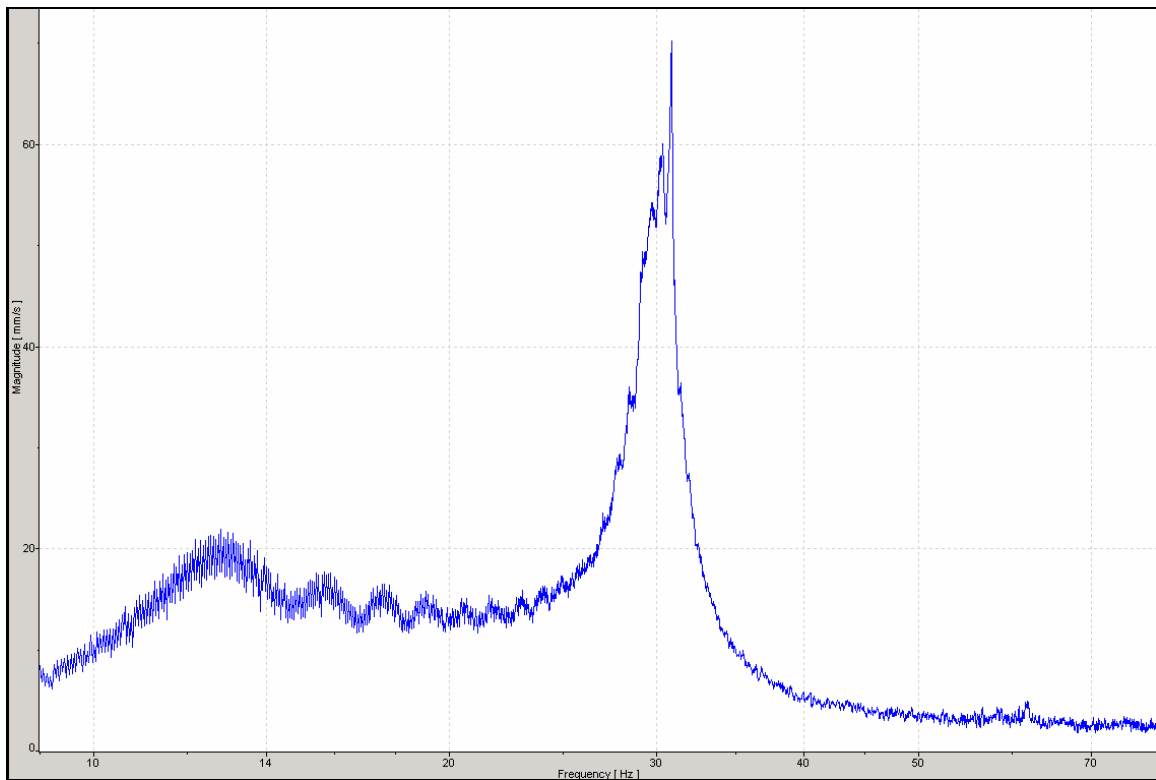


**Figure 63: 1-D Asymmetric Carbon-Epoxy Beam Configuration – Frequency Spectrum**

Once again the mode shape of the asymmetric configuration can be shown to resemble a beam experiencing a torque moment. This evidence combined with that found while testing using the laser vibrometer in a 3-D configuration leads to the next step of conducting a study using the 1-D configured laser vibrometer and a symmetric configured carbon-epoxy beam setup.



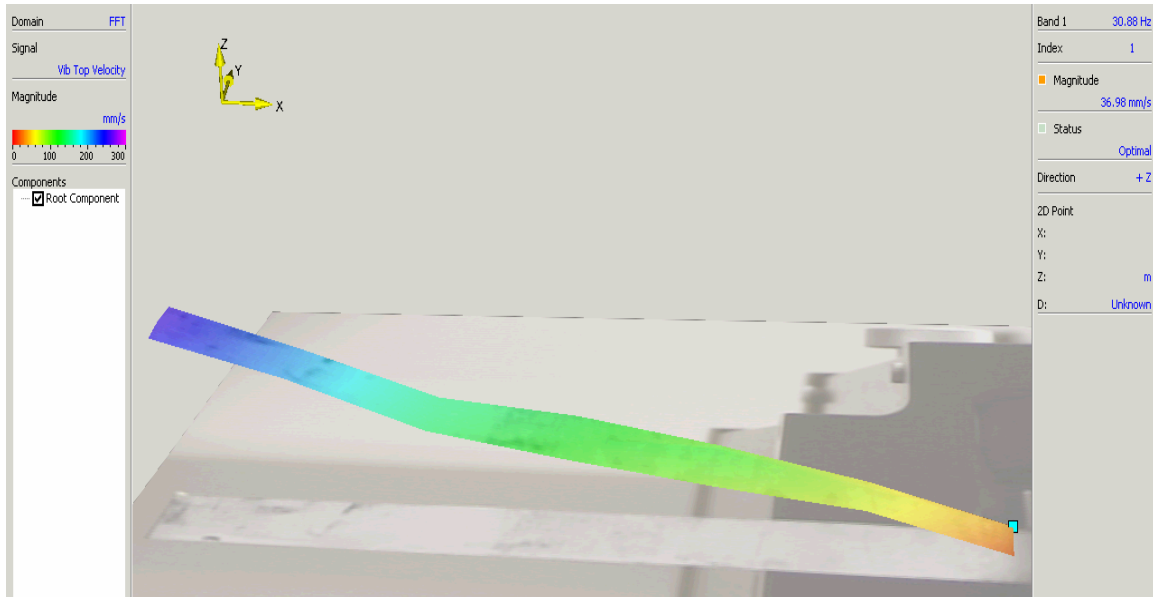


**Figure 64: 1-D Asymmetric Carbon-Epoxy Beam Configuration – Eigenvector Torque**

### **3.5.4 IM7/5250-4 Carbon-Epoxy Beam - Symmetric Shaker Configuration**

The experimental research with the laser vibrometer culminates with the 4-ply carbon-epoxy beam testing using the 1-D configured laser vibrometer while maintaining a symmetric placement about the shaker armature, as seen in Figure 21. Many challenges have been discovered and minimized up to this point, allowing for this section's research to become directed toward the original nonlinear vibration objectives. Numerous trials were conducted for this particular configuration to pinpoint nonlinear trends. The details and results of these efforts will be carried out in this section.

Nonlinearity existing in a structure will typically lead to jumps in the frequency response curves (13). Figure 65 shows an example of softening and hardening nonlinearity shown on frequency response plots (9:61).

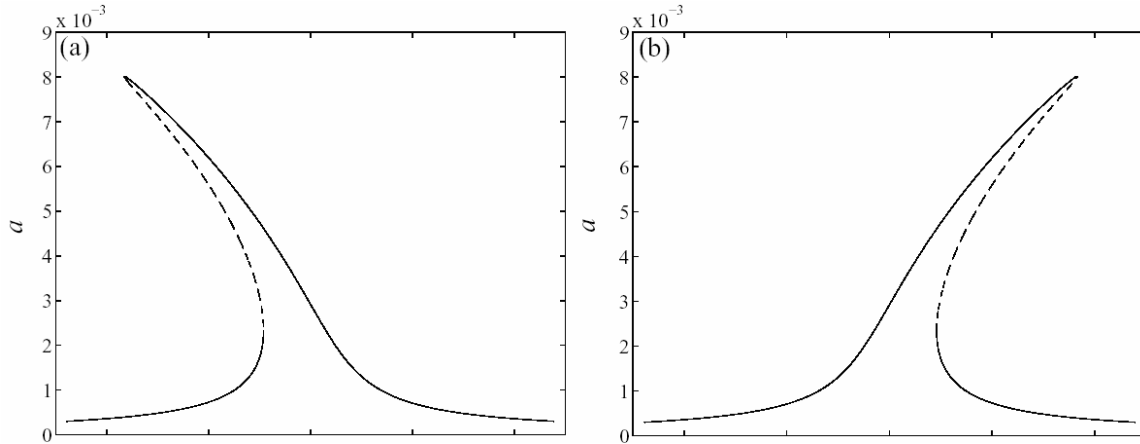


**Figure 65: Respective Softening/Hardening Nonlinearity in Frequency Response (9:61)**

Using the laser vibrometer, this curve can be generated through a series of forward and backward FFT sweeps. The “a” label for the vertical axis of Figure 65 represents response amplitude, which is usually represented by displacement. Each of the Figure 65 curves illustrates the jump frequencies, occurring at the peak of the respective curves. These plots are the result of a theoretical frequency response sweep at constant input amplitude. If the input forcing function is decreased, the curve will have the same general shape but will be scaled to a smaller size. It would fall inside or outside the function shown depending on whether the input is smaller or larger. For the softening example, a decrease in input forcing function would cause the natural frequency to increase at a given displacement. Likewise, for the hardening example, a decrease in input forcing function would cause the natural frequency to decrease at a given displacement. The original intent of this research was to document the softening or hardening nonlinearity as a result of the large flapping motion.

Methods similar to those used in all previous vibrometer testing were employed for the preliminary work of this section. One difference, however, is the use of the

Zoom-FFT feature of the PSV 8.4 software. This keeps the natural frequency of interest centered inside a user defined frequency bandwidth, as discussed further in Appendix D.

One other change was with the reference input used by the PSV 8.4 software. All former research has concentrated on determining the most suitable experimental methods. In these initial trials the input forcing amplitude in g's was documented, but the frequency response functions were not created with a purpose of theoretical comparison. Therefore, the former experiments used the same input reference signal as the output signal from the PSV Junction Box. This section changes the input reference signal to be the actual accelerometer voltage measurement recorded on the clamped boundary condition of the beam structure. This step establishes repeatable frequency response amplitude results.

The input g-force was determined by the value occurring approximately at resonance on the oscilloscope. A preliminary 0.2g input FFT scan was conducted with a grid placed along the surface of the beam. The specific settings established in the PSV software for this initial FFT are shown in Figures 66-69. For this scan, ten complex averages were measured and are shown in Figure 66. This particular test took additional time due to an error in selecting 0% overlap, as seen in Figure 67. Subsequent testing from this point always used 50% overlap. The first two natural frequency modes were captured in this FFT scan which ranged from 0-200 Hz, and are shown in Figure 70. Notice the scatter occurring beyond approximately 40 Hz in Figure 70. This is the result of a limitation with the laser vibrometer velocity decoder range. As was previously mentioned, the higher-valued velocity decoders are most precise when being used in conjunction with vibrations occurring at a corresponding velocity magnitude. Measuring

much smaller velocities, such as those existing beyond the first mode of Figure 70, causes scattered results.

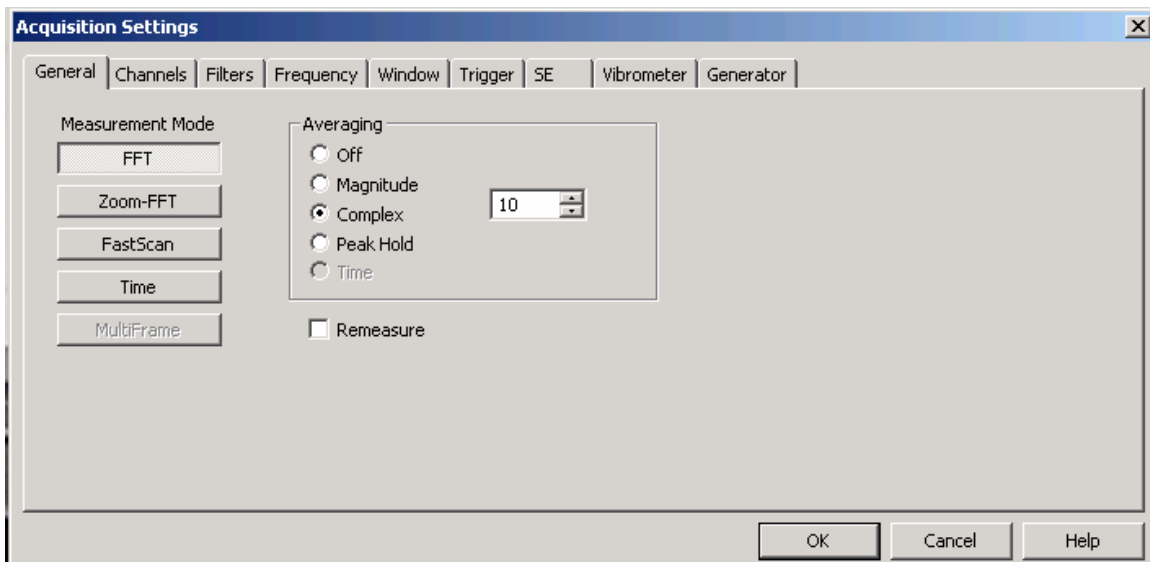


**Figure 66: 1-D Symmetric Carbon-Epoxy Beam FFT Configuration – General Settings**

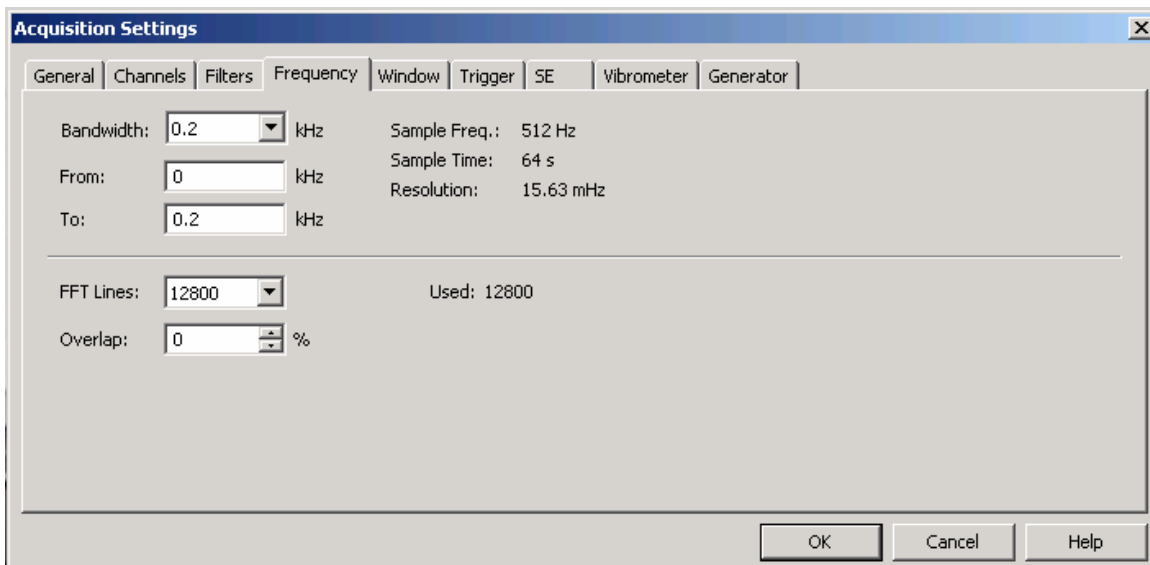


**Figure 67: 1-D Symmetric Carbon-Epoxy Beam FFT Configuration – Frequency Settings**

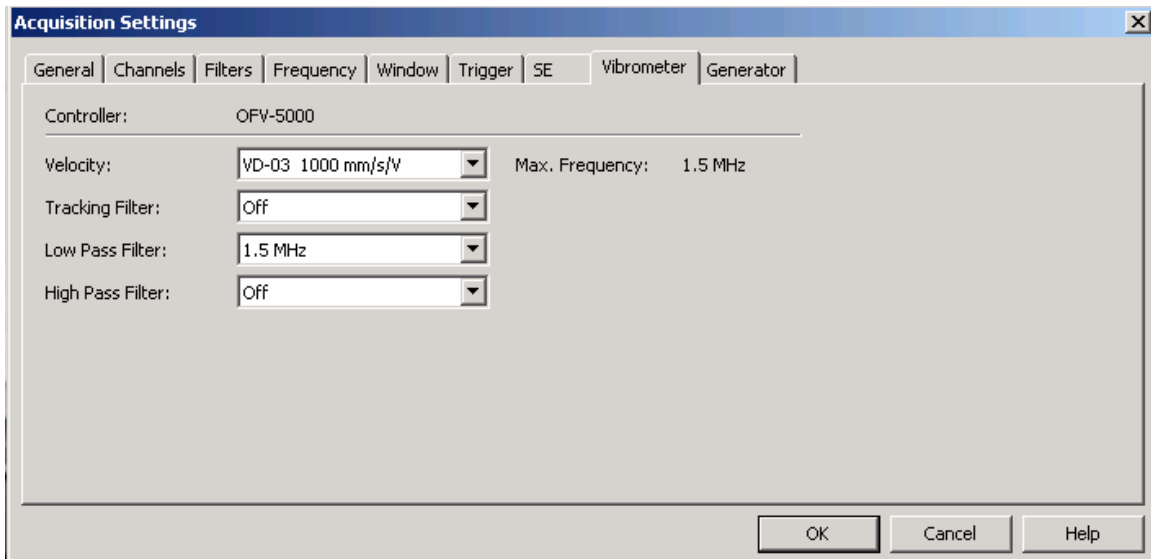


**Figure 68: 1-D Symmetric Carbon-Epoxy Beam FFT Configuration – Vibrometer Settings**

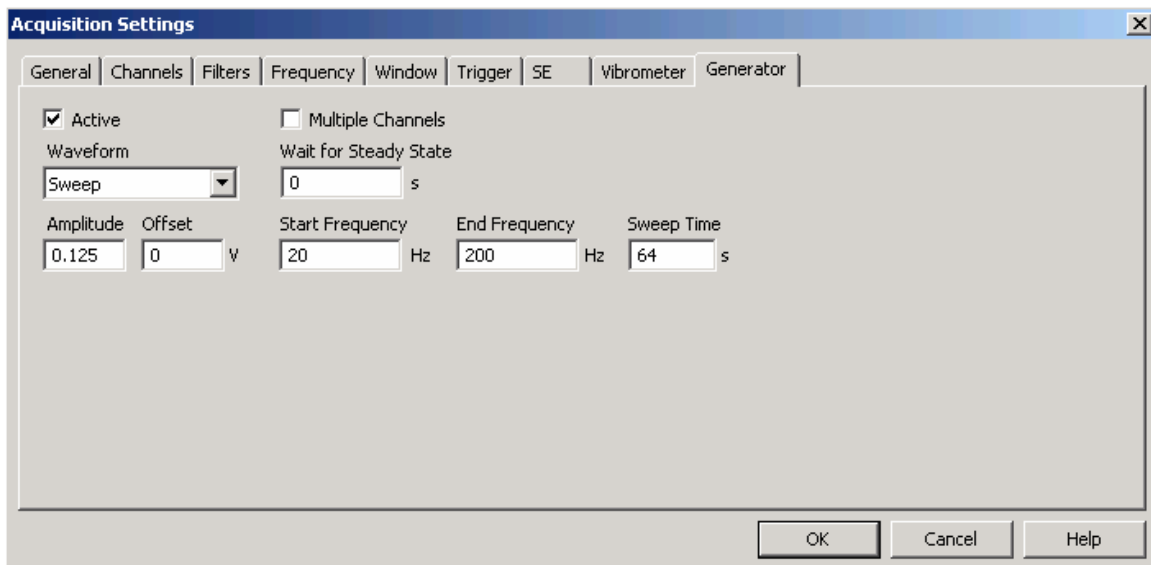


**Figure 69: 1-D Symmetric Carbon-Epoxy Beam FFT Configuration – Generator Settings**

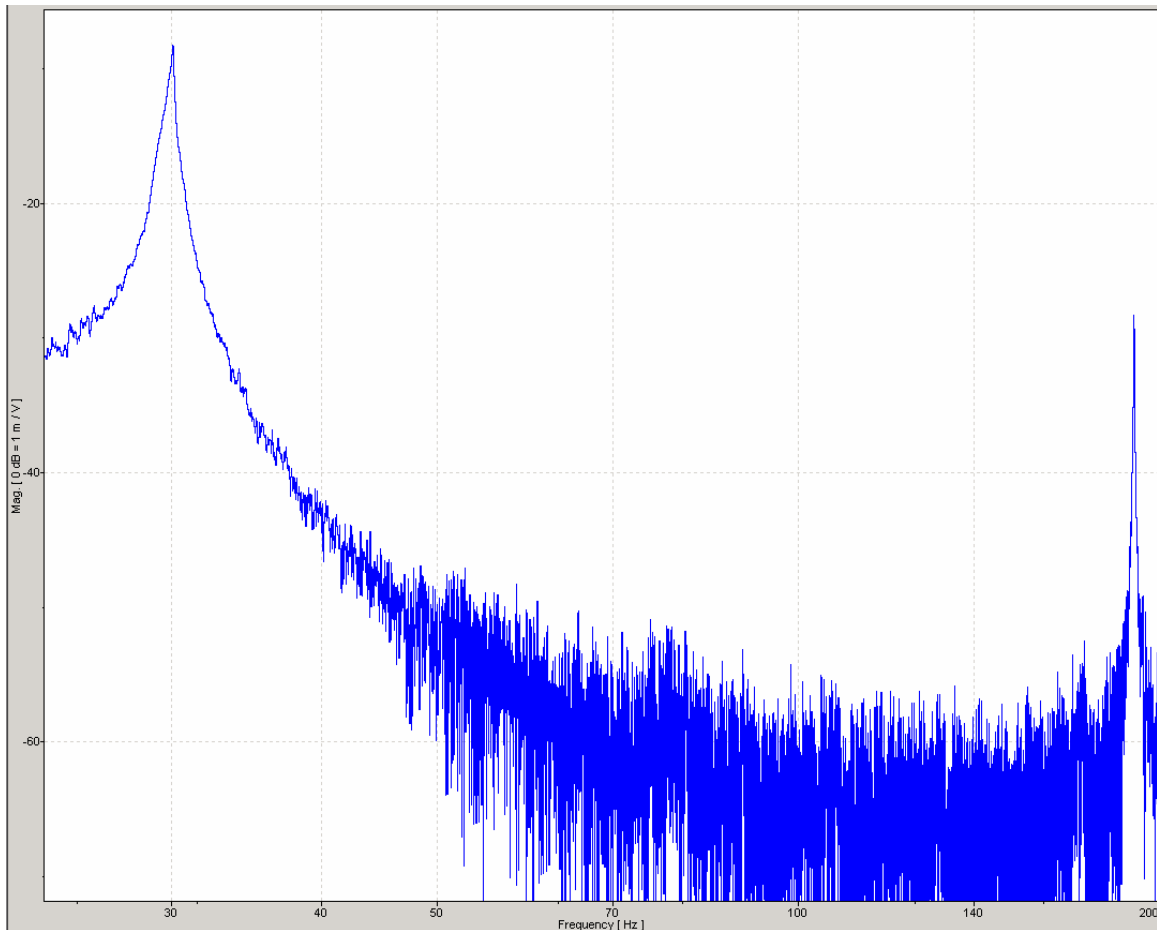


**Figure 70: 1-D Symmetric Carbon-Epoxy Beam Configuration – Frequency Spectrum**

Additionally, this scan resulted in the following representation of the 1<sup>st</sup> natural frequency mode shape occurring at 30 Hz for this IM7/5250-4 beam:

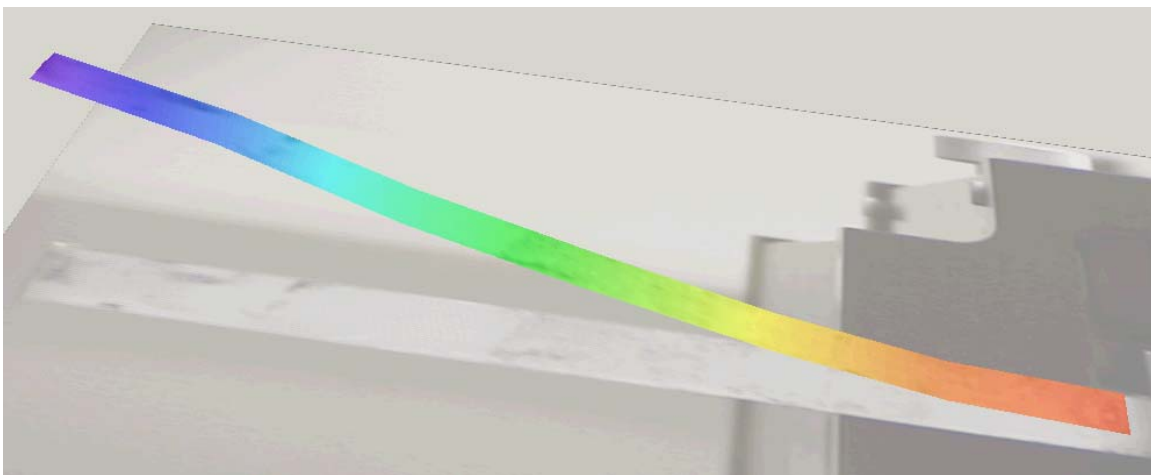


**Figure 71: 1-D Symmetric Carbon-Epoxy Beam Configuration – Eigenvector**

As one can see, torque is no longer being introduced into the eigenvector representation in the beams first mode as we had seen with the asymmetric testing. While the overall shape of Figure 71 may closely resemble that of a theoretical 1<sup>st</sup> mode shape as seen in Figure 1, a slight kink defect occurs near the tip of the beam. Again, this defect is possibly the result of a slight visible deformation in the carbon-epoxy beam.

The next set of experiments was run to document both the displacement magnitudes as well as the displacement transfer functions for this former amplitude range using the 1-D laser vibrometer. Examples of the acquisition settings used within the PSV program are included in Figures 72-77. Due to the variability of displacement introduced by higher amplitude shaking, a complex averaging of ten was established. Figure 75 shows how now the reference channel (the clamp-located accelerometer input) is active. This choice makes reliable transfer function calculations possible, while also removing rigid body motion effects.

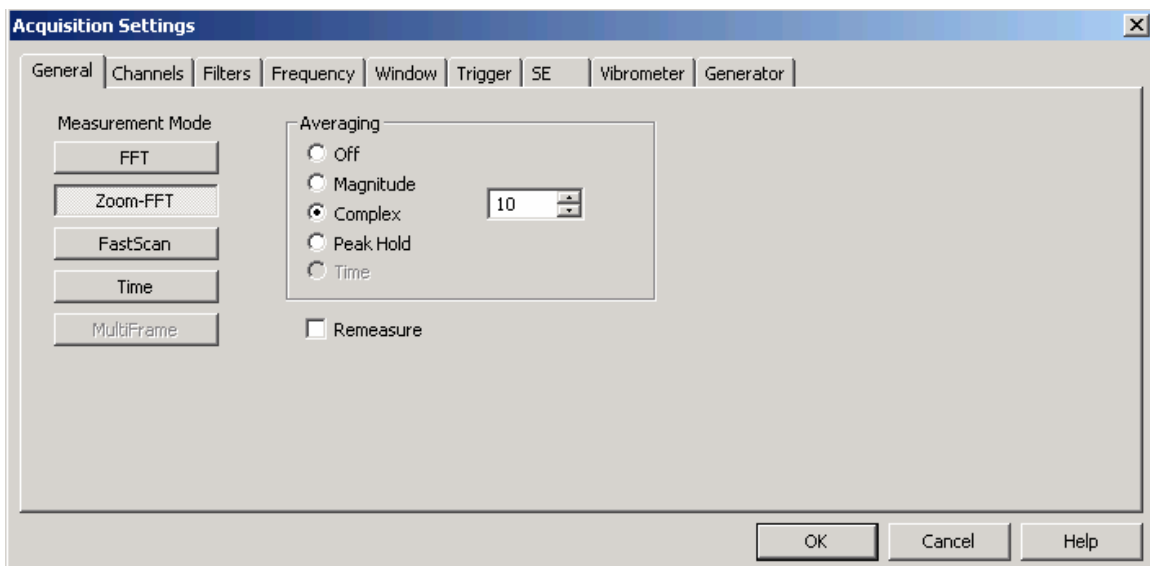


**Figure 72: 1-D Symmetric Carbon-Epoxy 29.5-30.5 Hz Zoom-FFT Config. – General Settings**

**Acquisition Settings**

General Channels Filters Frequency Window Trigger SE Vibrometer Generator

☐ Differential Input

Channel	Active	Ref	Index	Direction	Range	Coupling	ICP	Quantity	Factor	Unit
Vibrometer Top	<input checked="" type="checkbox"/>	<input type="checkbox"/>		+ Z	10 V	DC	<input type="checkbox"/>	Velocity	1000	mm/s / V
Vibrometer Left	<input type="checkbox"/>	<input type="checkbox"/>		+ Z	10 V	DC	<input type="checkbox"/>	Voltage	1	
Vibrometer Right	<input type="checkbox"/>	<input type="checkbox"/>		+ Z	10 V	DC	<input type="checkbox"/>	Voltage	1	
Reference 1	<input checked="" type="checkbox"/>	<input checked="" type="checkbox"/>		+ Z	10 V	DC	<input type="checkbox"/>	Voltage	1	

OK Cancel Help

**Figure 73: 1-D Symmetric Carbon-Epoxy 29.5-30.5 Hz Zoom-FFT Config. – Channel Settings**

**Acquisition Settings**

General Channels Filters Frequency Window Trigger SE Vibrometer Generator

Center Freq.: 0.03 kHz Sample Time: 100 s  
 Bandwidth: 0.001 kHz Resolution: 10 mHz  
 Range: 29.5 Hz - 30.5 Hz

FFT Lines: 101  
 Overlap: 50 %

0.03 kHz Center Freq

OK Cancel Help

**Figure 74: 1-D Symmetric Carbon-Epoxy 29.5-30.5 Hz Zoom-FFT Config. – Frequency Settings**

A Zoom-FFT range of 29.5-30.5 Hz was chosen for this set of tests.



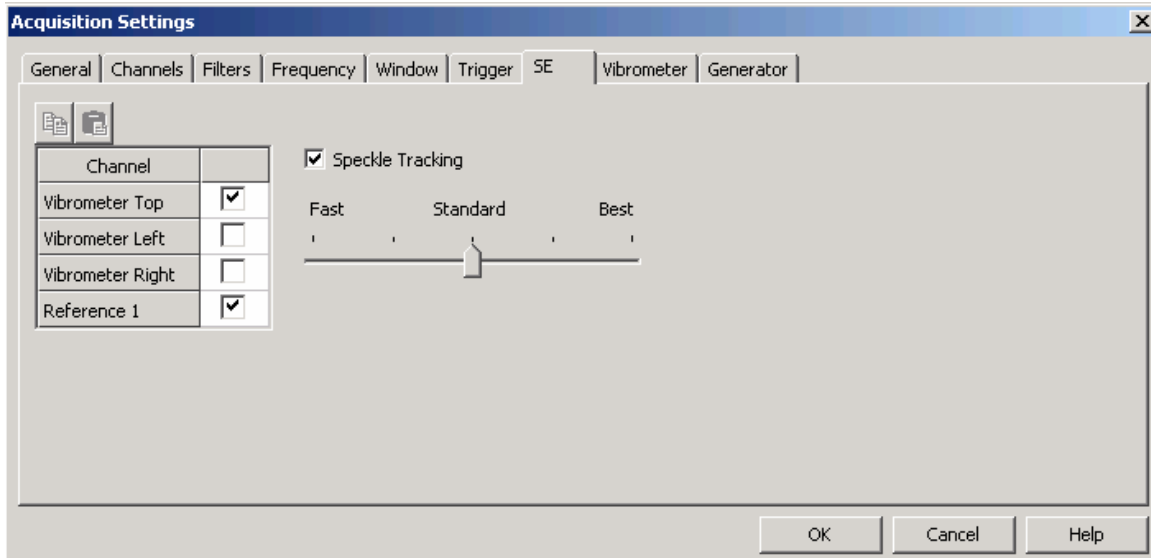


**Figure 75: 1-D Symmetric Carbon-Epoxy 29.5-30.5 Hz Zoom-FFT Config. – SE Settings**

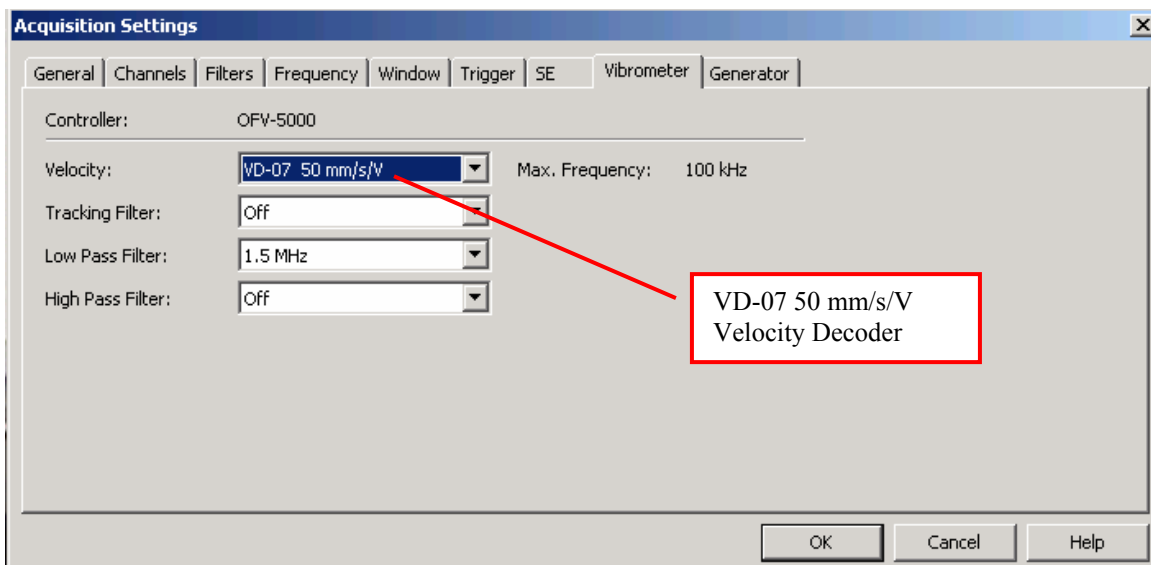


**Figure 76: 1-D Symmetric Carbon-Epoxy 29.5-30.5 Hz Zoom-FFT Config. – Vibrometer Settings**

Figure 76 shows the velocity decoder VD-07 being used. Any velocity decoder chosen was entirely dependent upon the output amplitude recorded by the laser vibrometer. Larger amplitudes require a greater velocity decoder range. The laser vibrometer is best suited for higher frequency vibrations, resulting in relatively small velocity ranges. For those beam vibration tests that approached the 10 m/s capability of the PSV laser vibrometer system, a very high sampling time and up to 20 complex averages was

required to generate accurate results. This fact is associated with the scatter discussion provided earlier regarding Figure 70. For these experiments, the timeframe to measure a single data point approached one hour. Again, the timeframe is directly dependent upon options such as FFT lines, frequency bandwidth, and complex averaging. To generate smooth spectrum and transfer function plots which can be used with confidence, these lengthy tests are a requirement when dealing with large deflections. This information must not be taken lightly in any decision to use this laser vibrometer for the purpose of high velocity tests of entire flapping wing structures while using many grid points.

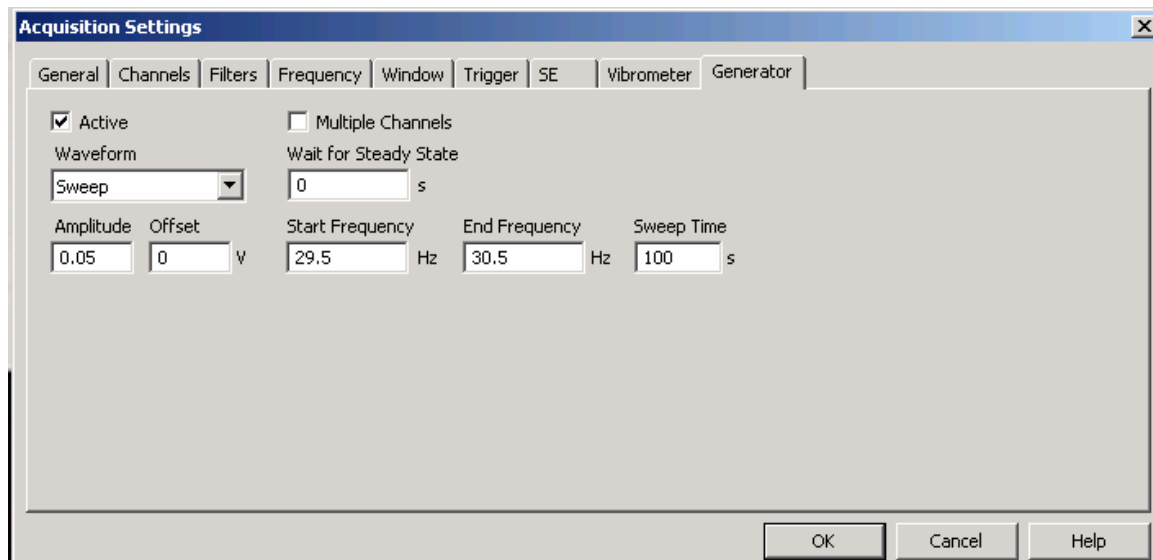


**Figure 77: 1-D Symmetric Carbon-Epoxy 29.5-30.5 Hz Zoom-FFT Config. – Generator Settings**

The 0.1g experiment only required a 100 second sweep time, 10 complex averages and 101 FFT lines. As it was previously mentioned, these requirements increased significantly as the beam velocities approached 10 m/s.

A table of the FRF results was saved from the PSV presentation mode. This table then was input into a Matlab code to create FRF plots and displacement frequency spectrum plots. This code has been provided in Appendix A. The displacement FRF

(with m/V magnitude) for this set of testing is shown by Figure 78. The top curve is the 0.2g test, and it can be seen how the frequency shifts toward the left until reaching the 3g test. Values beyond 3g approach a straight line causing the peaks become indistinguishable. Another feature displayed by the FRF curves is damping. As the input amplitude is increased, damping also is increased, resulting in the gradual straightening of the respective higher amplitude curves.

From the FRF table of values, a displacement frequency spectrum plot has been generated using an additional Matlab code which is also attached in Appendix A. This resulting plot is shown in Figure 79. During this testing, sweeps both of increasing and decreasing frequency were performed. This had no effect upon the resulting FRF magnitudes, and therefore no effect on the displacement frequency spectrums. One can see that a jump frequency effect is not shown by the Figure 78 and 79 curves as they were seen in Figure 65. However, the natural frequency is indeed changing, as indicated by the highlighted peaks, which is indicative of nonlinearity.

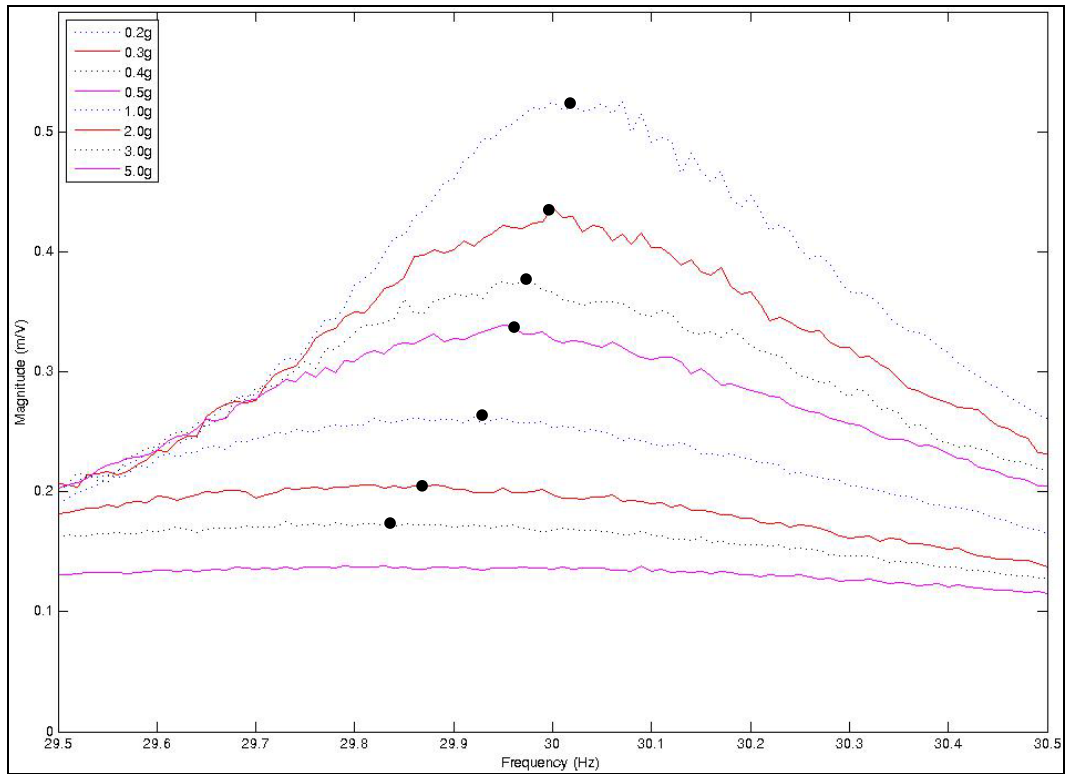


**Figure 78: Displacement Transfer Function of Carbon Epoxy Beam Tip – 1 Hz Bandwidth**

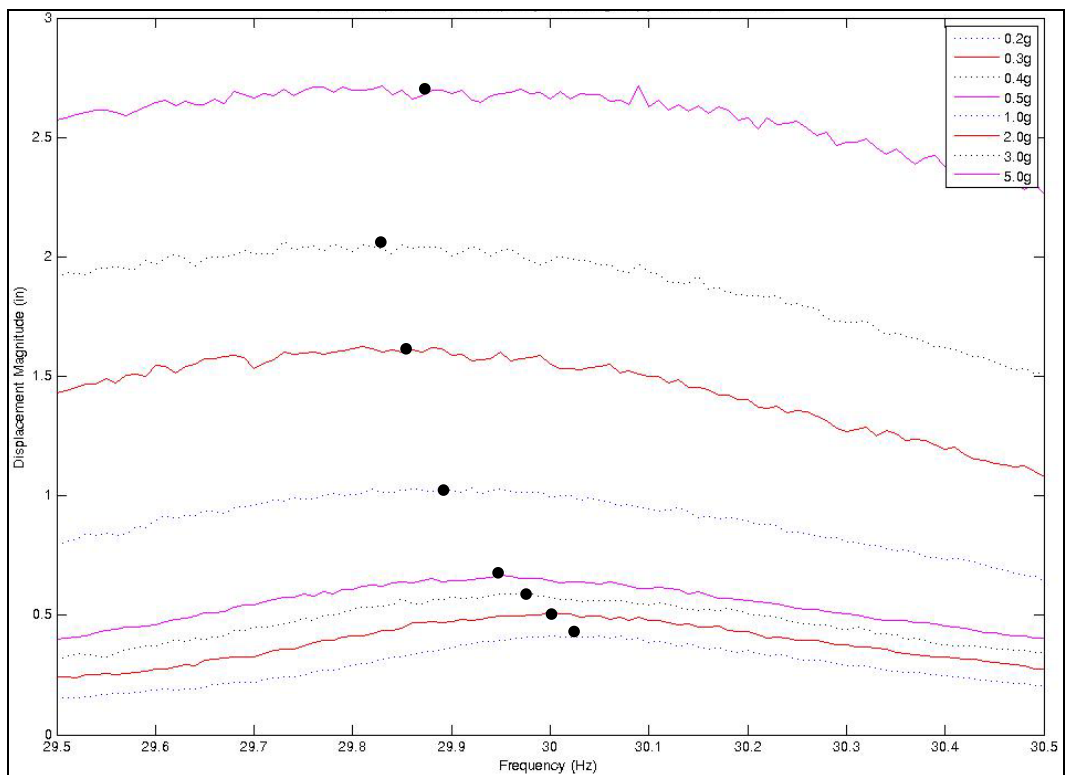


**Figure 79: Displacement Frequency Spectrum of Carbon Epoxy Beam Tip – 1 Hz Bandwidth**

The former experiments show that a 1 Hz bandwidth is not wide enough to accurately display the natural frequency magnitudes for each given test. More tests were then conducted, this time with a 10 Hz bandwidth centered on 30 Hz, to provide a better graphical representation of the frequency spectrum and the associated nonlinear vibration characteristics. These trials begin similar to the most recent set, only incorporating the bandwidth change. This is shown by the acquisition settings included in Figures 80 and 81.

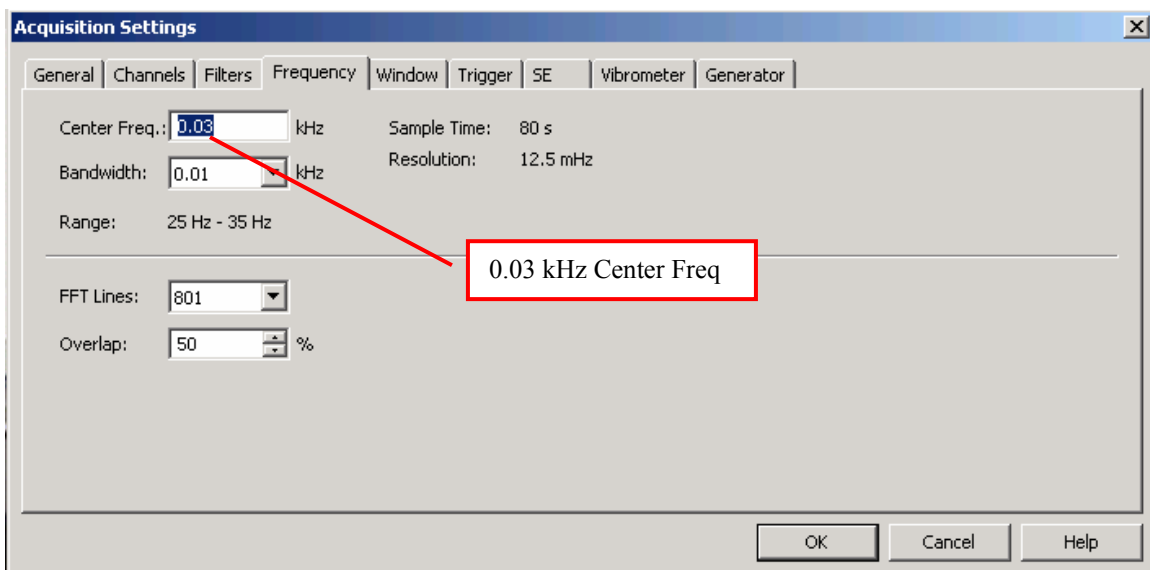


**Figure 80: 1-D Symmetric Carbon-Epoxy Beam 25-35 Hz Zoom-FFT Config. – Frequency Settings**

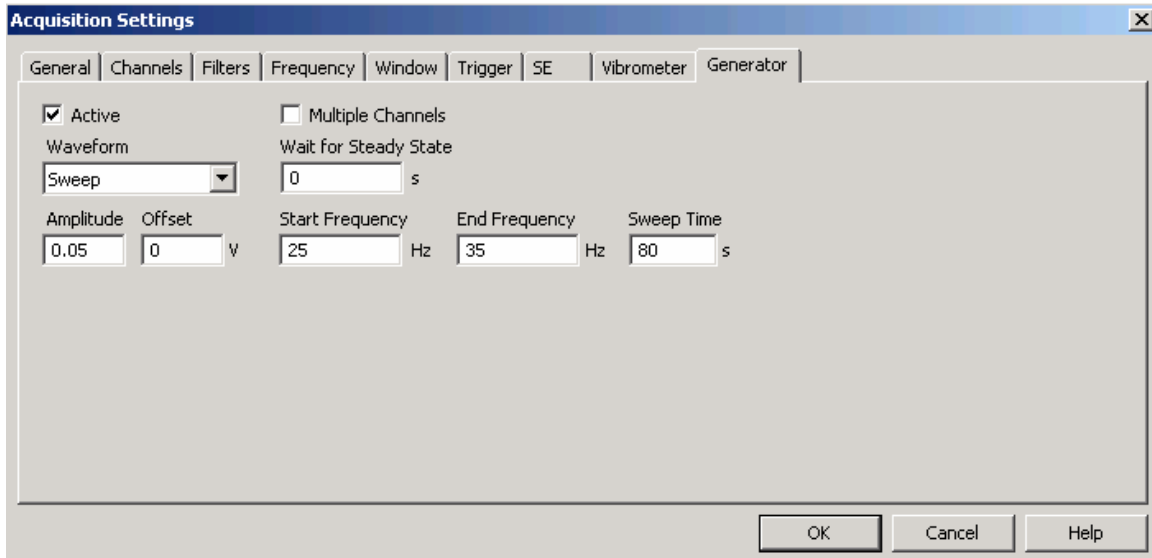


**Figure 81: 1-D Symmetric Carbon-Epoxy Beam 25-35 Hz Zoom-FFT Config. – Generator Settings**

A time domain representation of the velocity magnitude over the course of a set of sweeps for the 9.0g test is shown in Figure 82. Here one can see where the velocity has been maximized to nearly 10 m/s, which is the limit of the Polytec scanning laser vibrometers. This plot was created over the course of the test, and is generated from real-time velocity values.

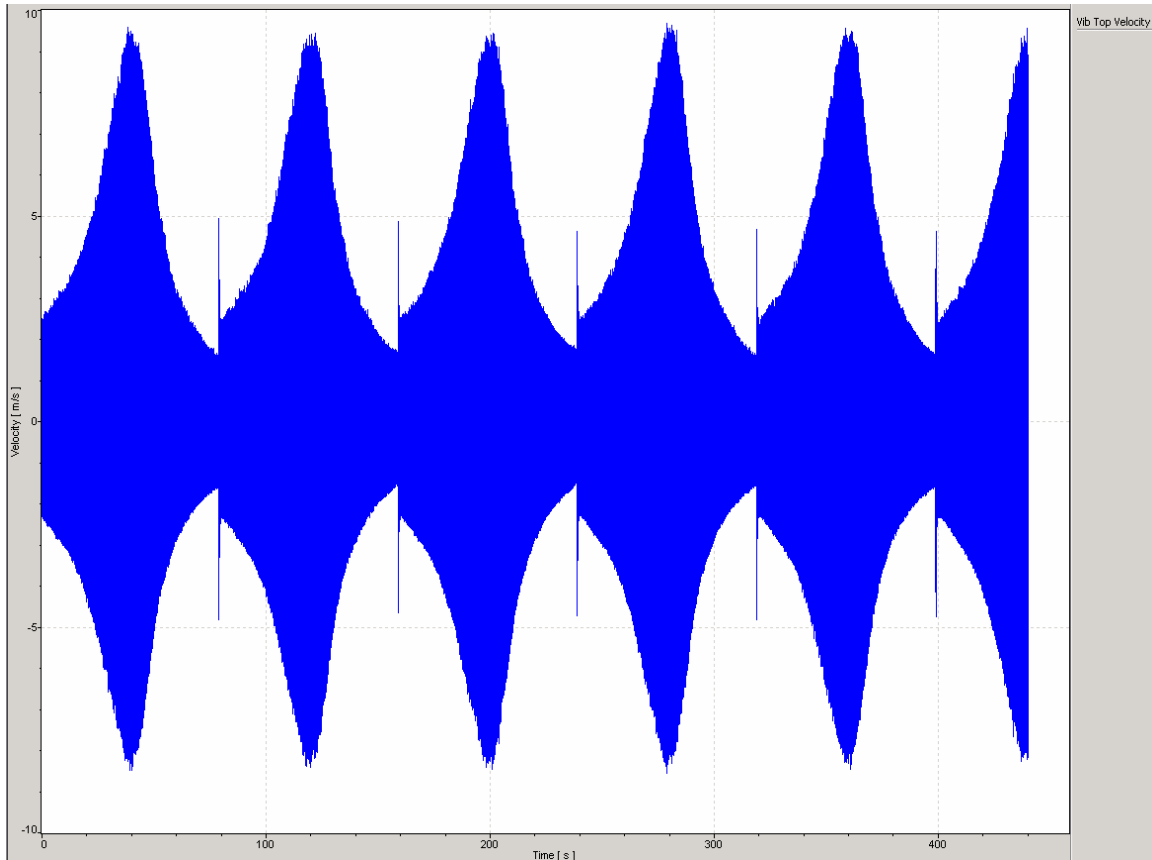


**Figure 82: 1-D Symmetric Carbon-Epoxy Beam – Tip 9.0g Velocity Illustration**

The results of the Zoom-FFT trials for these 10 Hz bandwidth tests were again tabulated and input into the Appendix A Matlab code for post-processing. The resulting FRF and frequency spectrum curves are shown by the next two figures. Notice the scatter in the peaks of the 0.4g, 0.6g, and 1.0g data, called out in Figure 83. This variability is the result of a large gap in the velocity decoders available for testing. The highest velocity decoder can record measurements of up to 10 m/s, as was previously mentioned, but the next highest will only record measurements of up to 1 m/s. It has been found over the course of this testing, that the 0.4g, 0.6g, and 1.0g tests had beam tip velocities that were just outside the range of the 1 m/s decoder, and required the 10 m/s decoder. The ideal solution would be to have more decoders, perhaps one with a 2 m/s limit, 3 m/s limit, and

so on. Since this ideal solution was not available, the use of the 10 m/s decoder for these lower velocities caused a scatter-effect as seen in these respective peaks. Even with this scatter, the trend of decreasing natural frequencies from 0.2-3.0g and increasing natural frequencies from 3.0-9.0g is visible in Figures 83 and 84.

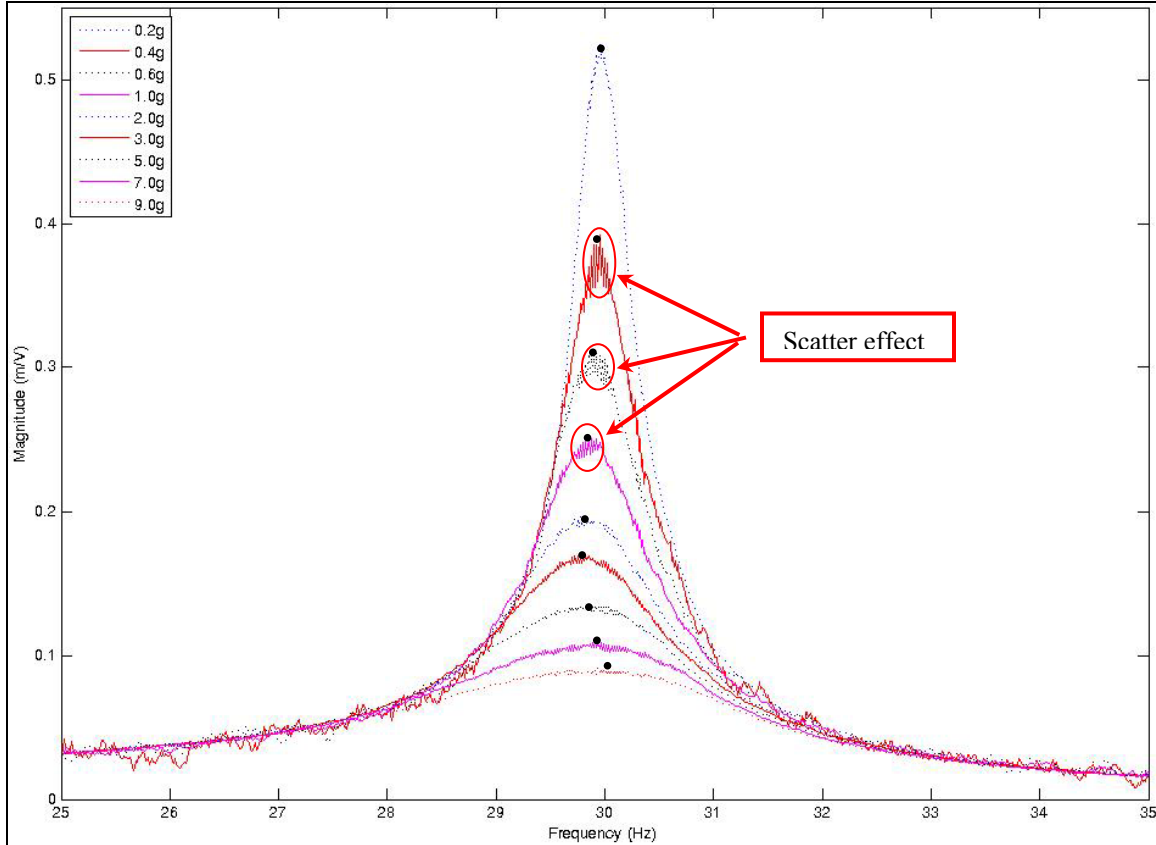


**Figure 83: Displacement Transfer Function of Carbon Epoxy Beam Tip – 10 Hz Bandwidth**



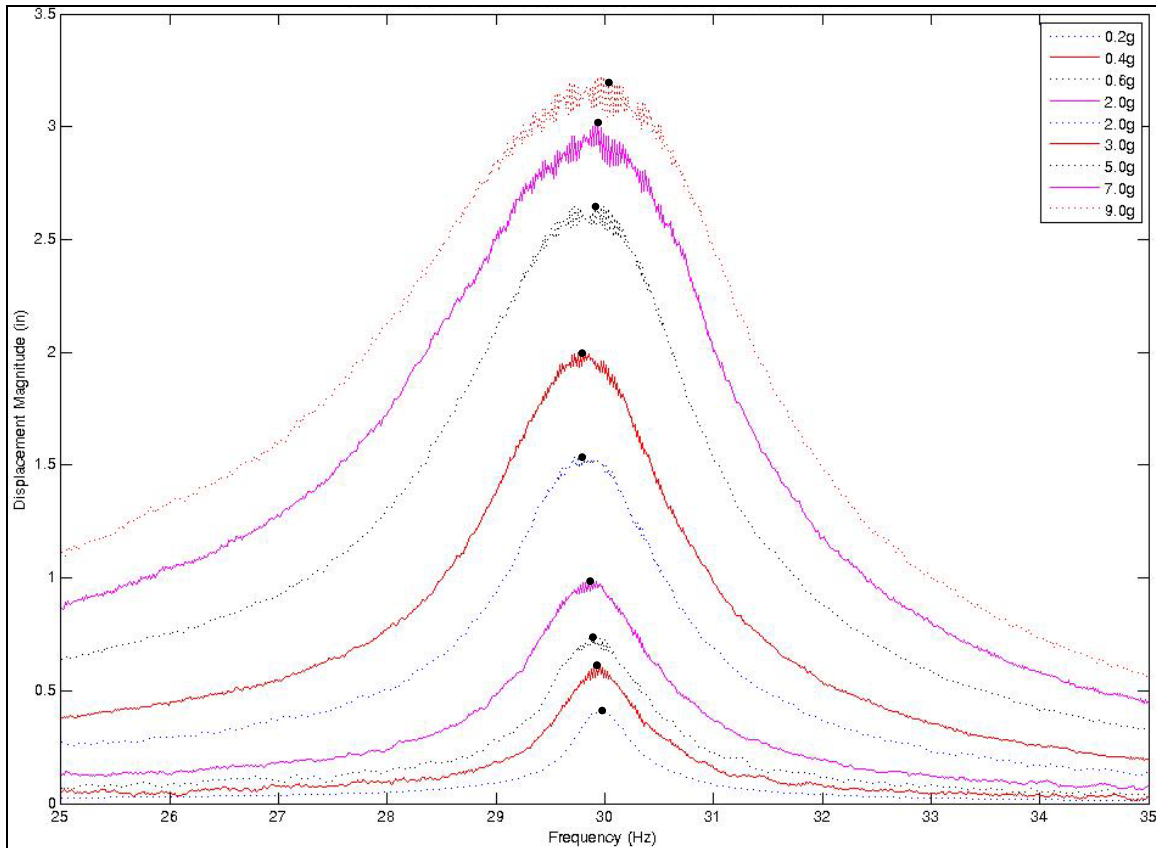


**Figure 84: Displacement Frequency Spectrum of Carbon Epoxy Beam Tip – 10 Hz Bandwidth**

A final collection of experiments has been performed to better document the approximate location of the peak natural frequencies, since it is not easily seen due to the peak scatter-effect. This test again used Zoom-FFT acquisition with a 5 Hz bandwidth centered on 30 Hz. One additional set of testing was included to account for the frequency response of the beam's midpoint, which is for comparison with the tip results. On both accounts, velocity phase plots were created to pinpoint the location of the beam's phase shift, which occurs near the frequency of resonance. Since by now the Zoom-FFT test method has been well demonstrated, no additional acquisition setting figures will be included.

The first experiment again was for the location  $\frac{1}{2}$ " from the beam tip. Phase plots were generated in the PSV 8.4 presentation mode, and the tabulated data making up these

plots was used to create Matlab variables. A Matlab program, which is located in Appendix A, was created to plot the occurrences of phase shift. Figures 85 and 86 provide pinpointed natural frequency locations for each respective test magnitude. Again these figures illustrate the nonlinear frequency decrease, or softening, from 0.2-3.0g's, and a hardening nonlinear trend occurring from 3.0-9.0g's. To be clear that this experiment has generated the same approximate results as shown by the previous beam tip displacement transfer functions and frequency spectrums, these 5 Hz bandwidth test result FRF and frequency spectrum are included as Figures 87 and 88. Each of the phase shift frequencies is labeled on the following figures, creating a better picture of where the actual natural frequency location is occurring.

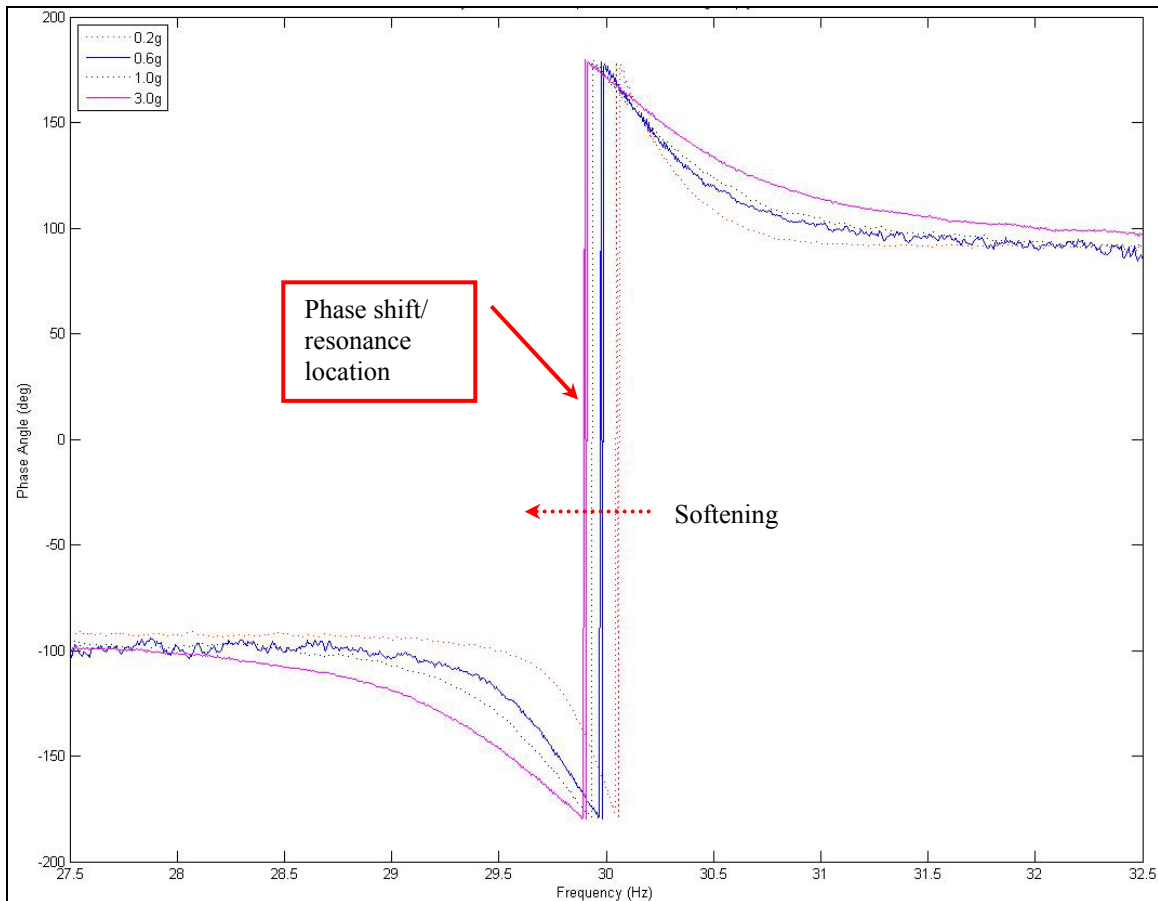


**Figure 85: Velocity Transfer Function Phase Shift - 0.2g-3.0g Tests of Carbon Epoxy Beam Tip**

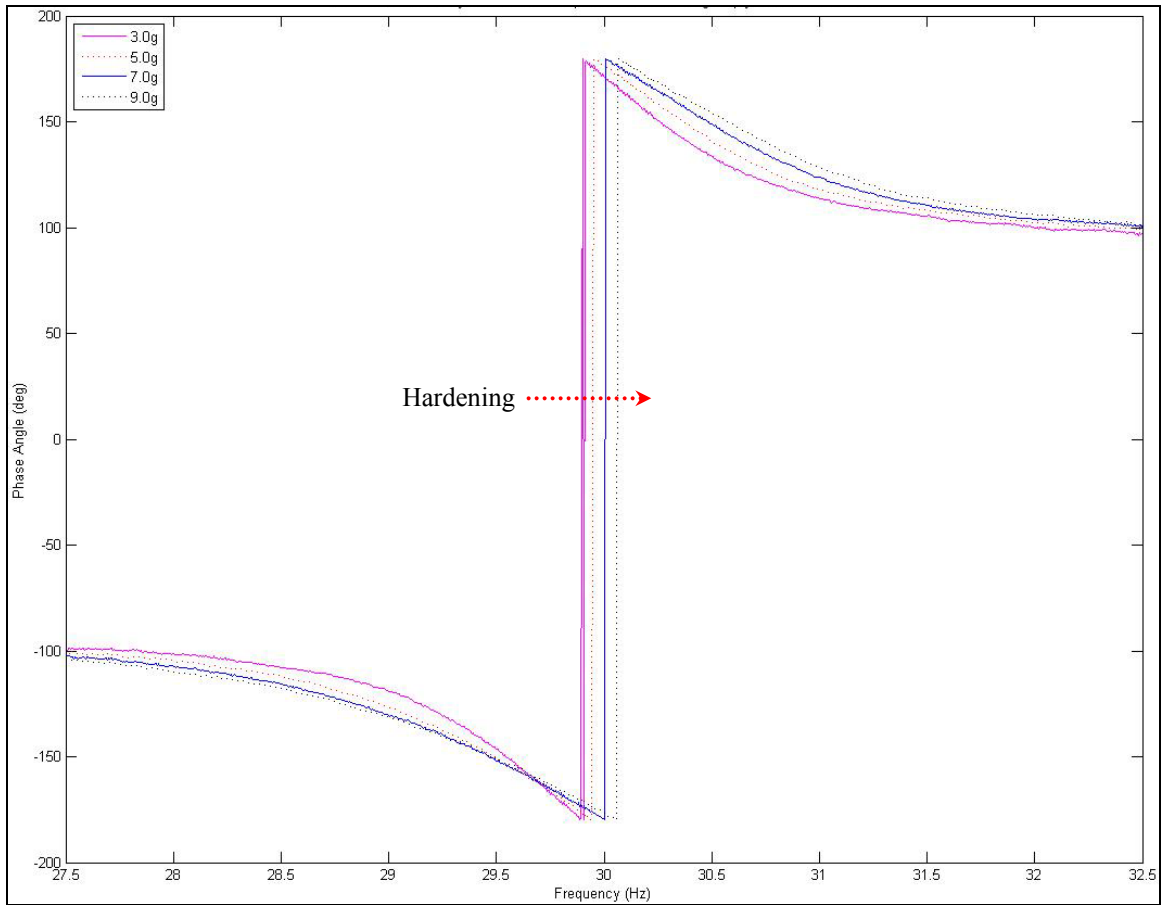


**Figure 86: Velocity Transfer Function Phase Shift - 3.0g-9.0g Tests of Carbon Epoxy Beam Tip**

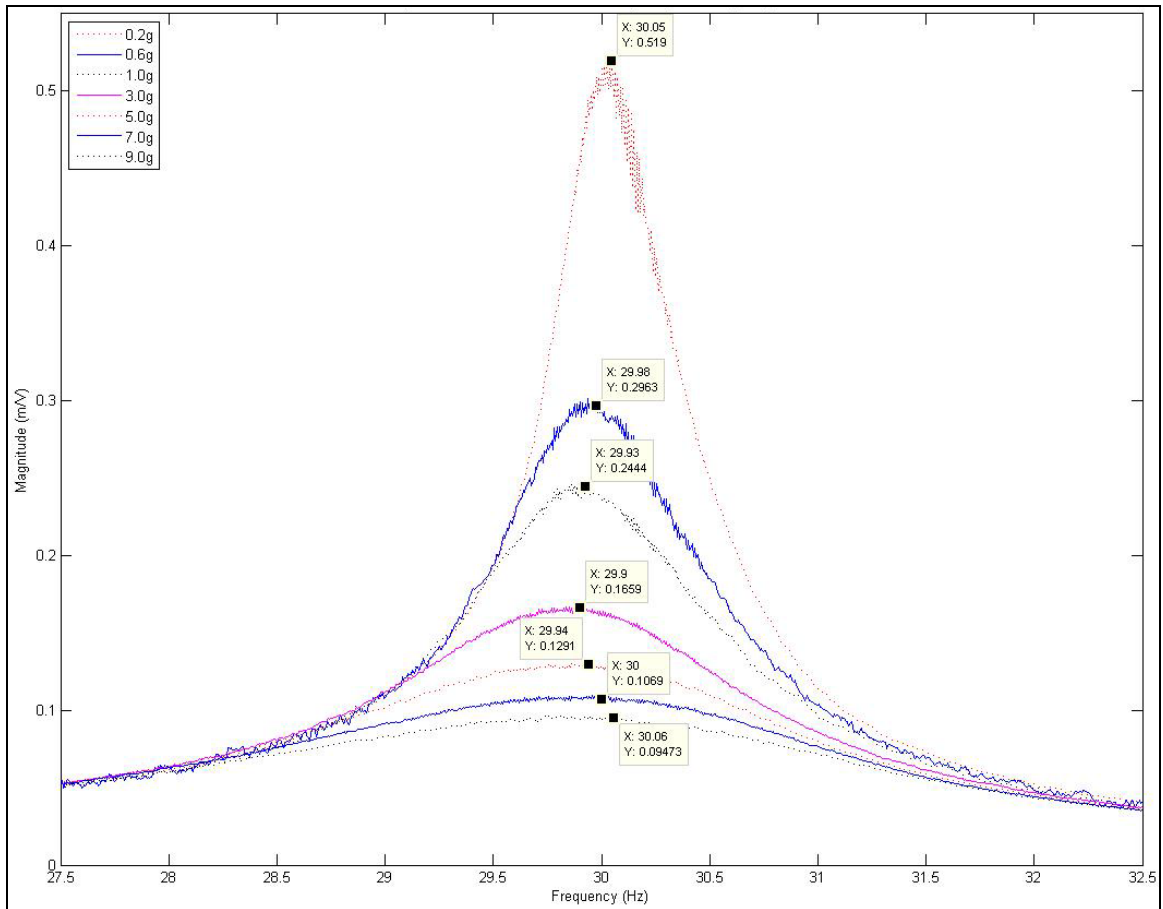


**Figure 87: Displacement Transfer Function of Carbon Epoxy Beam Tip – 5 Hz Bandwidth**

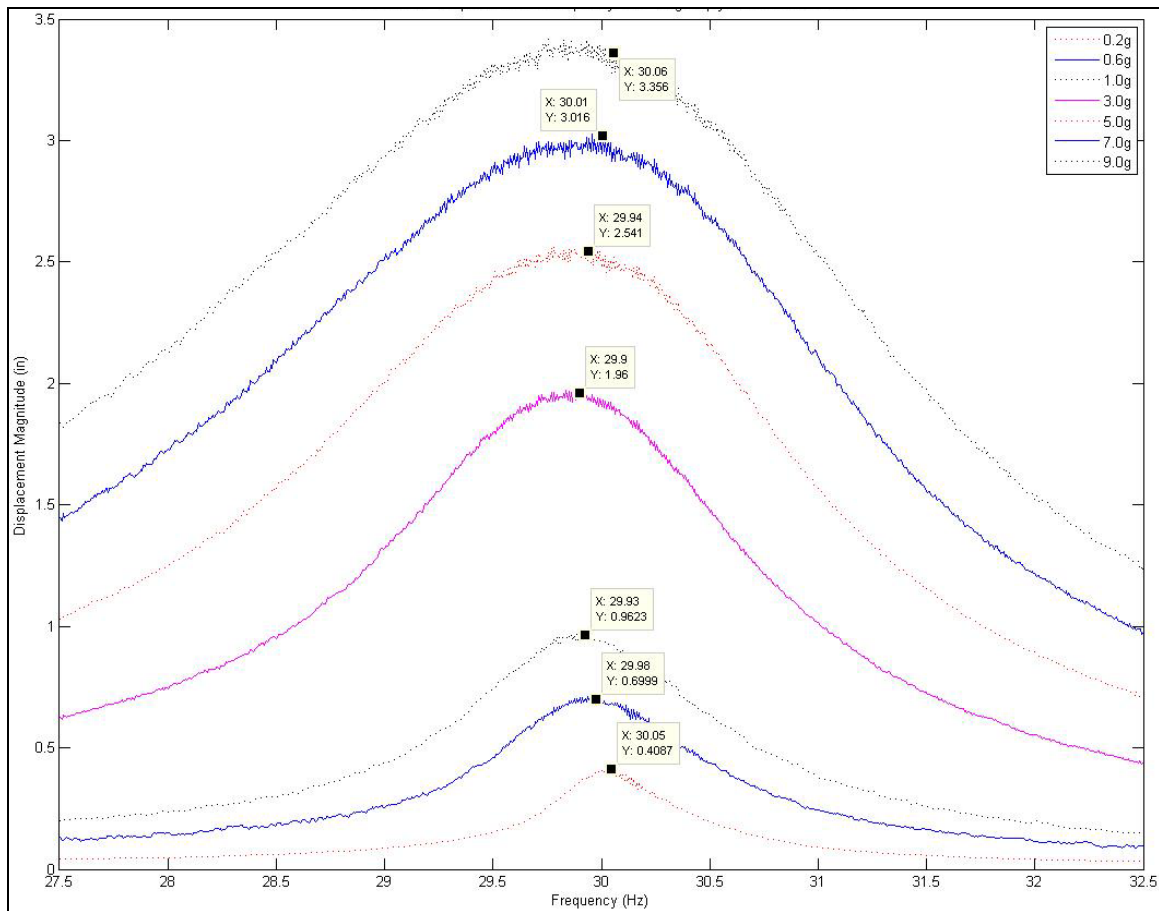


**Figure 88: Displacement Frequency Spectrum of Carbon Epoxy Beam Tip – 5 Hz Bandwidth**

Next, the beam midpoint results will be shown. Due to the large tip deflections, nearly 3.5 inches peak to peak, of the six inch length carbon epoxy beam, it has been decided to investigate and determine the natural frequencies for the previous amplitudes at a location closer to the root boundary condition. Same as before, this precise location three inches from the root was measured with calipers, and a spot was marked on which to position the laser beam. The laser vibrometer software setup was again very similar to all of the Zoom-FFT testing of the beam tip, but special attention was addressed to the velocity decoder, to ensure the proper decoder was used for each respective amplitude change. Again, the lowest valued decoder capable of recording the spot's velocities without overranging is most desirable. An example of the velocity difference that occurs

by shifting the laser test from the tip to the midpoint is shown by the following resulting velocity vs. time plot of the midpoint test at the 9.0g amplitude. Remember that at the beam's tip, 9.0g acceleration brought about a near maximum allowable velocity of 10 m/s.

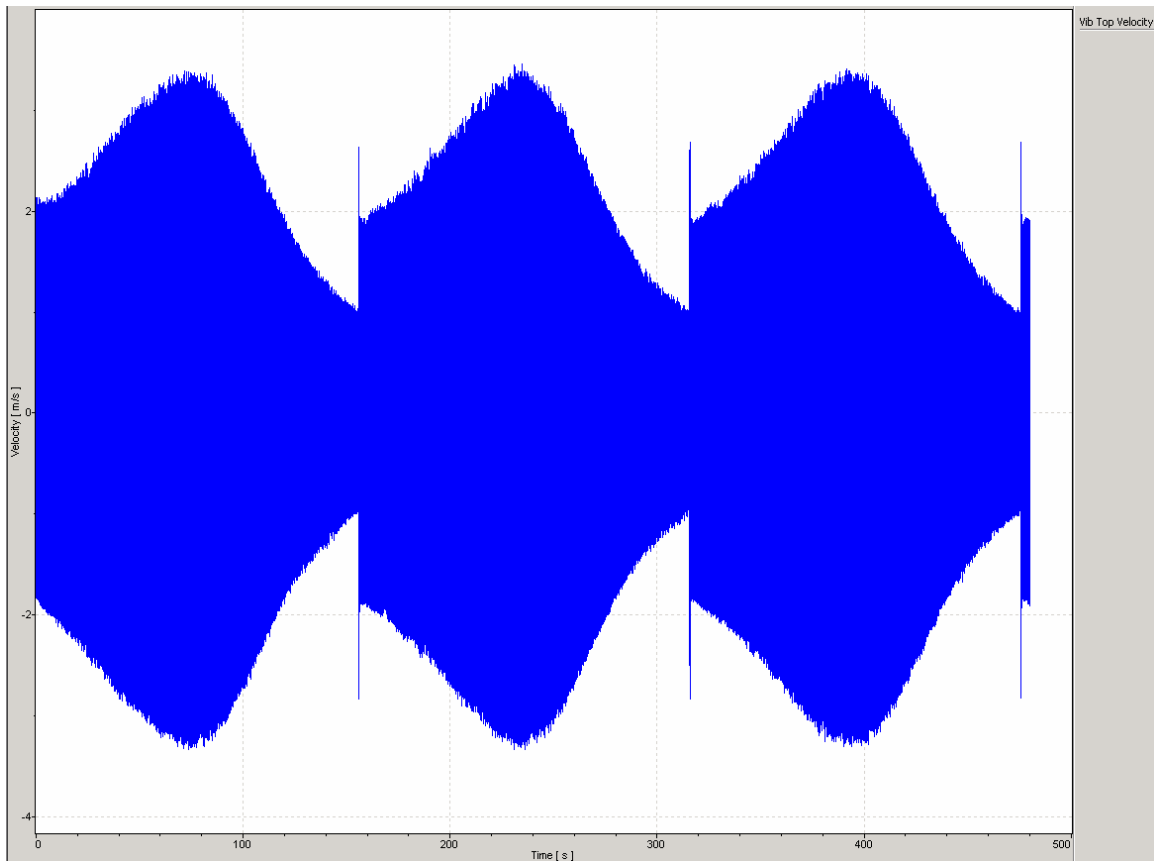


**Figure 89: 1-D Symmetric Carbon-Epoxy Beam – Midpoint 9.0g Velocity Illustration**

During post-processing of the midpoint experiments, velocity phase plots were again generated. It has been shown how the phase shift location marks the approximate natural frequency. Aside from the obvious velocity and displacement differences, the only other significant difference between the midpoint and the tip occurs during the frequency range beyond 3.0g's. The midpoint records a more pronounced hardening nonlinearity resulting in a 9.0g natural frequency of 30.18 Hz, whereas the 9.0g tip testing resulted in a natural frequency of 30.06 Hz. The midpoint phase, displacement

transfer function, and displacement frequency spectrum plots are included in Figures 90-93, respectively.

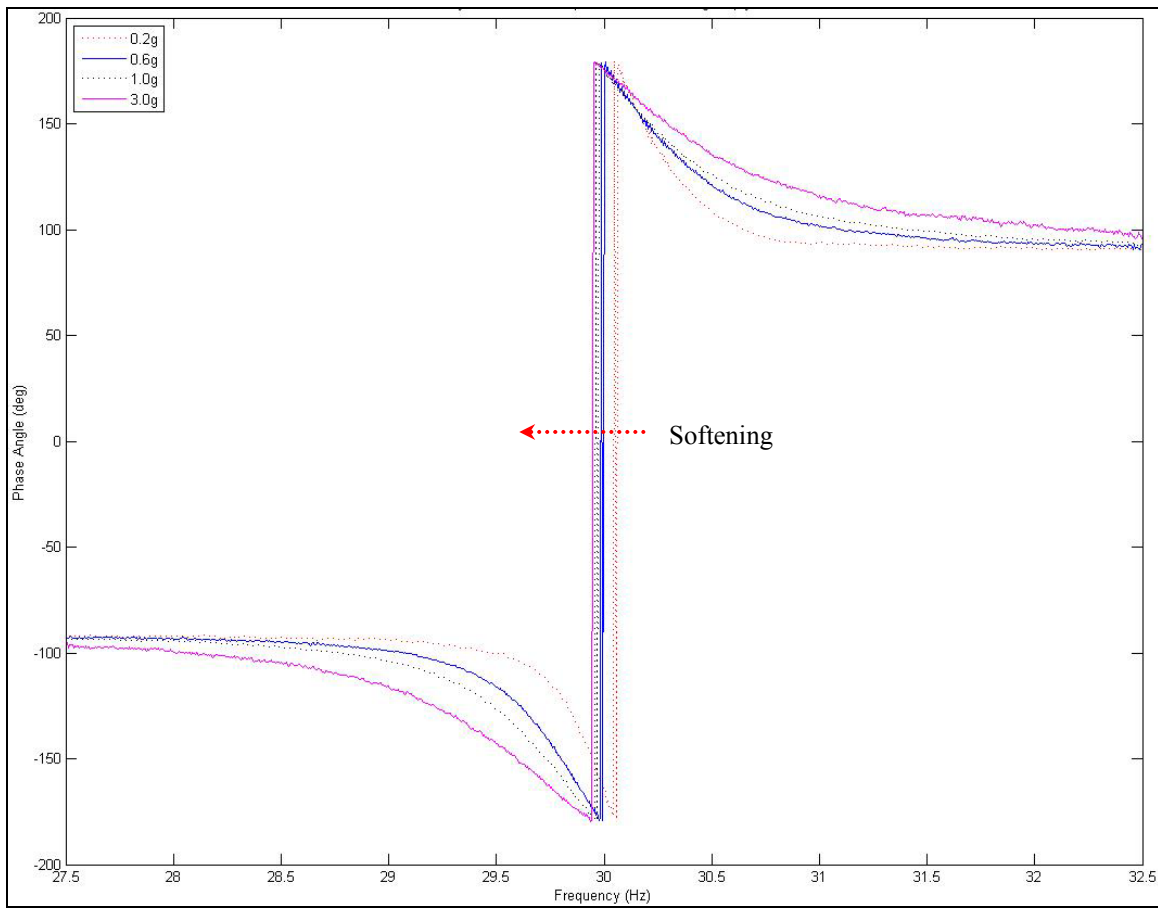


**Figure 90: Velocity Transfer Function Phase Shift– 0.2g-3.0g Tests of Carbon Epoxy Beam Midpoint**

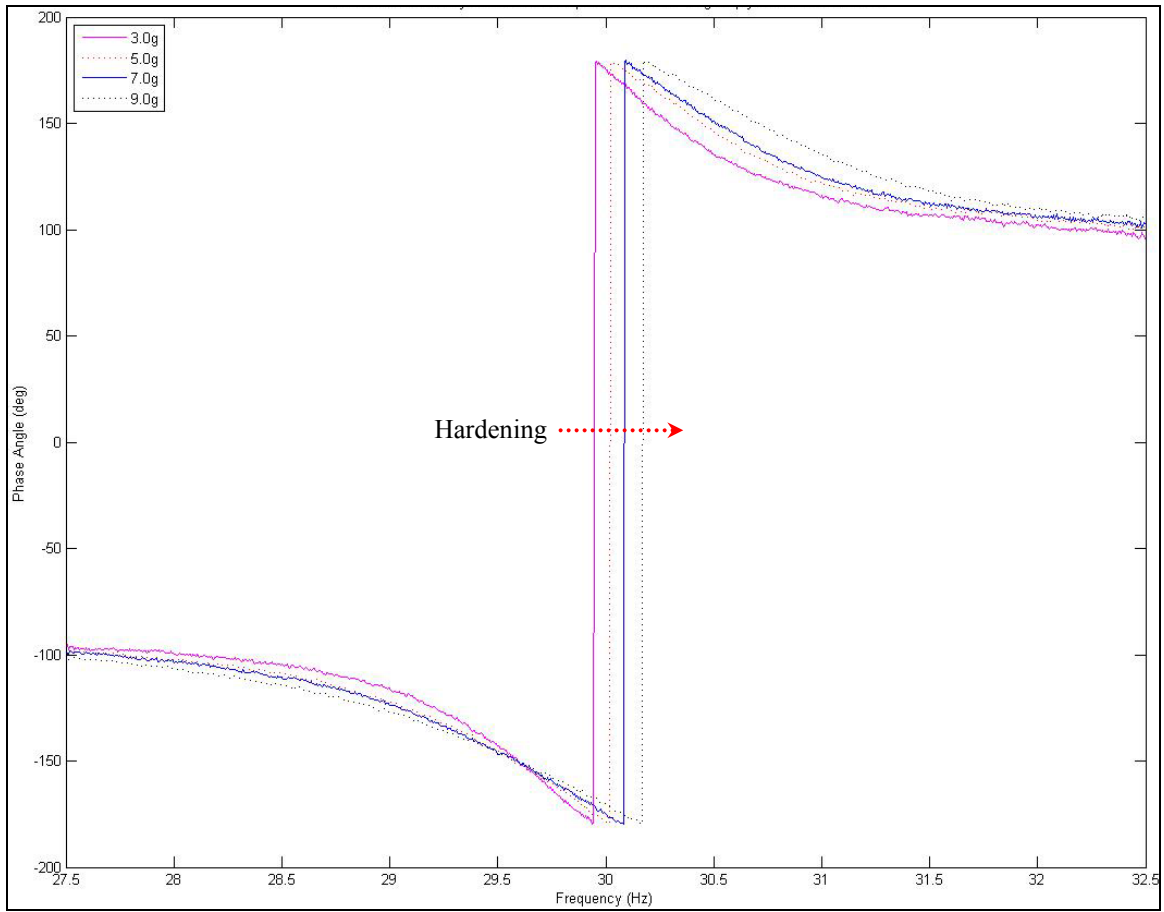


**Figure 91: Velocity Transfer Function Phase Shift – 3.0g-9.0g Tests of Carbon Epoxy Beam Midpoint**



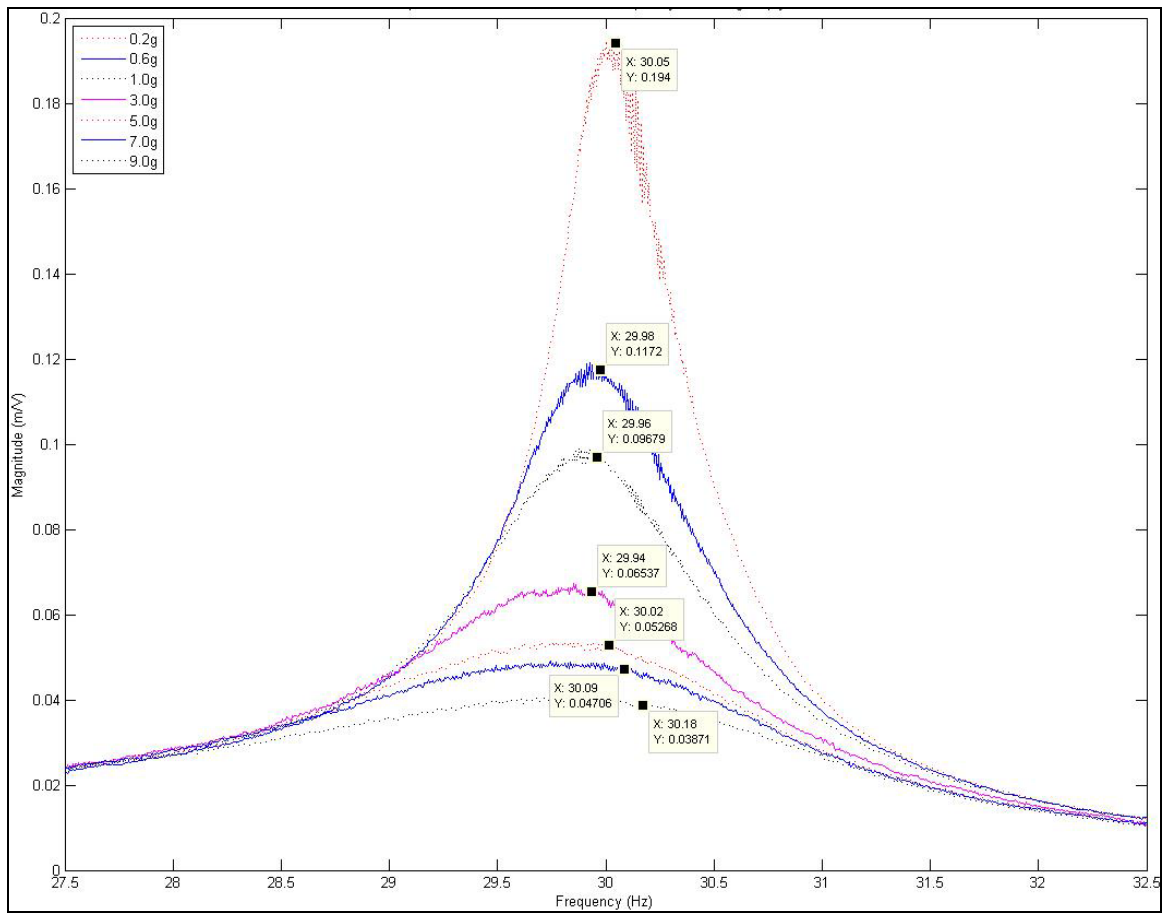


**Figure 92: Displacement Transfer Function of Carbon Epoxy Beam Midpoint – 5 Hz Bandwidth**

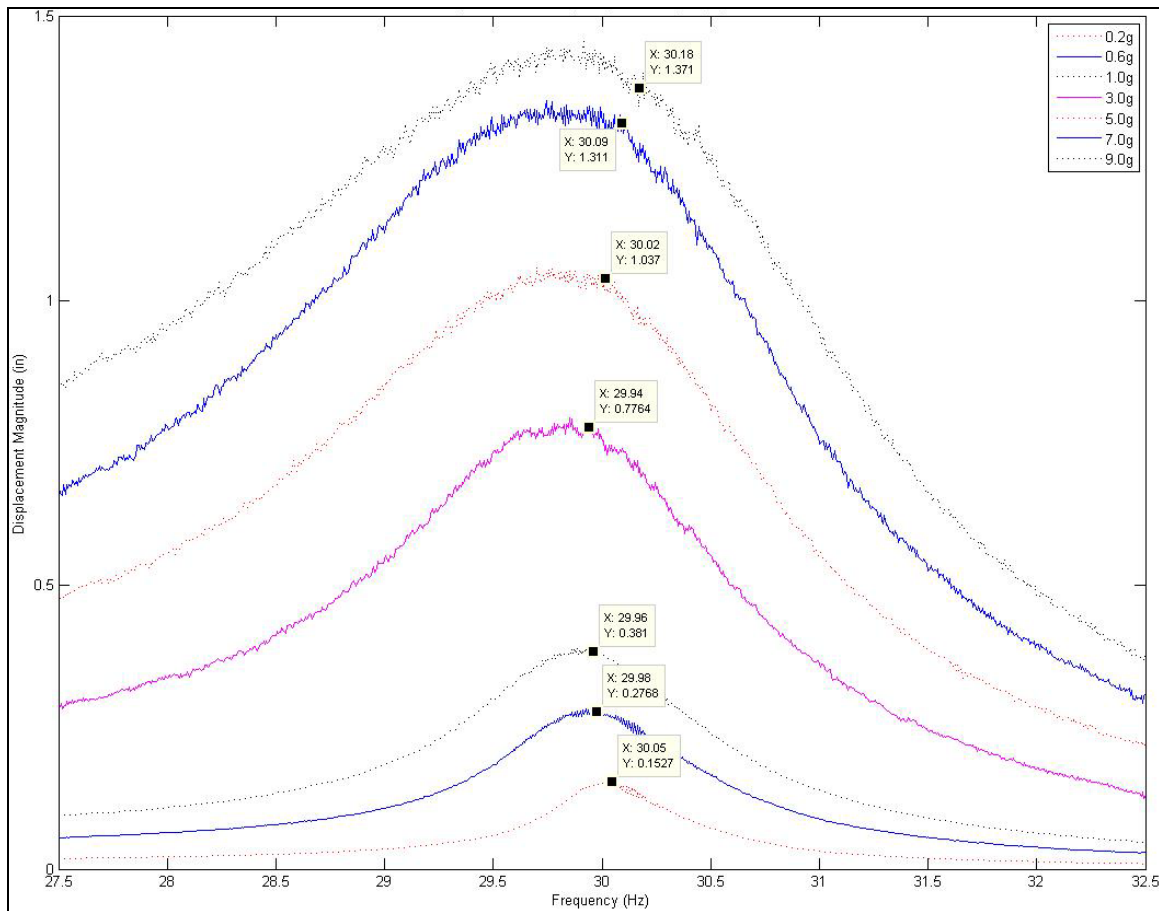


**Figure 93: Displacement Frequency Spectrum of Carbon Epoxy Beam Midpoint – 5 Hz Bandwidth**

One final experiment was carried out to confirm the accuracy of the natural frequency results which have been generated during all previous vibrometry testing. This experiment involved using both the laser vibrometer and two accelerometers, which are shown in Figures 94 and 95.

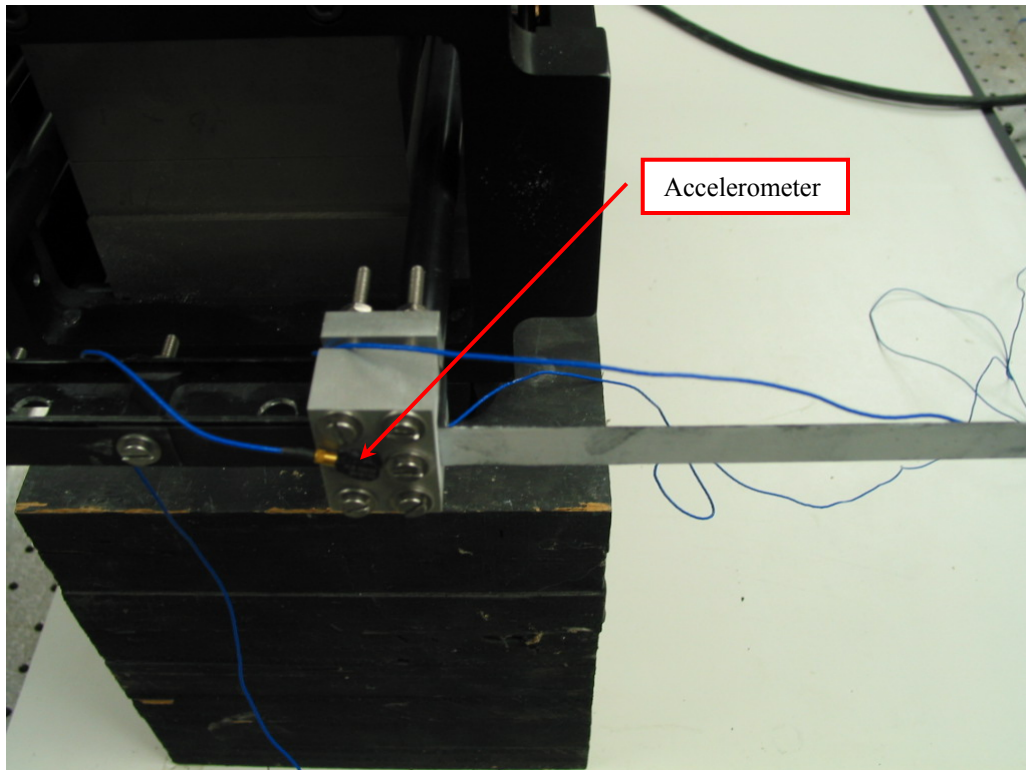


**Figure 94: Placement of Accelerometer on Clamp for Method Validation**

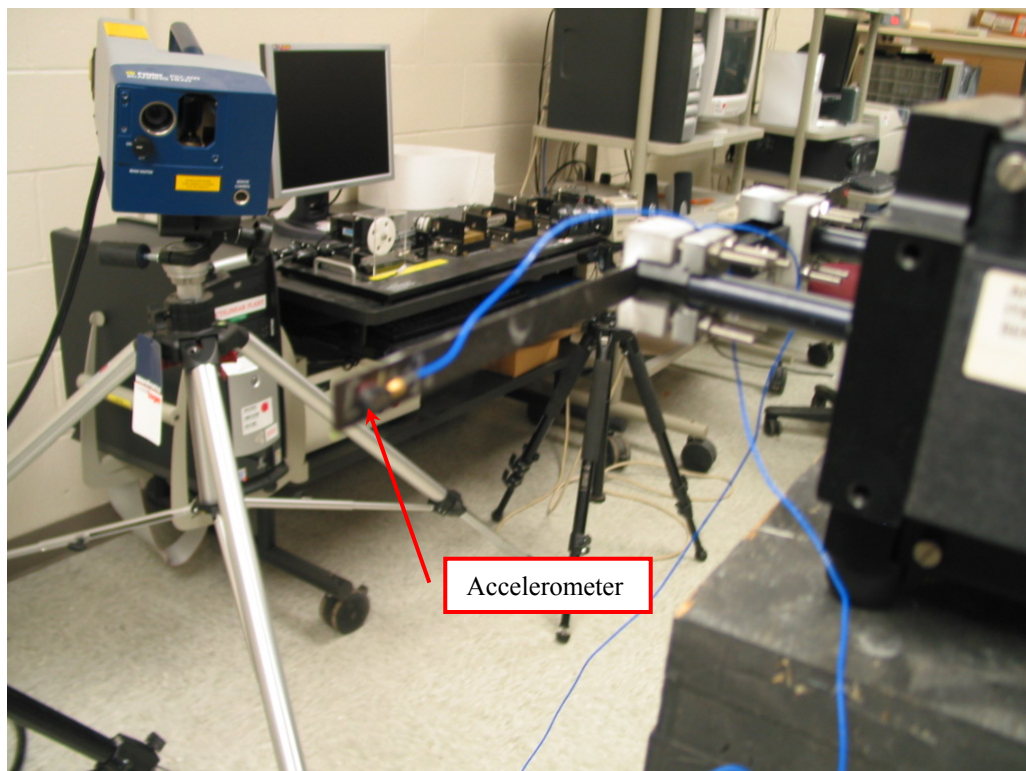


**Figure 95: Placement of Accelerometer on Beam Tip for Method Validation**

The SignalCalc vibration software program was used for this testing. SignalCalc allows for the direct input and measurement of accelerometer and/or laser vibrometer signals. The plan for this experiment was to place an accelerometer on the opposite side of the beam tip at the exact point where the laser would be positioned for vibrometer measurements. The original root clamp-located accelerometer was connected to input 1, the beam tip accelerometer to input 2, and the vibrometer's velocity signal to input 3 of the SignalCalc junction box, as shown in Figure 96.

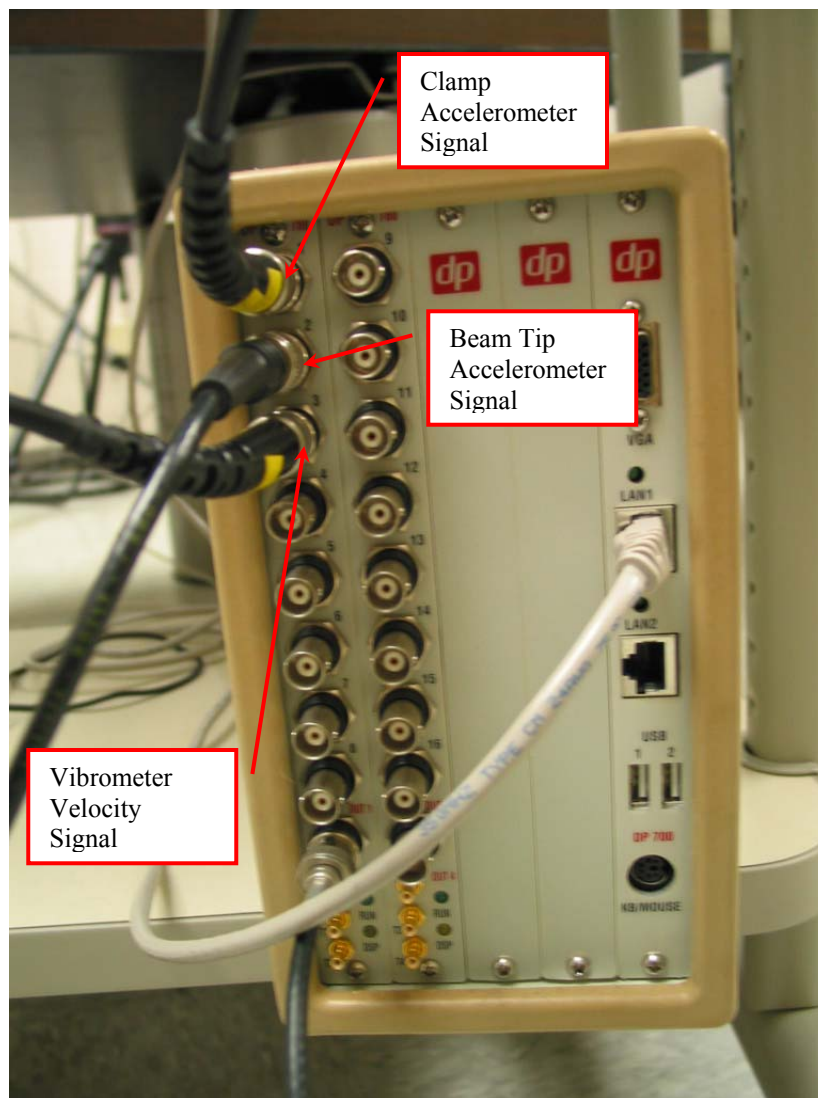


**Figure 96: Connection of Signal Leads into Junction Box**

Two different sets of transfer functions were created from these tests. Since the vibrometer is sending a velocity signal, and the accelerometers are sending acceleration, the transfer functions will have magnitudes that are not equal. To account for this difference, a scaling factor, seen in the Appendix A Matlab code, is applied. An illustration of a 1g test using the SignalCalc program is provided in Figure 97. This example used a frequency bandwidth of 10 Hz, and centered on the 21 Hz location. Similar to what was seen using the PSV software, 50% overlap was used with 10 complex averages. Additionally, 200 FFT lines of resolution were chosen. While this is an entirely different software program, the methods are very similar and comparable to the Polytec software previously discussed.

The upper plot in Figure 97 shows the frequency response functions comparing the beam tip accelerometer with the beam tip laser method of vibrometry. The lower plot shows the real-time voltage response of the clamp, indicating its movement through the course of a frequency sweep.

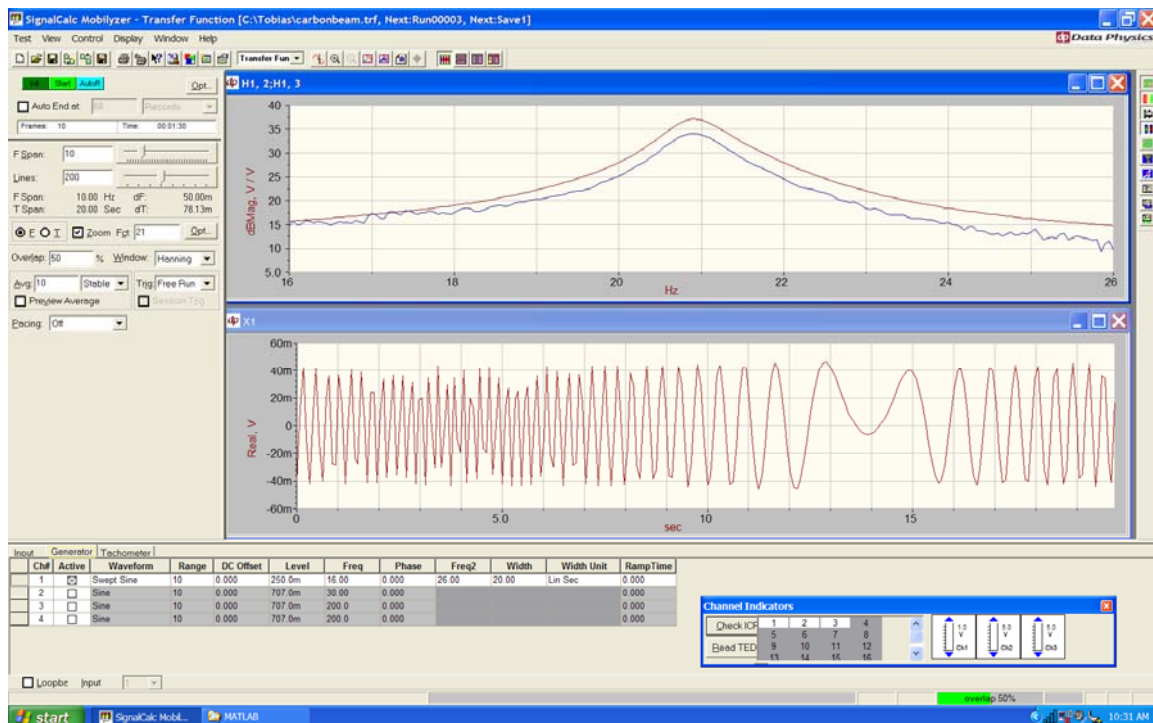


**Figure 97: SignalCalc Software Methods During 1g Comparison Testing**

The results of this comparison testing are provided by Figure 98. The primary goal of these experiments was to prove that indeed the natural frequencies determined by the laser vibrometer were consistent with other available methods. Only three separate input accelerations were evaluated. From these results, one obvious difference between the peak frequencies shown in Figure 98, as compared to any of the previous transfer function plots, is the location of the beam's natural frequencies. A frequency decrease of approximately 9 Hz has occurred as a result of the tip mass added by the beam tip accelerometer. A possible second resonance may be occurring as a result of the tip mass in the 5g testing. Two different nonlinear problems are shown in Figure 98, the original issue created as a result of material imperfection, and the second caused by the tip mass. While not the original intent of this experiment, the tip mass effect caused by the very



small accelerometer placed at the beam tip is significant evidence to support the use of non-contact methods when measuring the vibration of a micro air vehicle wing.

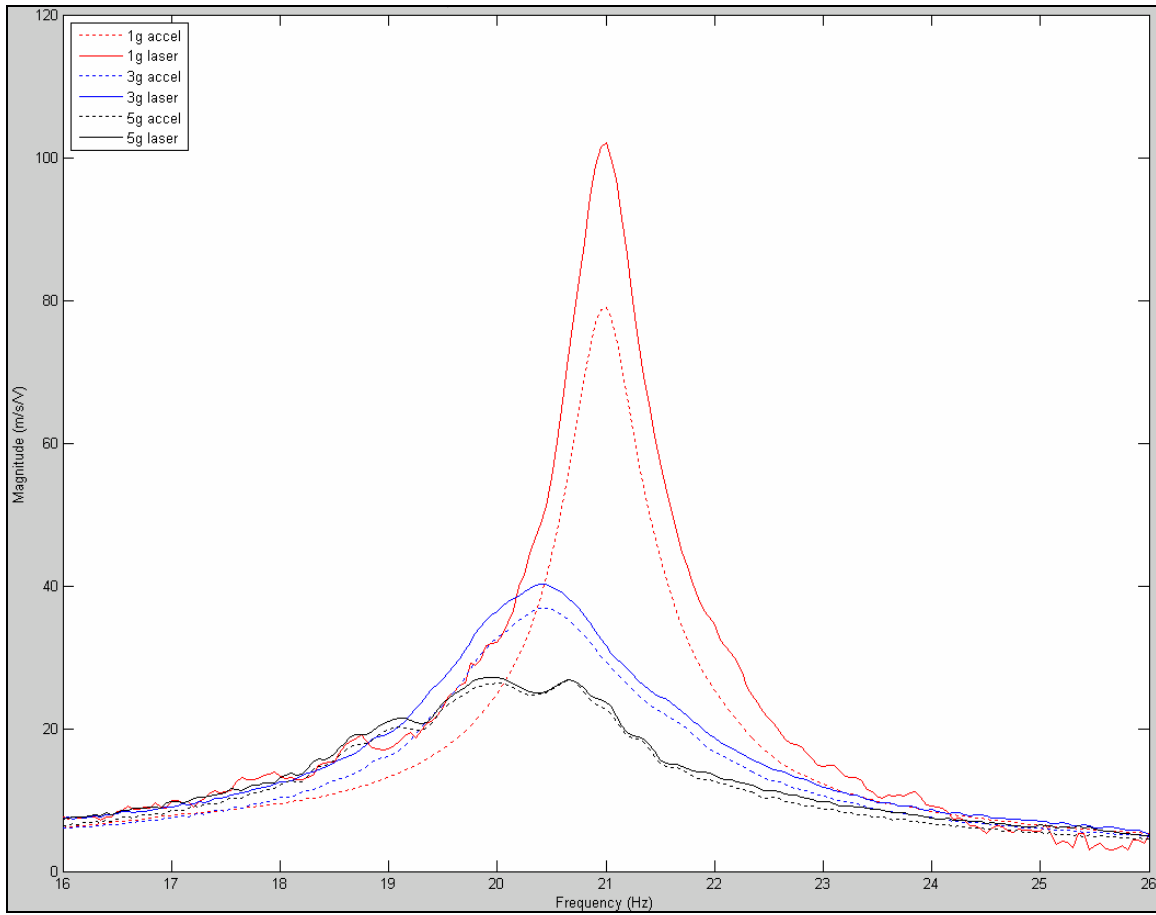


**Figure 98: Transfer Function Comparison of Vibrometer and Accelerometer Methods**

### 3.6 High Speed Optical Experimentation

A few limitations exist with the laser vibrometer which bring about the need for additional methods, such as an optical system, to calculate a flapping wing's displacement and/or velocity magnitude. For example, if a wing were to undergo very large flapping rotations, such as 180 degrees, the laser vibrometer could not be used to collect any vibration data. A high speed camera would be capable of recording this movement, and through the analysis methods previously discussed, the wing's movement could be accurately characterized. Additionally, rigid body movement may be removed

by using the Motion Tools analysis software if the methods described in Section 3.3.6 are followed.

To demonstrate the feasibility of this technique, some experiments were carried out to document displacement of the beam tip at varying input voltages. First the aluminum beam was set up for evaluation. To calculate actual deflection, both the beam tip and beam root were recorded in the camera images. The beam's length of 10.1" required a positioning of the camera far enough away from the beam that in the pictures, the ruler measurement units were not distinguishable. This led to testing only the 6" carbon-epoxy beam. An example of one of these tests is shown in Figure 99.

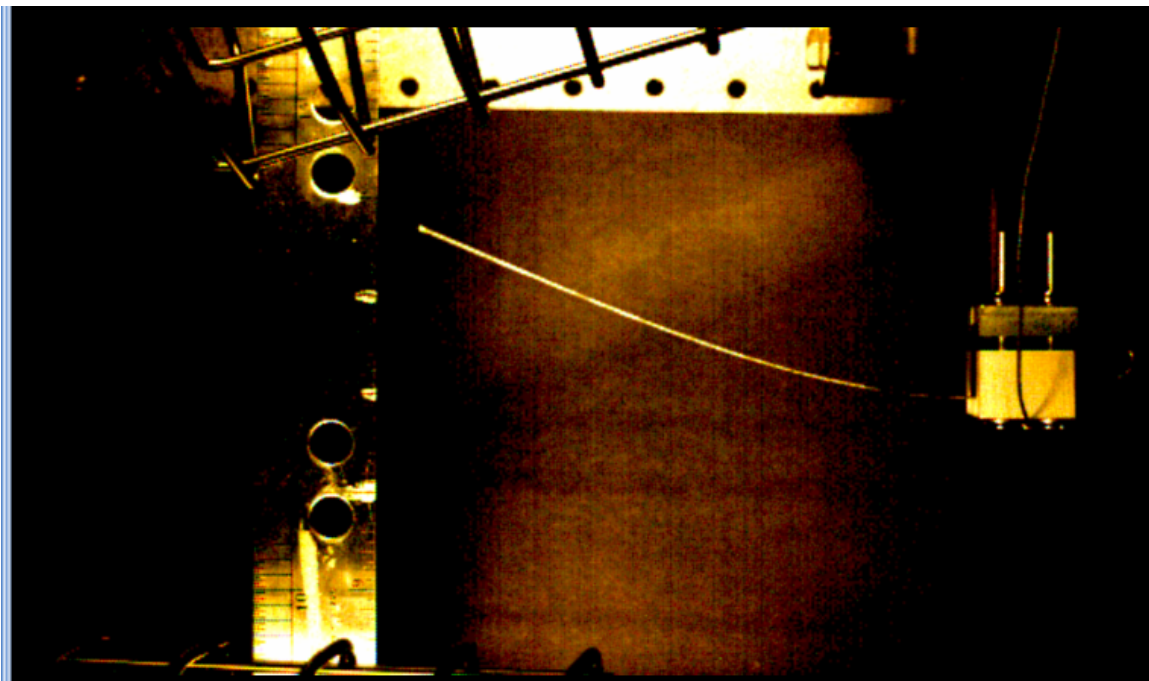


**Figure 99: Example Frame of the High Speed Camera Carbon Epoxy Testing**

The camera method is incapable of measuring characteristics of a structure's entire surface. Only an edge can be observed and analyzed using an optical system. With this camera software package, phase plots or frequency response functions can not



be generated. This puts cameras at a disadvantage over the other non-contacting vibration measurement method.

Numerous trials were conducted using both the symmetric and single carbon epoxy beam configurations. During these experiments, the out-of-plane movement induced during the asymmetric testing was very apparent at higher amplitudes. The videos would show the clamp rotating in an elliptical pattern rather than in a straight line. Unfortunately, it was not possible to make out this rotation by looking at still photos. The video observations clearly match the torsion effect shown by the laser vibrometer eigenvector plots of the asymmetric testing.

The results of two optical tests provide documentation of this method's capabilities. For these tests, the symmetric carbon epoxy beam configuration was used. A manual frequency sweep was carried out using a waveform generator connected through an amplifier to the shaker. A single desired frequency, for example 30 Hz, was input to the waveform generator, and the beam was allowed to vibrate for at least ten seconds to establish a steady state condition. At this time the camera was turned on and the movements were recorded, frame by frame. The Motion Tools analysis was performed and peak-to-peak displacement magnitudes of this movement were saved to Microsoft Excel files. The beam tip displacement was measured and so was the root displacement, to remove rigid body motion. The difference between these two was the maximum peak-to-peak displacement for each given frequency. These steps were repeated over a range of frequencies from 27 to 34 Hz, and the results were plotted. The results provided in Figure 100 show two different input magnitudes, 450mV and 900mV. These amplitudes were programmed into the waveform generator.

Using curve smoothing, if one compares the two different input curves, a slight peak frequency increase seems to occur as the amplitude is increased. While these amplitudes exceed that of the vibrometer testing, it is interesting to note how a similar increase, or hardening effect, was present in the higher amplitude 1-D vibrometer testing.

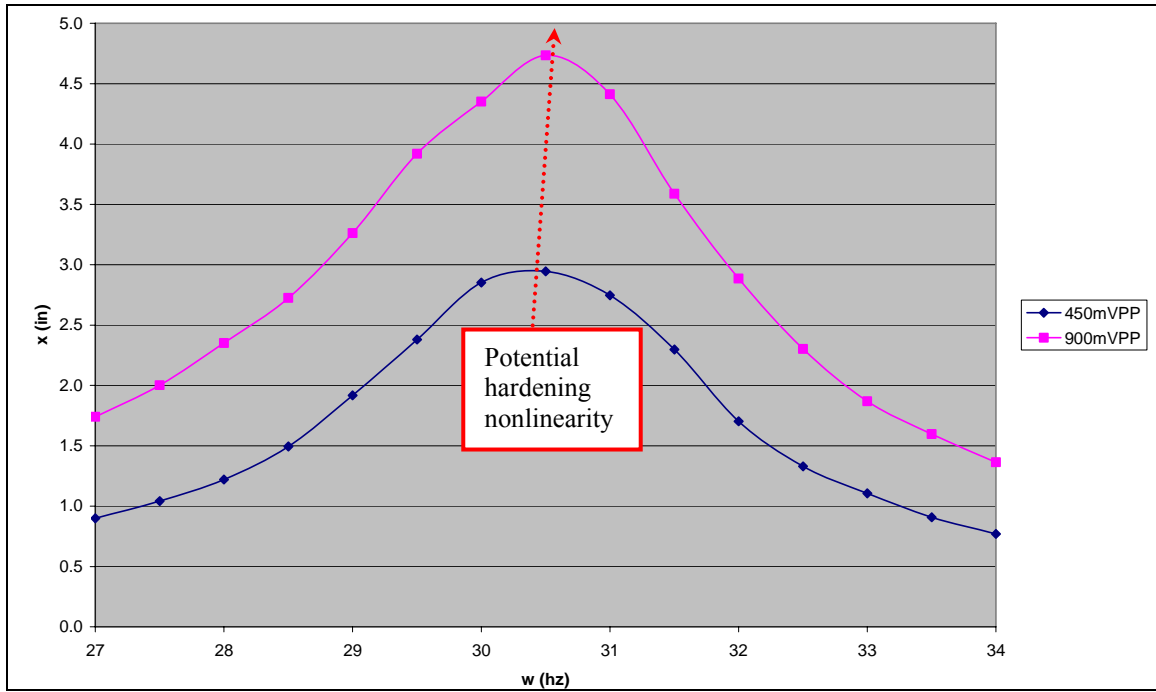


Figure 100: Symmetric Carbon-Epoxy Peak-to-Peak H.S. Camera Tip Displacement vs. Frequency

## **IV Conclusions**

### **4.1 Experimental Methods**

The intent of this thesis was to determine the best suitable experimental methods to document nonlinear vibration of a flapping MAV-type wing. Finite element analysis, beam theory, and composite theory were used in the computational vibration analysis and beam sizing. A high speed camera and two configurations of a scanning laser vibrometer were employed to carryout the experimental focus of this research. Two beams consisting of different material structures were tested.

The first set of scanning laser vibrometer experiments used a three dimensional configuration. Both an aluminum beam and a carbon-epoxy beam were investigated using the 3-D laser vibrometer system. While 3-D laser vibrometers are ideal for numerous structural dynamics applications, they did not prove to be the most valuable choice for testing of a flapping wing.

As a result of the 3-D laser vibrometer complications, a new set of experiments was designed using a 1-D configured laser vibrometer. The 1-D vibrometer proved to be capable of generating accurate natural frequency comparisons with the results found from analytical methods. Most importantly, the 1-D vibrometer was able to characterize the vibration of a beam undergoing large deflections. Numerous trials were conducted to determine the best possible experimental setup. It was found that two beams symmetrically oriented on a shaker proved to generate the most accurate vibration responses. Coincidentally, this configuration very much resembles the wingtip-fuselage-wingtip configuration of an actual flapping wing vehicle. The mode shapes of the symmetric carbon-epoxy beam testing generated from the 1-D configured setup did not

show the twisting that was documented during the single beam testing. Therefore, it is recommended that any further studies using the shaker procedure would consist of symmetric configurations. Carbon-epoxy 1-D testing was able to provide frequency response functions and frequency spectrums that illustrated the nonlinear natural frequency changing with respect to amplitude. A natural frequency decrease occurred from 0.2-3.0g's and an increase existed beyond 3.0g's.

A separate investigation was carried out to verify the accuracy of natural frequencies as calculated by the vibrometer. These experiments involved testing the carbon-epoxy beam simultaneously with the laser vibrometer as well as an accelerometer located at the same approximate spot. The conclusions of these tests show that indeed the laser vibrometer is an accurate method for determining natural frequency, and documenting nonlinearity of a flapping-wing type structure. This beam tip and accelerometer comparison showed that, by placing even these very small accelerometers on a very light weight vibrating structure, the carbon-epoxy, significant changes to the vibration characteristics occur. This greatly supports the choice of using non-contact methods to acquire nonlinear vibration data from flapping wing MAVs, rather than other vibration collection methods.

A final set of experiments was designed to provide insight into the capabilities of a high speed camera as applied to the same flapping tests. It was shown that while a high speed camera is very capable of measuring displacement and/or velocity of a beam, it has many limitations when compared to the scanning laser vibrometer. The camera is unable to capture movement occurring over the entire structural surface; rather just the edges can be tracked. Additionally, the camera is unable to generate frequency spectrum data

which is necessary for pinpointing natural frequencies, phase information, and documenting response transfer functions.

Additional flapping wing MAV testing would benefit from using a combination of the positive aspects of the previous methods. The 3-D vibrometer could solve for the entire structures eigenvalues and eigenvectors without introducing large movements. If one were to measure, for example, up to the quarter-span location, the 3-D vibrometer could be used with larger deflections. The 1-D vibrometer is capable of characterizing large flapping motion, up to but not to exceed 10 m/s or significant angles of rotation. The high speed camera is best suited analyzing flapping motion exceeding the geometric rotation and/or velocity limitations of the 1-D laser vibrometer.

The following list summarizes the conclusions of Section 4.1:

- **3-D Laser Vibrometry is limited for large flapping applications**
- **Asymmetry of the experimental setup causes significant problems**
- **1-D Vibrometry is ideal for nonlinear vibration characterization of flapping**
- **High speed camera is limited to time domain and surface edge measurements**
- **Non-contact vibration testing is essential to guarantee accurate results**
- **An appropriate combination of discussed methods is ideal for future testing**

## **4.2 Proposed Topics for Further Study**

A capability to test inside a vacuum environment would be very useful to compare and contrast with the ambient air pressure tests. However, this type of testing is accompanied by numerous challenges. Since MAV research involves testing of small structures, limitations exist in what methods can be utilized for data acquisition. The laser vibrometer is a very useful and much needed tool which should also be used if possible with the vacuum testing - this is especially good for determining what modes & mode shapes we are dealing with. It has been shown that the vibrometer is limited to lesser displacements and velocities than may be ultimately desired. The camera system could be used as well with the vacuum, but with a more complex structure its usefulness would diminish. Calculation of wingtip, leading edge and trailing edge displacements and velocities should always be possible when using the camera. Other acquisition methods such as strain gauges or multiple accelerometers along the surfaces would likely interfere with the structures true vibration characteristics. An example of this effect was shown during the tip mass accelerometer and laser vibrometer comparison study.

Since it was stated that a MAV needs to have its greatest dimension less than or equal to 6", it would be useful to study wings that meet this constraint. This effort would require development of a membrane-structure system that, when combined, could be used in a flapping application. A mixture of finite element analysis, experimentation, and partial differential equation analysis could be applied to aid in the design and testing of a MAV wing. Finally, one could investigate damage detection or simulation of these wing structures.

## Appendix A

### A.1 Matlab Code to Calculate Beam Length for an Aluminum Beam

```
% This program will calculate beam length
% Material used is 2024 T3 Aluminum Alloy
% Filename: aluminum_beam_length
% Created by Adam Tobias on 11 July 2006
clear; clc;

% The following are the inputs for frequency, thickness, and width
w1 = input('What is the frequency in Hz? ');
h1 = input('What is the beam thickness in inches? ');
b1 = input('What is beam width in inches? ');

% will convert thickness and width to units & Hz to rad/s
h2 = h1 * 2.54E-2;
b2 = b1 * 2.54E-2;
w2 = w1 * 2*pi;

% Area of beam cross section
A = b2*h2;

% Moment of inertia of beam cross section
I = (b2*h2^3)/12;

% Modulus of Elasticity of 2024 T3 in Pascals, kg/(m s^2)
E = 7.31E10;

% Density of 2024 T3 in kg/m^3
rho = 2780;

% ZetaSq = Zeta Squared
ZetaSq = 1.875104;

% The following calculates the length of the beam in meters
L1 = (((ZetaSq^4)*E*I)/((w2^2)*rho*A))^(1/4);

% Here is beam length converted to inches
Length_Inches = L1/(2.54E-2);
fprintf('The length of the beam is %g inches.\n', Length_Inches)
```

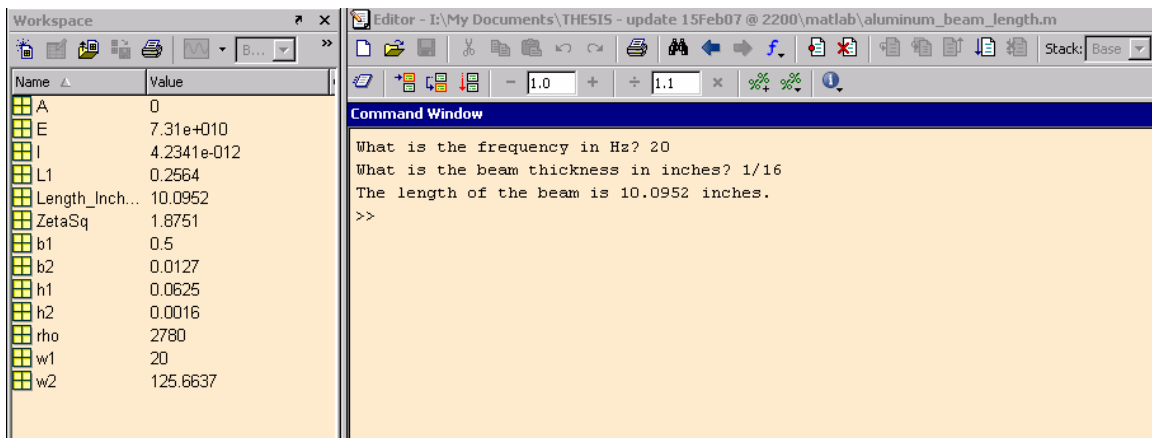


**Figure 101: Matlab Aluminum Beam Length Result**



## A.2 Matlab Code to Calculate Beam Length for a Carbon-Epoxy Beam

```
% Program to find Quasi-Isotropic Laminate Modulus of Elasticity
% Program name: composite_beam_length_4ply
% Created by Adam Tobias on 25 August 2006

clear;
clc;

% First I will define material properties of IM7/5250-4
% [0,90,90,0]

% rho = density in kg/m^3
rho = 1540; %estimated from IM7/5250-4 density

% w1 = input('What is the frequency in Hz? ');
w1 = 30;
fprintf('The frequency is %g Hz.\n', w1)

% will convert Hz to rad/s
w2 = w1 * 2*pi;

% ZetaSq = Zeta Squared
ZetaSq = 1.875104;

% E1 = Axial modulus in GPa
E1 = 176.79E9;

% E2 = Transverse modulus in GPa
E2 = 10.2E9;

% v12 = Poisson's ratio v12
v12 = 0.277;

% v21 = Poisson's ratio v21
v21 = v12*E2/E1;

% G12 = Shear modulus G12 in GPa
G12 = 6.29E9;

% next I will define the four fiber directions in radians
theta1 = 0;
theta2 = 90*pi/180;

% Here I will define m and n, m = cos(theta), n = sin(theta)
m1 = 1;
m2 = 0;

n1 = 0;
n2 = 1;

% thickness of each layer is 0.05inches, t is converted to meters
t = 0.005*2.54E-2;
fprintf('The thickness of the beam is %g meters.\n', t)
```

```

% width of the beam is 0.5 inches, b is converted to meters
b = 0.5*2.54E-2;
fprintf('The width of the beam is %g meters.\n', b)

% Q11 = Reduced stiffness coefficient Q11
Q11 = E1/(1-v12*v21);

% Q12 = Reduced stiffness coefficient Q12
Q12 = (v21*E1)/(1-v12*v21);

% Q22 = Reduced stiffness coefficient Q22
Q22 = E2/(1-v12*v21);

% Q66 = Reduced stiffness coefficient Q66
Q66 = G12;

% Stiffness coefficients for each respective fiber orientation in GPa
Qbar11_theta1 = (Q11*m1^4)+(2*(Q12+2*Q66)*(m1^2)*(n1^2))+(Q22*n1^4);
Qbar11_theta2 = (Q11*m2^4)+(2*(Q12+2*Q66)*(m2^2)*(n2^2))+(Q22*n2^4);

Qbar12_theta1 = (Q11+Q22-4*Q66)*(m1^2)*(n1^2)+Q12*((n1^4)+(m1^4));
Qbar12_theta2 = (Q11+Q22-4*Q66)*(m2^2)*(n2^2)+Q12*((n2^4)+(m2^4));

Qbar22_theta1 = (Q11*n1^4)+(2*(Q12+2*Q66)*(m1^2)*(n1^2))+(Q22*m1^4);
Qbar22_theta2 = (Q11*n2^4)+(2*(Q12+2*Q66)*(m2^2)*(n2^2))+(Q22*m2^4);

Qbar16_theta1 = (Q11-Q12-2*Q66)*(m1^3)*(n1)+(Q12-
Q22+2*Q66)*(n1^3)*(m1);
Qbar16_theta2 = (Q11-Q12-2*Q66)*(m2^3)*(n2)+(Q12-
Q22+2*Q66)*(n2^3)*(m2);

Qbar26_theta1 = (Q11-Q12-2*Q66)*(m1)*(n1^3)+(Q12-
Q22+2*Q66)*(n1)*(m1^3);
Qbar26_theta2 = (Q11-Q12-2*Q66)*(m2)*(n2^3)+(Q12-
Q22+2*Q66)*(n2)*(m2^3);

Qbar66_theta1 = (Q11+Q22-2*Q12-
2*Q66)*(m1^2)*(n1^2)+Q66*((n1^4)+(m1^4));
Qbar66_theta2 = (Q11+Q22-2*Q12-
2*Q66)*(m2^2)*(n2^2)+Q66*((n2^4)+(m2^4));

% now I will combine the four different Qbar matrices
% first for theta1 (zero degree layer)
Qbar_theta1 = [ Qbar11_theta1 Qbar12_theta1 0;...
    Qbar12_theta1 Qbar22_theta1 0;...
    Qbar16_theta1 Qbar26_theta1 Qbar66_theta1];

% next is theta2 (90 degree layer)
Qbar_theta2 = [ Qbar11_theta2 Qbar12_theta2 0;...
    Qbar12_theta2 Qbar22_theta2 0;...
    Qbar16_theta2 Qbar26_theta2 Qbar66_theta2];

z0=-2*t; z1=-t; z2=0; z3=t; z4=2*t;

```

```

A = (Qbar_theta1*((z1-z0)+(z4-z3)))+(Qbar_theta2*((z2-z1)+(z3-z2)));

a_star = (4*t)*inv(A);

% Modulus of Elasticity of IM7/5250-4 Carbon Epoxy in Pascals,
kg/(m s^2)
E = 1/(a_star(1,1));
fprintf('The equivalent Elastic Modulus is %g Pascals.\n', E)

D = (1/3)*((Qbar_theta1*(z1^3-z0^3)))+(Qbar_theta1*(z4^3-z3^3))+...
    (Qbar_theta2*(z2^3-z1^3))+(Qbar_theta2*(z3^3-z2^3));

% E*I = D11 * b
EI = b*D(1,1);

% Area of beam cross section
Area = 4*t*b;
fprintf('The area of the beam cross section is %g meters^2.\n', Area)

% The following calculates the length of the beam in meters
L1 = (((ZetaSq^4)*EI)/((w2^2)*rho*Area))^(1/4);

% Here is beam length converted to inches
Length_Inches = L1/(2.54E-2);
fprintf('The length of the beam cross section is %g inches.\n',
Length_Inches)

```

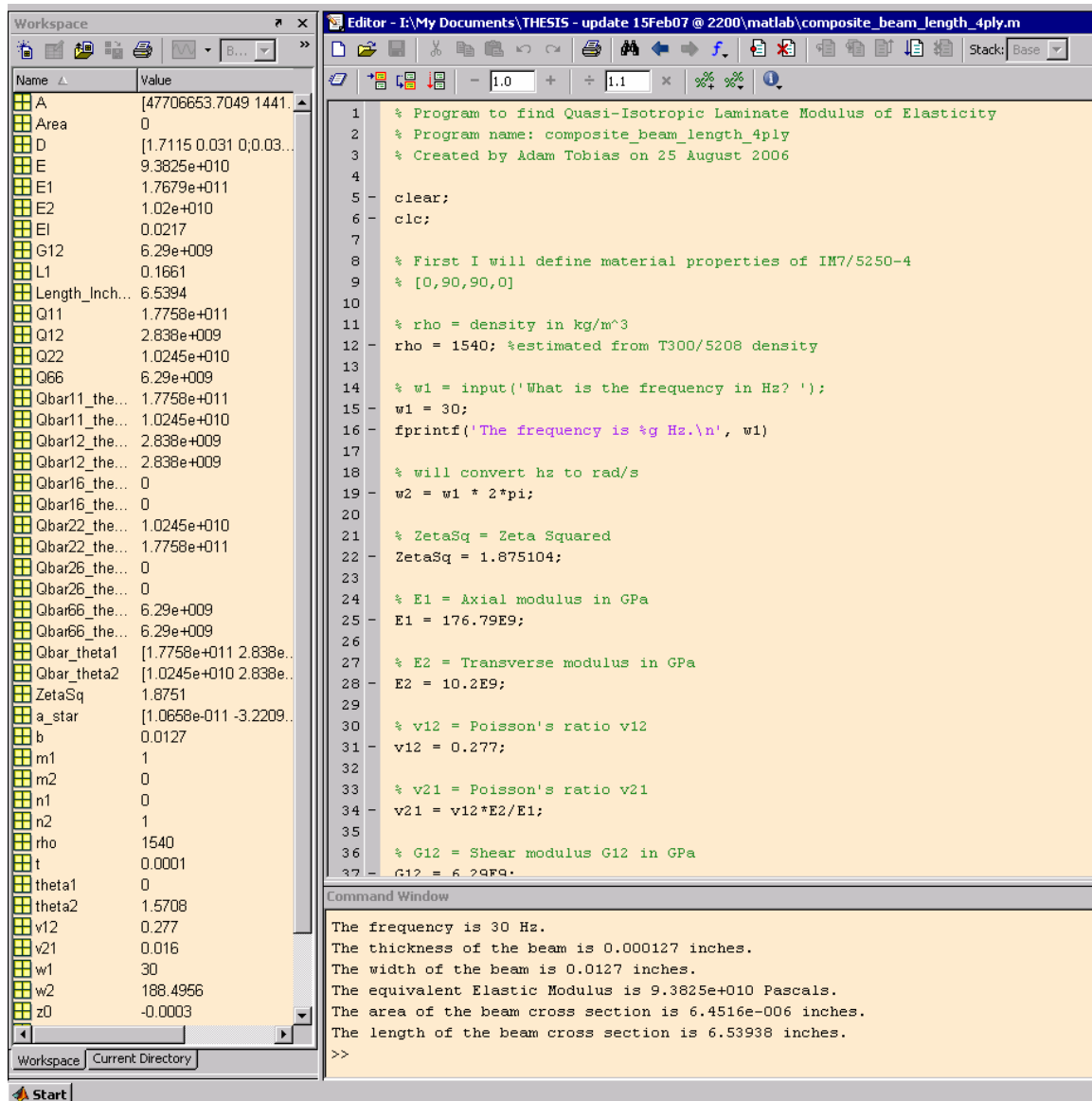


Figure 102: Matlab Carbon-Epoxy Beam Length Result

### A.3 Matlab Code to Plot PSV FRFs and Displacement Frequency Spectrums

```
% section will convert the displacement transfer functions to
% displacements in inches. I multiply the original value (m/V) by the
% test input voltage and by 39.37in/m to convert to inches for the
% displacement

% The bandwidth always is the same and ranges from 25 Hz to 35 Hz

load original_TF_arrays

disp_p2g(:,1)=test_p2g(:,1);
disp_p2g(:,2)=test_p2g(:,2)*.02*39.370;

disp_p6g(:,1)=test_p6g(:,1);
disp_p6g(:,2)=test_p6g(:,2)*.06*39.370;

disp_1g(:,1)=test_1g(:,1);
disp_1g(:,2)=test_1g(:,2)*.1*39.370;

disp_3g(:,1)=test_3g(:,1);
disp_3g(:,2)=test_3g(:,2)*.3*39.370;

disp_5g(:,1)=test_5g(:,1);
disp_5g(:,2)=test_5g(:,2)*.5*39.370;

disp_7g(:,1)=test_7g(:,1);
disp_7g(:,2)=test_7g(:,2)*.7*39.370;

disp_9g(:,1)=test_9g(:,1);
disp_9g(:,2)=test_9g(:,2)*.9*39.370;
```

```

% This final section generates Displacement/Volt Transfer Functions
% vs frequency plots and also displacement vs frequency plots

figure(1); plot(test_p2g(:,1),test_p2g(:,2),'r:'), hold on
plot(test_p6g(:,1),test_p6g(:,2),'b-')
plot(test_lg(:,1),test_lg(:,2),'k:')
plot(test_3g(:,1),test_3g(:,2),'m-')
plot(test_5g(:,1),test_5g(:,2),'r:')
plot(test_7g(:,1),test_7g(:,2),'b-')
plot(test_9g(:,1),test_9g(:,2),'k:')

set(gca,'XLim',[27.5 32.5]), xlabel('Frequency (Hz)')
set(gca,'YLim',[0 0.55]), ylabel('Magnitude (m/V)')
h = legend('0.2g','0.6g','1.0g','3.0g','5.0g','7.0g','9.0g',2);
set(h,'Interpreter','none');
title('Plot of x=5.5" Displacement Transfer Function vs Frequency for
6" length 4ply Carbon Fiber Beam')

figure(2); plot(dis_p2g(:,1),dis_p2g(:,2),'r:'), hold on
plot(dis_p6g(:,1),dis_p6g(:,2),'b-')
plot(dis_lg(:,1),dis_lg(:,2),'k:')
plot(dis_3g(:,1),dis_3g(:,2),'m-')
plot(dis_5g(:,1),dis_5g(:,2),'r:')
plot(dis_7g(:,1),dis_7g(:,2),'b-')
plot(dis_9g(:,1),dis_9g(:,2),'k:')

set(gca,'XLim',[27.5 32.5]), xlabel('Frequency (Hz)')
set(gca,'YLim',[0 3.5]), ylabel('Displacement Magnitude (in)')
h = legend('0.2g','0.6g','1.0g','3.0g','5.0g','7.0g','9.0g',1);
set(h,'Interpreter','none');
title('Plot of x=5.5" Displacement vs Frequency for 6" length 4ply
Carbon Fiber Beam')

```

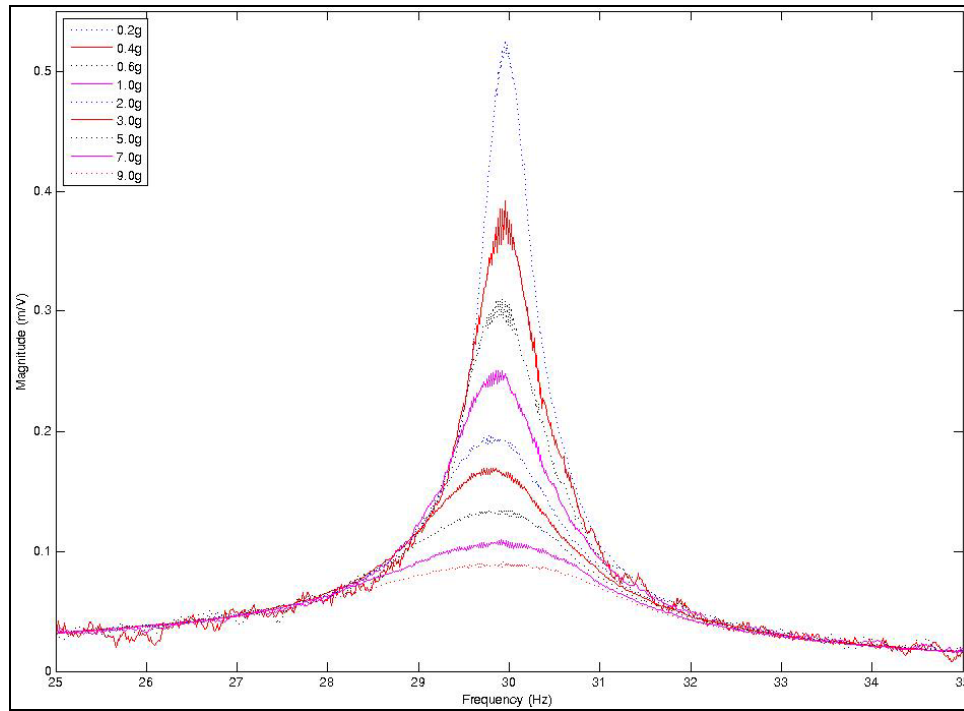


**Figure 83: Displacement Transfer Function of Carbon Epoxy Beam Tip – 10 Hz Bandwidth**

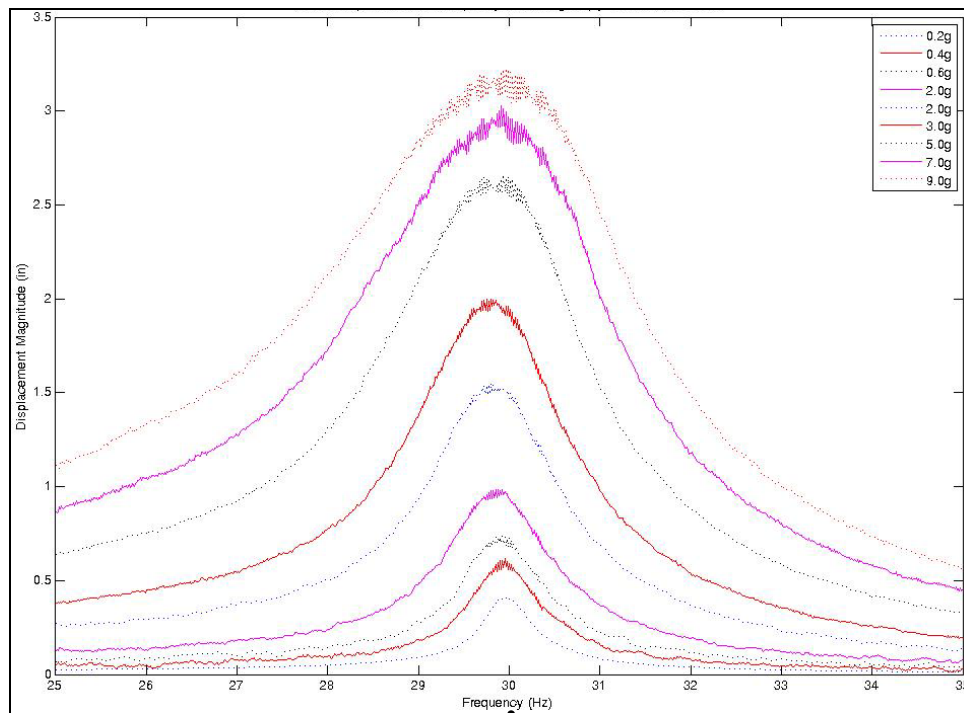


**Figure 84: Displacement Frequency Spectrum of Carbon Epoxy Beam Tip – 10 Hz Bandwidth**

#### A.4 Matlab Code to Plot PSV Phase Plots

```
% This section generates phase plots for 0.2g's to 3.0g's

load original_phase_arrays

figure(1); plot(test_phase_p2g(:,1),test_phase_p2g(:,2),'r:'), hold on
plot(test_phase_p6g(:,1),test_phase_p6g(:,2),'b-')
plot(test_phase_1g(:,1),test_phase_1g(:,2),'k:')
plot(test_phase_3g(:,1),test_phase_3g(:,2),'m-')

set(gca,'XLim',[27.5 32.5]), xlabel('Frequency (Hz)')
set(gca,'YLim',[-200 200]), ylabel('Phase Angle (deg)')
h = legend('0.2g','0.6g','1.0g','3.0g',2);
set(h,'Interpreter','none');
title('Plot of x=5.5" velocity transfer function phase shift for 6"
length 4ply Carbon Fiber Beam')

% This section generates phase plots for 3.0g's to 9.0g's
figure(2); plot(test_phase_3g(:,1),test_phase_3g(:,2),'m-'), hold on
plot(test_phase_5g(:,1),test_phase_5g(:,2),'r:')
plot(test_phase_7g(:,1),test_phase_7g(:,2),'b-')
plot(test_phase_9g(:,1),test_phase_9g(:,2),'k:')
set(gca,'XLim',[27.5 32.5]), xlabel('Frequency (Hz)')
set(gca,'YLim',[-200 200]), ylabel('Phase Angle (deg)')
h = legend('3.0g','5.0g','7.0g','9.0g',2);
set(h,'Interpreter','none');
title('Plot of x=5.5" velocity transfer function phase shift for 6"
length 4ply Carbon Fiber Beam')
```

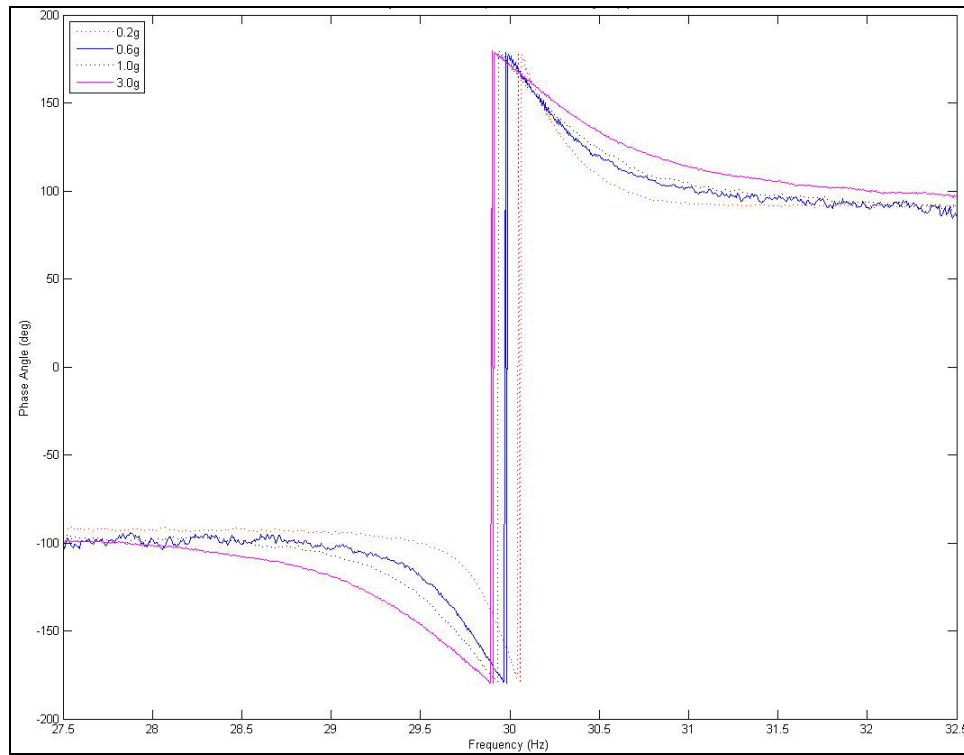
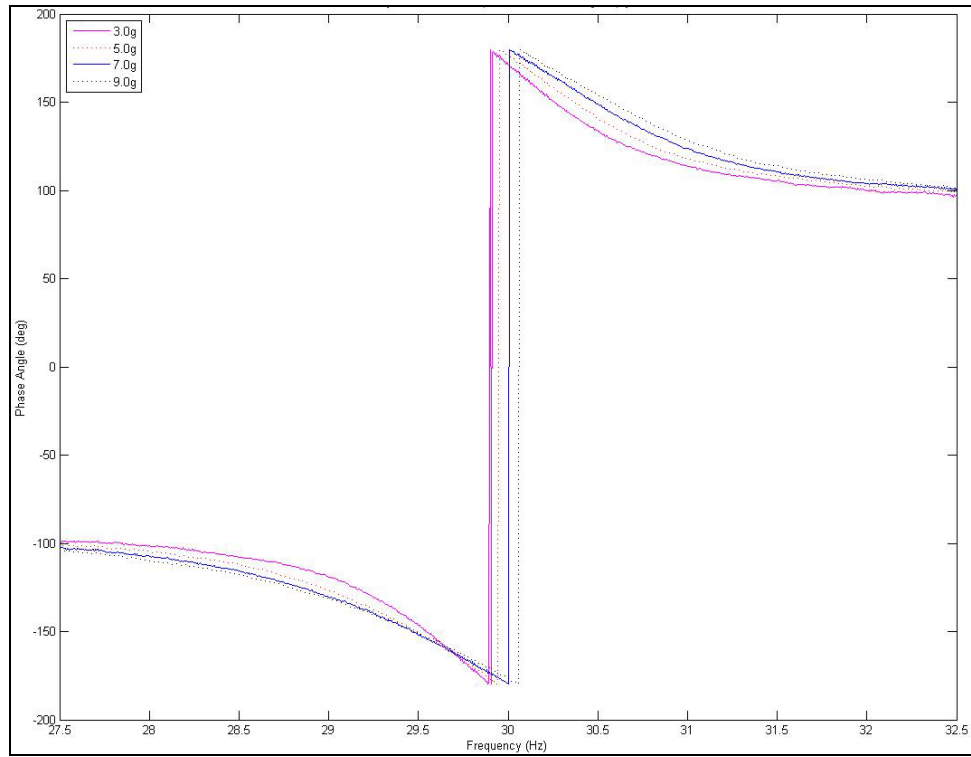


Figure 85: Velocity Transfer Function Phase Shift - 0.2g-3.0g Tests of Carbon Epoxy Beam Tip





**Figure 86: Velocity Transfer Function Phase Shift - 3.0g-9.0g Tests of Carbon Epoxy Beam Tip**

### A.5 Matlab Code to Plot Vibrometer & Accelerometer FRF Comparison

```
% This program will plot the FRF comparison of the accelerometer data
collection vs the laser vibrometer data collection

% converts velocity transfer functions to acceleration by multiplying
by jw, then converting to radians, and then by multiplying an arbitrary
% constant of "5"

clear; clc;

load 1g.mat
H1_2__1g=abs(H1_2);
for i=1:201
    H1_3(i,2)=H1_3(i,2).*(j*H1_3(i,1)*pi/180)*5;
end
H1_3__1g=abs(H1_3);
clear H1_2 H1_3 ChanName ChanNum DP_Info Sensitivity SerialNo Unit

load 3g.mat
H1_2__3g=abs(H1_2);
for i=1:201
    H1_3(i,2)=H1_3(i,2).*(j*H1_3(i,1)*pi/180)*5;
end
H1_3__3g=abs(H1_3);
clear H1_2 H1_3 ChanName ChanNum DP_Info Sensitivity SerialNo Unit

load 5g.mat
H1_2__5g=abs(H1_2);
for i=1:201
    H1_3(i,2)=H1_3(i,2).*(j*H1_3(i,1)*pi/180)*5;
end
H1_3__5g=abs(H1_3);
clear H1_2 H1_3 ChanName ChanNum DP_Info Sensitivity SerialNo Unit

figure(1); plot(H1_2__1g(:,1),H1_2__1g(:,2),'r:'), hold on
plot(H1_3__1g(:,1),H1_3__1g(:,2),'r-')
plot(H1_2__3g(:,1),H1_2__3g(:,2),'b:')
plot(H1_3__3g(:,1),H1_3__3g(:,2),'b-')
plot(H1_2__5g(:,1),H1_2__5g(:,2),'k:')
plot(H1_3__5g(:,1),H1_3__5g(:,2),'k-')
set(gca,'XLim',[16 26]), xlabel('Frequency (Hz)')
set(gca,'YLim',[0 120]), ylabel('Magnitude (m/s/V)')
h = legend('1g accel', '1g laser',...
    '3g accel', '3g laser', '5g accel', '5g laser',2);
set(h,'Interpreter','none');
title('Comparison of Laser Vibrometer vs Accelerometer Methods')
```

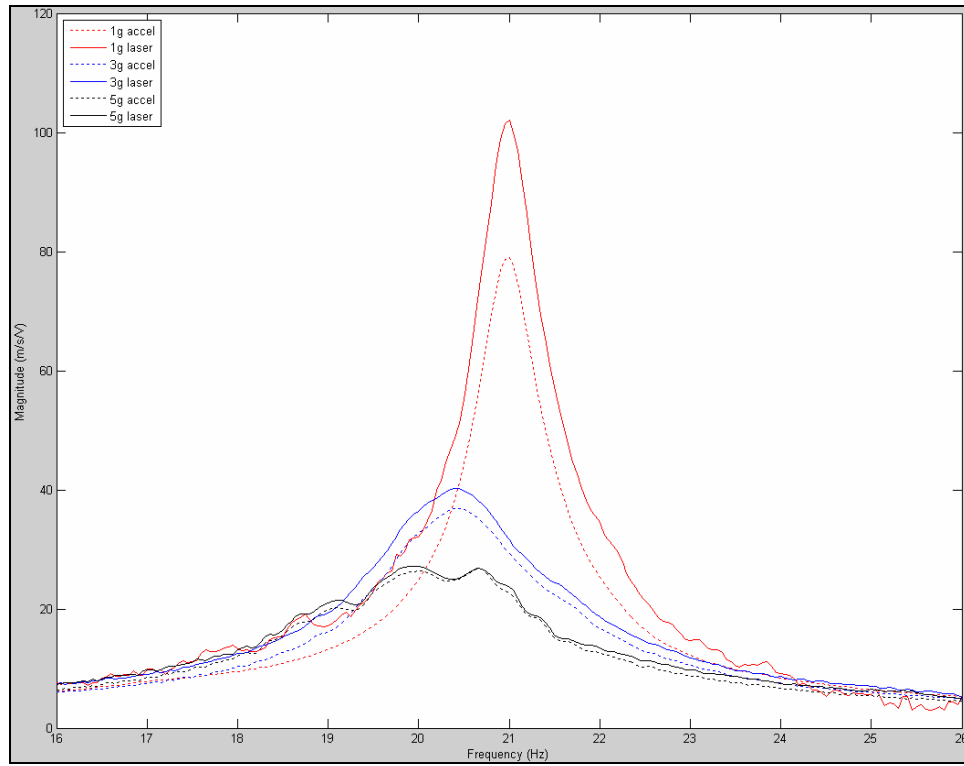


**Figure 100: Transfer Function Comparison of Vibrometer and Accelerometer Methods**

## Appendix B

This appendix details how one can create and analyze the modal information of a composite beam or plate using the ABAQUS finite element analysis software.

### **Part Module:**

Create Part – be sure to select 3-D modeling space, deformable type, and the base features of shell shape and planar type, as indicated.

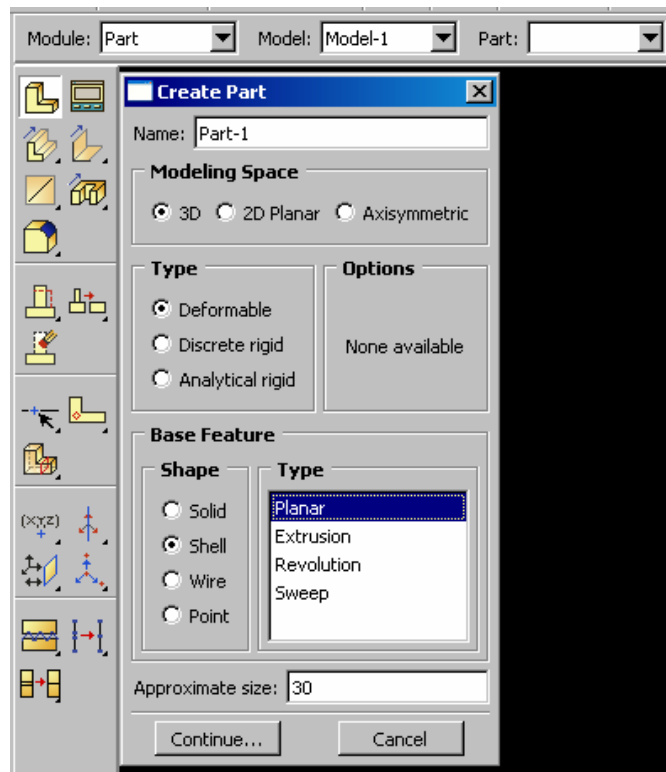


**Figure 103: ABAQUS Part Creation Tool**

## Draw 2-D shape and add dimensioning

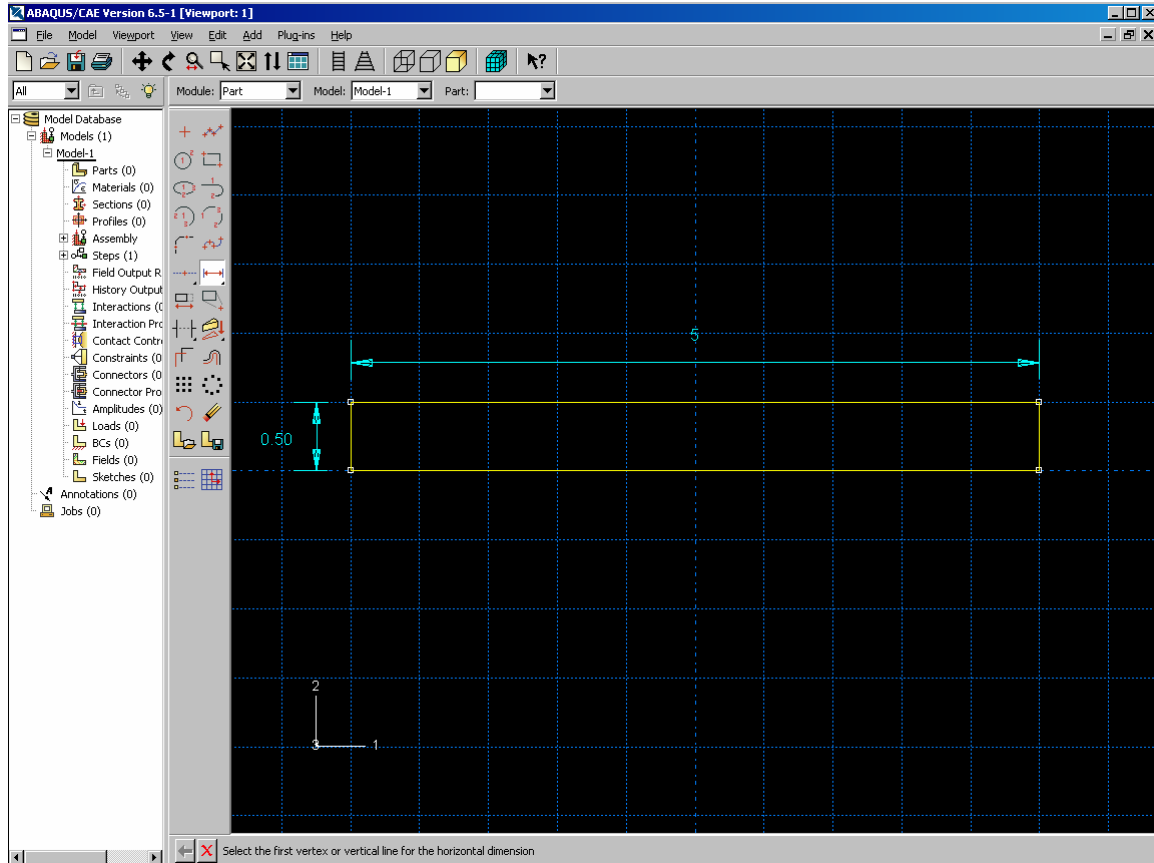


**Figure 104: ABAQUS Part Drawing**

Select “Done” to finish part

### **Property Module:**

Create material properties as appropriate using “Create Material” tab

- First enter a mass density, if you have a mass density in units of (lb/in<sup>3</sup>), be sure to make conversion to the mass units used by Abaqus. To do this divide by 384.
  - o For example, T300/5208 Laminate density is 0.056 lb/in<sup>3</sup>. To use with Abaqus you must divide by 384... which gives 1.46E-4

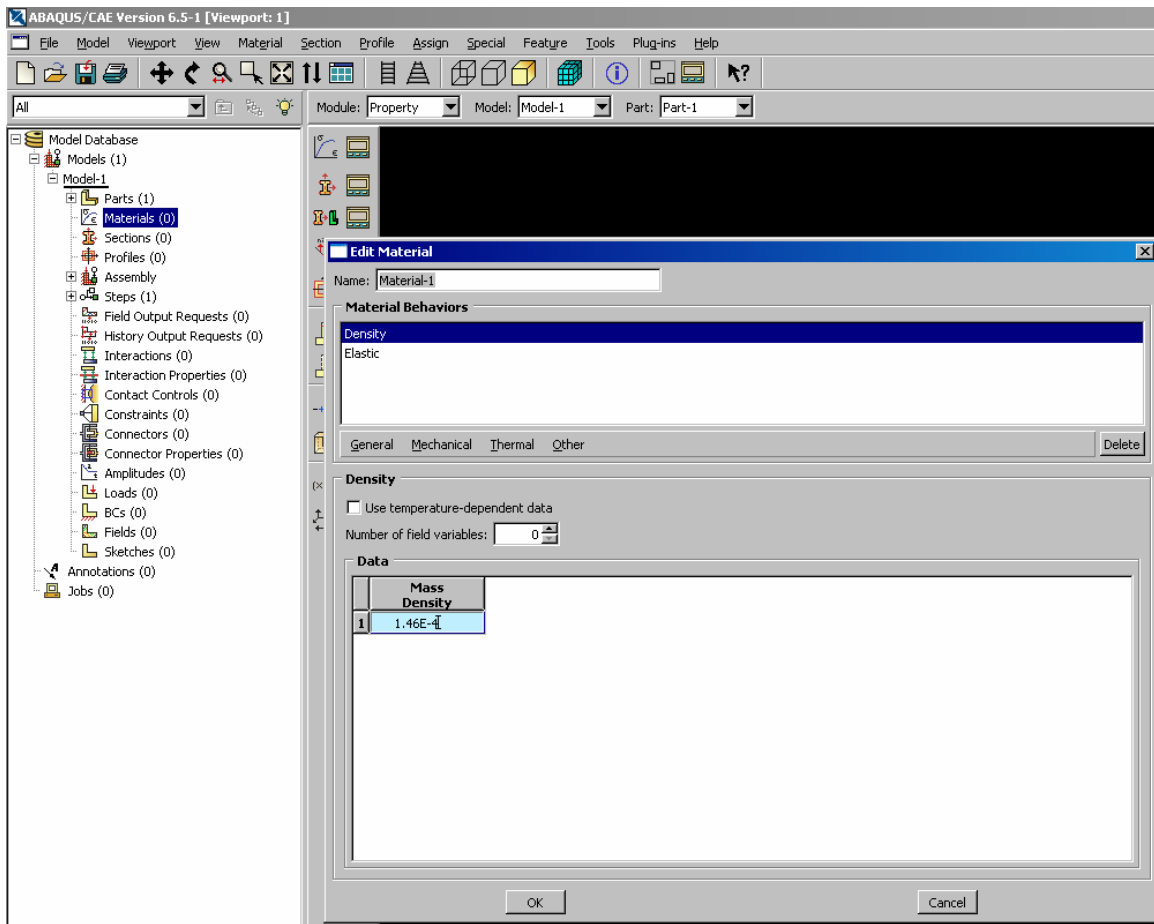


Figure 105: ABAQUS Material Density Editor

Next select the tab for Mechanical-Elasticity-Elastic. Change the Elastic type to lamina.

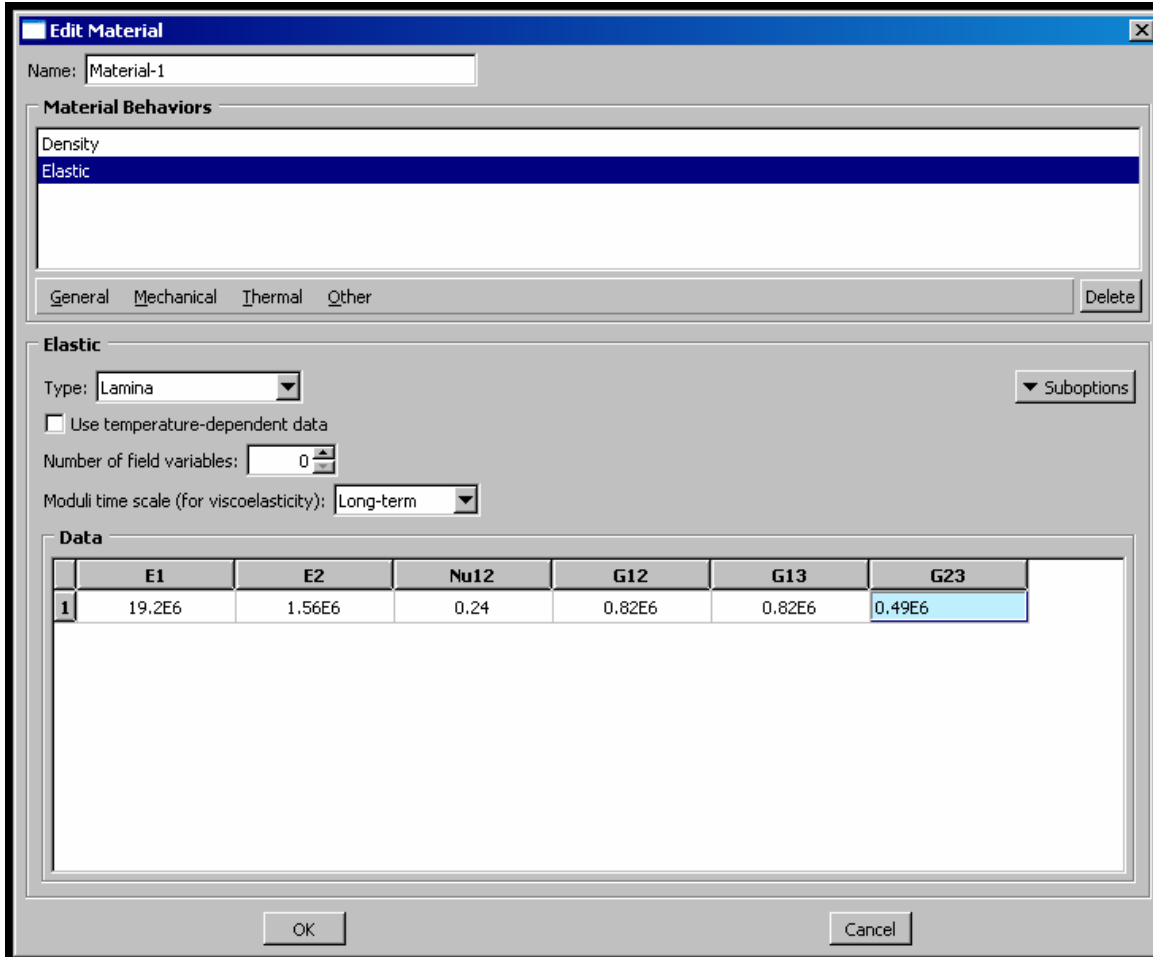


Figure 106: ABAQUS Material Elastic Properties Editor

Create section using the shell/composite option

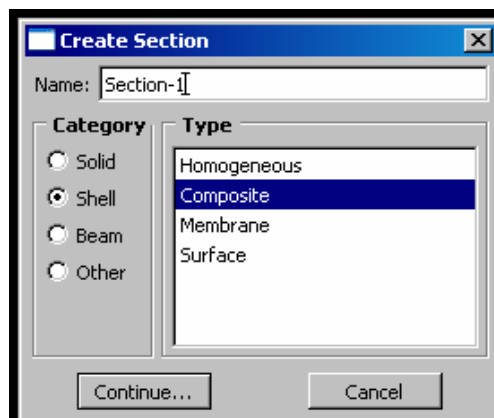
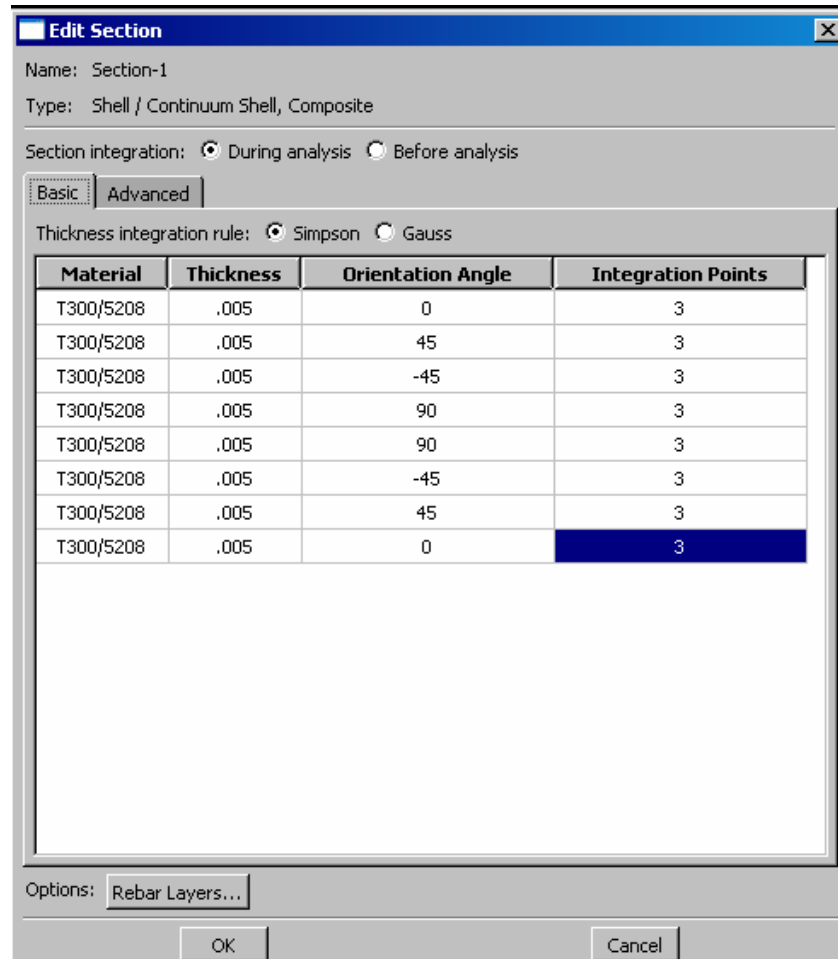


Figure 107: ABAQUS Section Creation

Select Continue

Next select the material type you just created (or another if you have multiple material types in the material), enter the thickness (make sure units correct, this example uses inches), and enter orientation angle.



**Figure 108: ABAQUS Section Editor**

Select “Assign Section” and click on the object to be assigned the properties that you have just finished defining. Select appropriate section (this example only uses one section, which is made up of 8 composite layers) and select “OK”



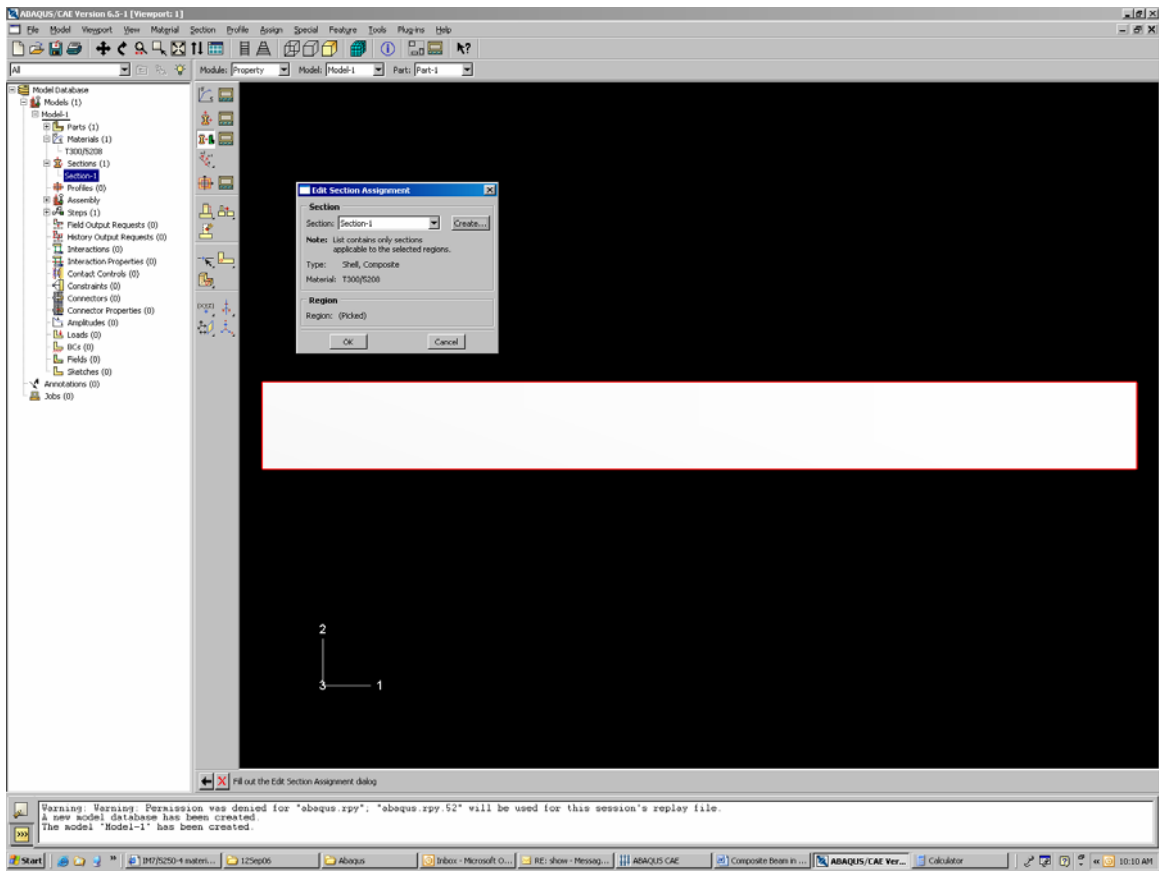


**Figure 109: ABAQUS Section Assignment Tool**

If the beam or plate is made up of multiple differing composite material layers, repeat this procedure for each layer. The entire beam should appear green once all the portions of the geometry have been assigned a section. Select “Done” when finished.

**Assembly Module:**

Select “Instance Part” and insure the “Independent (mesh on instance)” box is selected.

Select “OK”

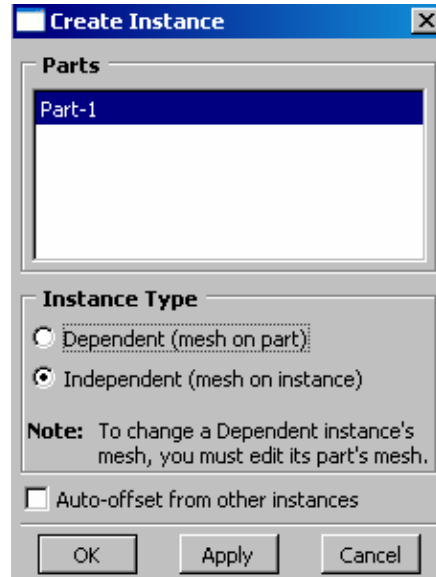


**Figure 110: ABAQUS Instance Creation**

**Step Module:**

Select “Create Step” and then “Linear Perturbation” under procedure type and then select “Frequency” and “Continue”

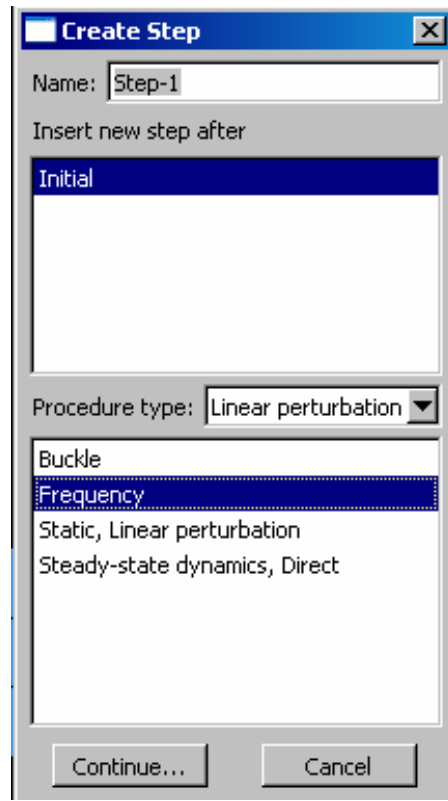


**Figure 111: ABAQUS Step Creation**

Select “Value” and type in the number of natural frequencies desired. Select “OK”

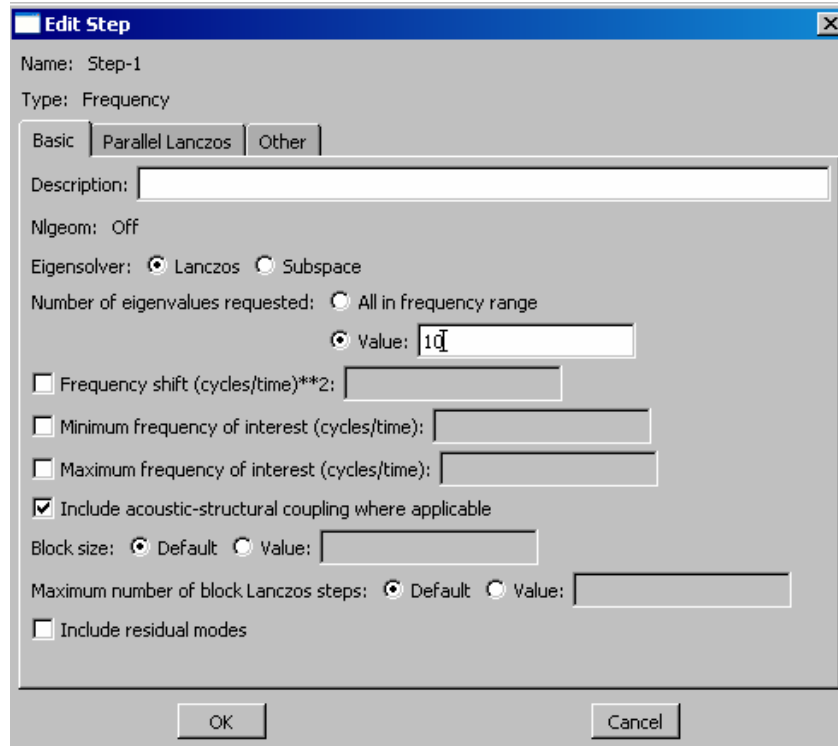


Figure 112: ABAQUS Step Editor

### **Load Module:**

Select “Create Boundary Condition” and chose “Symmetry/Antisymmetry/Encastre”

select continue and then select appropriate boundary that you are trying to constrain.



Figure 113: ABAQUS Boundary Condition Creation

Select “Done” when finished, then chose the desired boundary condition and select “OK”

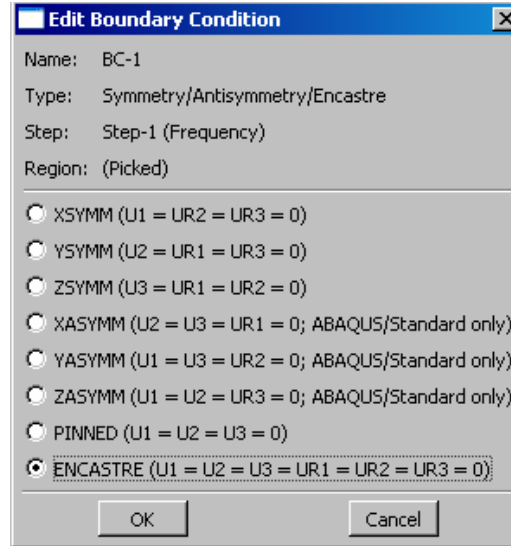


**Figure 114: ABAQUS Boundary Condition Editor**

Abaqus will then show arrows designating the fixed degrees of freedom



**Figure 115: ABAQUS Boundary Condition Designation**

### **Mesh Module:**

Select “Seed Part Instance” and chose an “Approximate global size”, select “OK”

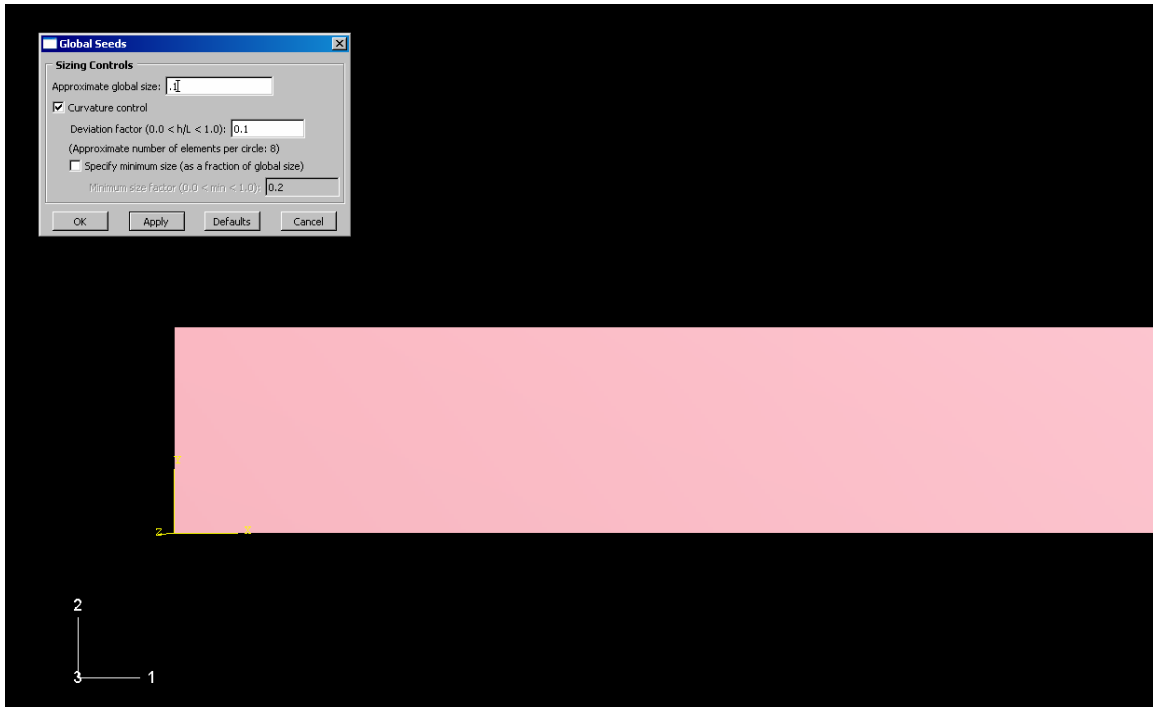


**Figure 116: ABAQUS Global Seed Control**

Next select “Assign Element Type”



**Figure 117: ABAQUS Assign Element Type**

Choose “Shell” family and leave other options at their defaults

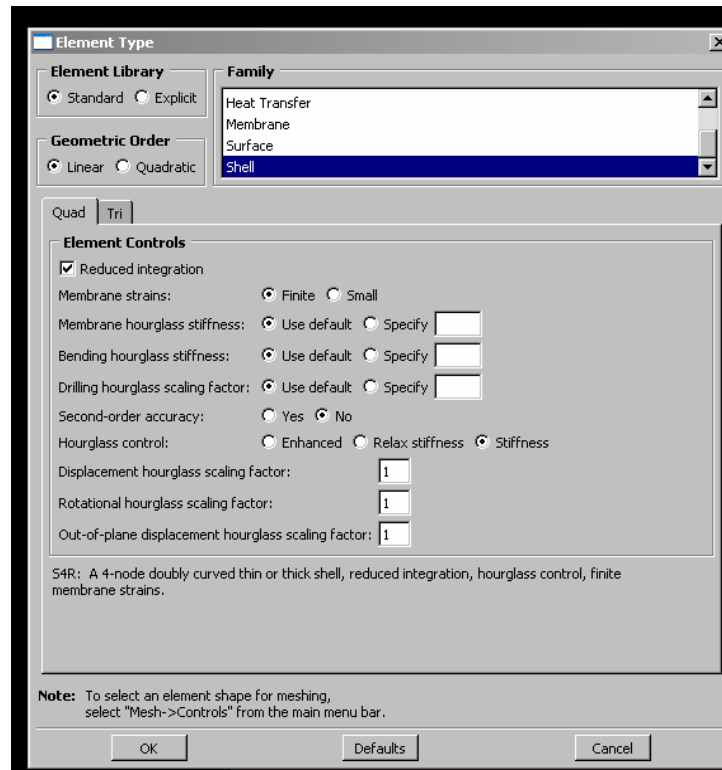


**Figure 118: ABAQUS Element Type Editor**

Select “Mesh Part Instance” and select “Yes” at the bottom of the window

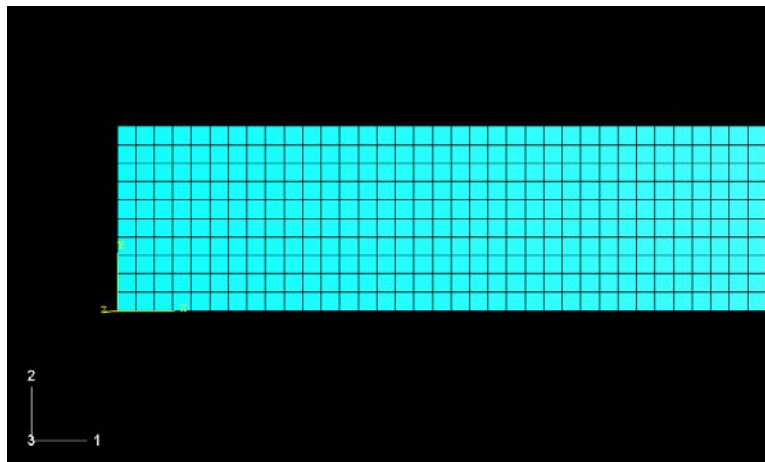


**Figure 119: ABAQUS Mesh Part Instance**

**Job Module:**

Select “Create Job”

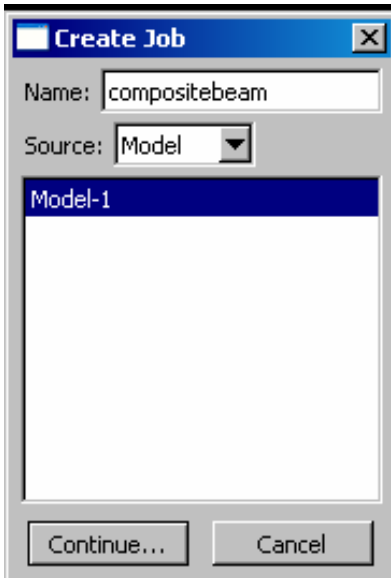


**Figure 120: ABAQUS Create Job Toolbox**

Select “Continue” and accept default settings.

Select “Job Manager” and select “Submit”

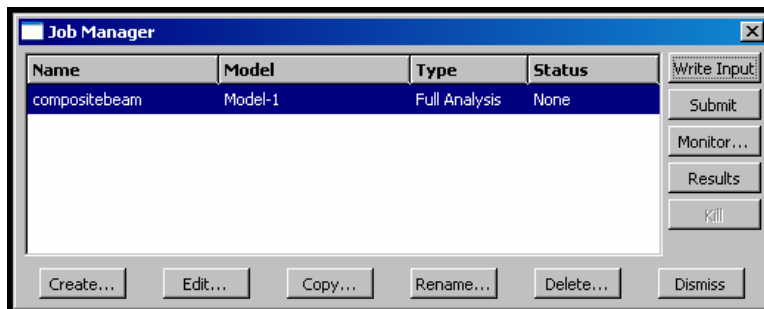


**Figure 121: ABAQUS Job Manager**

Once the job has completed successfully select “Results” from the “Job Manager” dialog box to view the frequency results

Select the “Plot Contours” button to see the mode shapes (the color scale in this example is vertical displacement). Use arrows at the bottom of the window to view all of the different frequencies and mode shapes.



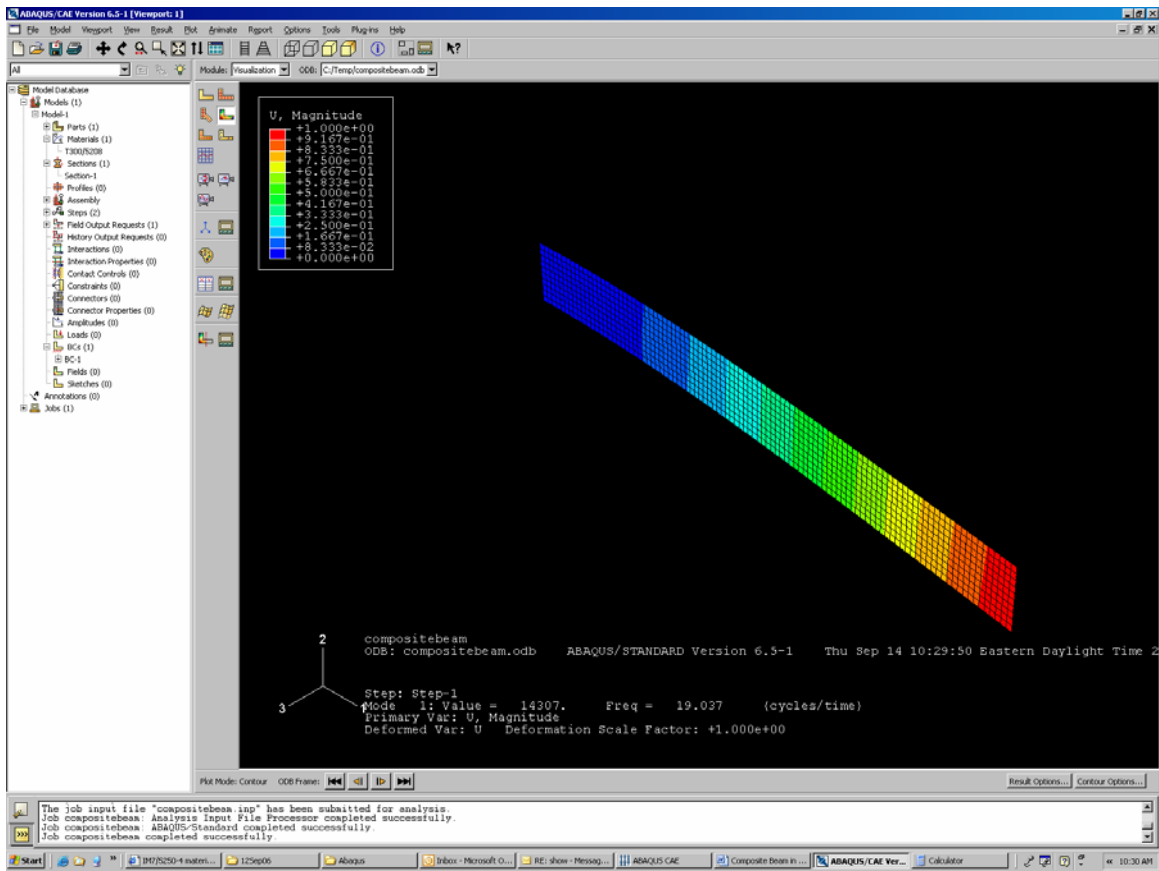


**Figure 122: ABAQUS Relative Displacement Plot of 1<sup>st</sup> Bending Mode**

**\*\*In order to see the stresses, forces, displacements, strains, or many other outputs, return to the “Step” module and select “Create Field Output”**

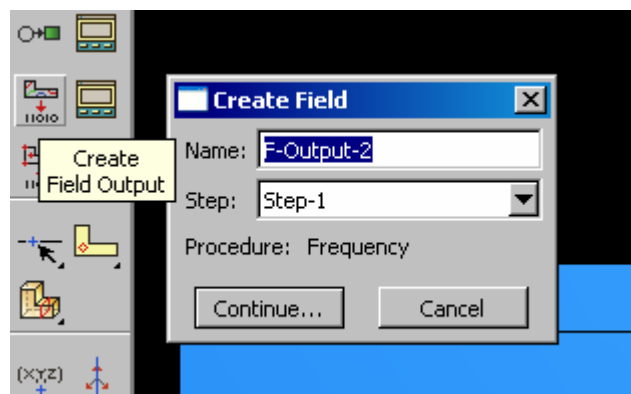


**Figure 123: ABAQUS Field Creator**

Select “Continue” and then chose desired outputs and select “OK”

For this example I have chosen Stresses as the additional output.

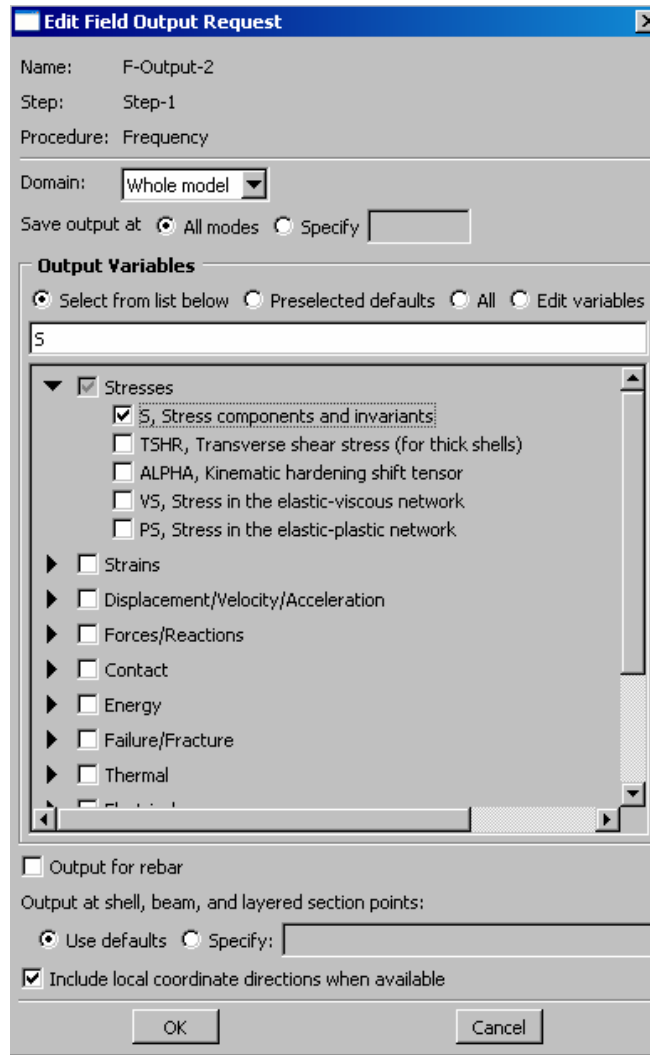


**Figure 124: ABAQUS Field Editor**

The go back to the “Job” module and resubmit the job. Select “Results” and then the “Plot Contours” tab to view the stress through the thickness of the composite.

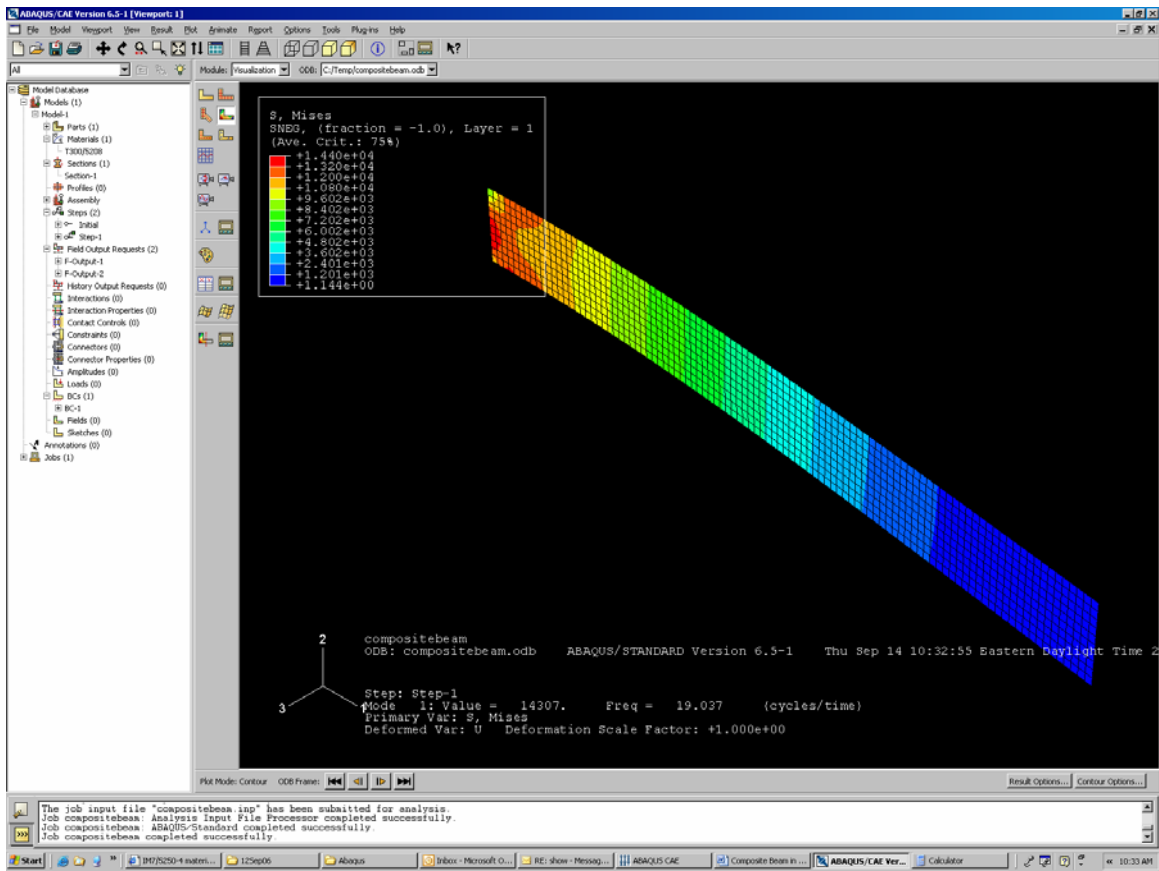


**Figure 125: ABAQUS Stress Contour Plot**

Scroll through the mode shapes the same way as described above to see the effects of varying the material properties through the thickness of the material.

Abaqus help was referenced in order to create this section. The Chapter 7 Linear Dynamic Abaqus reference test should be consulted for further help or explanation of steps.

## Appendix C

### Step-by-step instructions for the 3-D Laser Vibrometer

Note: This list of procedures is provided as a guide to aid a person needing to learn to use the Polytec Scanning Laser Vibrometer (PSV). These instructions are very thorough, but may have left out information pertinent to specific test requirements. Please also be sure to reference the Polytec Software, Hardware, and Theory Manuals, as well as the PSV 3-D Quick Start Guide, as needed in support of your testing.

#### BASIC SETUP FOR 3-D TESTING

1. Turn on PSV computer
2. Turn on the 3 vibrometer controller boxes
3. Open PSV 8.3 Program using icon on the desktop
4. Open the laser and camera lens covers on all three vibrometer scanning heads
5. Set up vibrometers to a height approximately level with the object being tested
6. The scanning head with the operating video camera should be positioned in the center
7. Select *Acquisition Mode* (a red starburst icon) in the PSV Program
8. Make sure the *Toggle Scanning Head* icon to the right of *Acquisition Mode* is selected
9. On the far right of the screen is the optics toolbox, make sure that all 3 lasers are checked on
10. Click the center button in the optics toolbar to center the laser's position
11. Adjust all 3 scanning heads manually so that the lasers point to the center of the object being tested
12. Make sure the *top* scanning head camera is zoomed out completely and the object to be scanned is in the center of the picture on the monitor, then autofocus the camera using the button in the optics toolbox
13. Now zoom in the focus of the camera using the *focus* bar in the optics toolbox, so that the object being tested now takes up the full area (width and/or height) of the monitor picture.
14. Autofocus the camera
15. Ensure that all 3 lasers are still positioned in the center of the object being tested
16. Click the autofocus button for each of the lasers (designated *AF* in the optics toolbox). To select each laser to autofocus one at a time, you must use the *Scanning Head* pull down menu in the optics toolbox and choose Top, Left, and Right. You may also autofocus all 3 lasers at once by holding down the *Shift* key and left clicking on *AF*.
17. If you would prefer to zoom in further at this point to a specific area of the item being tested, you may use the zoom "magnifying glass" icon. You can zoom in and out with the magnifying glass icons without affecting the focus of the camera. Think of it as doing the same as the zoom feature in Microsoft Word.
18. At this point the basic setup is complete. Next is the 2-D Alignment.

## 2-D ALIGNMENT

1. Even though you will be doing a 3-D test, you must first always do a 2-D (standard) Alignment.
2. Before aligning, right click on the screen and select *Delete All* to delete all previously stored alignment points
3. Before moving the lasers, decide on 4-10 alignment points for each head. If the object is relatively basic, such as a flat beam or plate, 4-6 points may be used. If it is complex, such as a 3-D wing, 8-10 points should be used.
4. Now shut off 2 of the 3 lasers by unchecking the respective *Laser* box in the optics toolbox
5. Make sure the remaining “on” laser is the one toggled in the *Scanning Head* pull down menu
6. Use the center button on the mouse to move the laser to the first alignment point
7. Autofocus the laser and then left click with the cursor centered exactly over the laser spot
8. Repeat steps 6 and 7 for the other two Scanning Heads (remember to switch lasers by using the *Scanning Head* pull down menu)
9. Now repeat steps 6-8 for all remaining alignment points
10. Once you have defined all of your 2-D alignment points, select the 2-D alignment icon again to close the alignment. If the alignment is successful, it will close uneventfully; otherwise you will receive a message telling you the alignment did not succeed. Redo or perhaps add more alignment points.
11. This completes the 2-D alignment

## 3-D ALIGNMENT

1. First, determine the coordinate system you would like to use. For example:

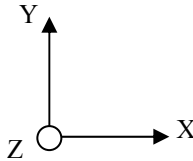


**Figure 33: 3-D Alignment Coordinate Axes**

2. Click on the *3-D Alignment* icon on the top toolbar
3. Make sure *Auto* is checked “on” in the 3-D Alignment toolbox
4. Turn on all 3 lasers using the optics toolbox
5. Choose *Origin, Axis, Plane* as the Coordinate Definition Mode in the 3-D Alignment toolbox
6. For now, set the target quality to 0.3mm
7. Choose *Set New Alignment Point* in the toolbox
8. Now move all 3 lasers to the chosen origin and autofocus them all

9. Wearing the green glasses, use the remote control to position all 3 lasers on exactly the same spot
  - a. For the remote control: Having the *Grid Mode* selected and pressing the *up* arrow switches lasers; Using *Free Mode* combined with the four directional arrows moves the selected laser around.
10. Once all 3 lasers are at the same point, make sure the top scanning head is selected and then position the cursor directly onto the center of the laser spot, and left click
11. Now change to the left scanning head and click directly on the laser alignment point
12. Do the same with the right scanning head
13. Right click on the alignment point and select *Origin* from the menu bar that pops up
14. The first alignment point has been created
15. Now move the 3 lasers to the next chosen alignment point, such as a point on the +x-axis, and autofocus them again
16. Repeat steps 9-12, and when complete, right click on the alignment point and select the appropriate coordinate definition, such as +x-axis
17. Repeat this process with a minimum of 4 and maximum of 7 total alignment points. Similar to the 2-D alignment, the number chosen depends upon the complexity of the object being tested. When in doubt, choose 7. This just takes about 5 more minutes than choosing 4.
18. It is a good idea to make the 3<sup>rd</sup> alignment point one such as +x/y
19. All remaining alignment points should be labeled *Alignment Point* when defined by step 13
20. Once all alignment points have been defined, select *Calculate* on the 3-D Alignment toolbox. If the target quality is not within your chosen desired quality (0.3mm), you have two choices:
  - a. Either redo the entire 3-D alignment and try to be more accurate with your alignment, reduce exterior lighting, coat the object being tested in case it is shiny
  - b. Or, increase the value of the target quality and re-click *Calculate*
21. When finished, go to the top menu bar *Setup* and click *Align 3-D Coordinates* to finish

## CREATE GRID

The grid establishes the grid points across the entire shape of your object. In the 3-D laser scan, all of the points that you have defined will be used. The more grid points, the longer the duration of a test scan, but the better your results will be.

1. Select the grid creation icon to begin
2. Another toolbar pops up
3. Select the *Professional* icon
4. Determine which shape you would like to use to define the grid for your object
5. Experiment with the different shapes to learn how to create different grids
6. Know that if your object is not perfectly level, you can rotate the grid object
7. Change the density of the grid points as desired
8. Once you have created a grid, uncheck the grid creation icon

## GEOMETRY SCAN

1. Go to the scan menu and choose *Geometry Scan*
2. A laser will jump to all grid points to scan the item's geometry
3. If the test goes well, you will get a message that *Geometry Scan Succeeded*, otherwise, go back to the grid creation tool and make any necessary changes. Sometimes points created may inadvertently not actually be on the object.
4. When finished with the geometry scan, select *Assign Focus Fast* or *Assign Focus Best* depending upon which you prefer
  - a. Assign focus fast is great for simple planar objects that are made of the same material, such as an aluminum plate
  - b. Assign focus best is desirable when an object has multiple surface properties and/or is a complex 3-D shape. Keep in mind that depending upon the number of grid points you have, assign focus best can take a long time.
5. Once this is complete, you are ready to begin testing.

## ACQUISITION BOARD SETTINGS AND TESTING

A basic introduction into some common A/D settings will be provided in these instructions. Of course the software offers many features and one should consult the PSV Software and Theory as needed to determine the features most appropriate for their testing.

1. Connect the amplifier to your tester (shaker or horn). Use the blue sided APS Dynamics amplifier for the shaker
2. Turn on the amplifier, make sure the switch is on voltage and the small dial is turned counterclockwise until it stops
3. Click the A/D icon on the computer
4. There are 9 different tabs ranging from *General* to *Generator*, begin with *General*
5. For an initial test, always choose the measurement mode *FFT*
6. If you choose to use complex averaging, 3 is a good choice
7. In the *Channels* tab, make sure the channels *Vibrometer 3-D* and *Reference 1* are checked *active*
8. In the *Filters* tab, if you don't want to use a filter, select *no filter*
9. In the *Frequency* tab, select the desired Bandwidth and range, the smaller Bandwidth the more precision in the test. Use a range corresponding to the frequency range you will be testing
10. The FFT lines improve test results, more lines = slower test
11. The *Window* tab may be left at *Rectangle Functions* if desired
12. The *Trigger* tab may be left off
13. *SE* tab is speckle tracking, select it on and choose Fast
14. The *Vibrometer* tab defines the velocity range. If the amplitude is too great, the software will indicate *over range*. Also, there is a light on the front of all 3 control boxes that must be watched for over ranging as well. Adjust the velocity range so that no over ranges occur. If the max velocity range is chosen and the test still over ranges, you must reduce the test amplitude.

15. The *Filters* tab may be left as Off/1.5MHz/Off
16. Now select the *Generator* tab
17. Check the box *Active* and choose the waveform desired. For initial scans, a sweep or chirp waveform are common, but many others are available
18. If applicable, define the *Start* and *End frequency range* and the *Sweep Time*. Keep in mind that the Sweep Time may be kept similar to the sample time found in the *Frequency* tab.
19. Choose the lowest possible amplitude of 0.05V initially, and increase from there. Remember that you have turned the amplitude dial off on the amplifier and when you turn the generator on you must increase the amplification, otherwise nothing will happen
20. When finished making changes to the Acquisition Settings, select *OK*
21. Next, turn on the generator using the icon that looks like a sine wave. Remember to turn up the amplitude on the amplifier to that desired
22. To perform sample tests, turn on the *Continuous* icon. An analyzer window pops up and you should see a graph of velocity vs. time
23. If you would like to see velocity vs frequency (FFT), select the far left icon in the analyzer window and choose *FFT*
24. Experiment with the different icons in the analyzer to see what is available
25. The far right icon is an *Auto Scale* feature that will zoom in/out your graph to create the best fit
26. When you are satisfied with your scan samples, you are ready to run a scan test
27. Choose either the *Single Shot* or the *Scan* icon
  - a. Single Shot only looks at one specific point and provides the same results you see in the continuous scan sampling done previously
  - b. Scan tests all grid points for the desired frequency or frequency range
28. When finished a message will popup saying that the scan is complete and the total of time that the scan took to complete
29. Now you may go to the presentation mode to see the results of your scan

## PRESENTATION MODE

1. Toggle into presentation mode by selecting the *Presentation* icon
2. Experiment with the choices in presentation mode
3. To see the frequencies of the different modes for your object, select the top left *Change View* icon and choose *Average Spectrum*
4. To choose only the frequency peaks, select the *Frequency Bands* icon
5. Using the mouse, drag and select a tight range around each given frequency peak
6. The peaks will be automatically calculated in a *Frequency Band Definition* toolbox
7. When finished, click the top right X on that toolbox to close it
8. A message pops up saying "Band Definition Changed", select *Yes*
9. Now the pull down *Frequency Band* toolbar has the peaks that you found
10. Choose the one that you wish to see



11. Now the animation may be played to see what happens at the respective frequencies. Feel free to look at the *X, Y, Z* directions together or separate. You may also zoom and rotate the animation as desired
12. Animations and graphics may be saved using the *File* pull down menu
13. If you would like to look at raw data for all frequencies tested, you may export an ASCII or Universal file. Here you will see all velocity magnitudes and their corresponding frequencies

## Appendix D

This appendix is responsible for covering the various acquisition settings available to the user. The *General* acquisition settings consist of measurement mode and averaging options, as seen in Figure 126.

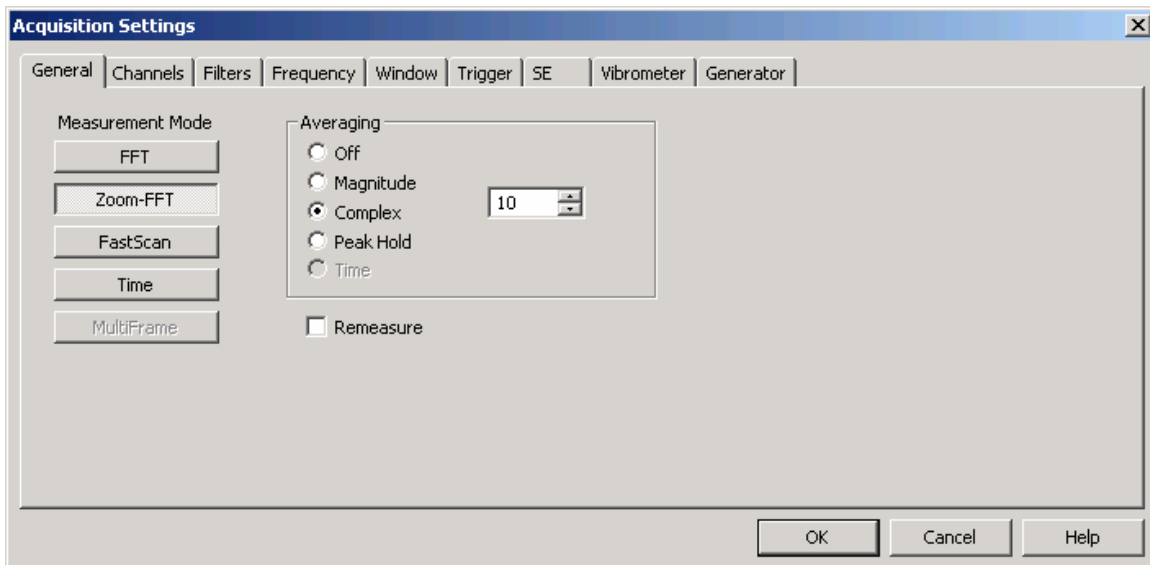


**Figure 126: Acquisition General Settings**

Throughout the course of testing for this project, the Fast Fourier Transform (FFT), Zoom-FFT and FastScan measurement modes were used on many occasions. Complex averaging was also used extensively throughout the testing. The FFT measurement mode conducts vibration analysis over a user defined range of frequencies. This option can be used to determine approximately the modal frequencies of an object. If the modal frequencies are already known, or if a basic FFT test has already been accomplished, the user may choose to conduct a Zoom-FFT test. This measurement mode establishes a center frequency chosen by the user and conducts a vibration analysis around that frequency. Finally, a FastScan may be used to look at one individual frequency. This can be very useful if the user desires to use a greater number of grid points to complete a

more thorough vibration analysis of the structure's respective modal frequencies. A FastScan can be completed in just a fraction of the time when compared to both the FFT and Zoom-FFT methods. If one chooses to use averaging, the signal-to-noise ratio of the frequency spectra can be improved (16:Ch 7.2).

In the Channels toolbox the user can activate the required measurement channels and set their parameters for the data acquisition. The following figure shows the settings required for a test using only the top laser vibrometer. The Direction column allows the user to enter the direction of the vibration. The default setting is +Z, however you can also select another direction as necessary. The direction of the vibrometer channel sets the orientation of the scanning head system. The Range option selects the input voltage range of the data acquisition board for each respective channel. Input coupling of vibrometer channels must be set to DC (16:Ch 7.2).

Channel	Active	Ref	Index	Direction	Range	Coupling	ICP	Quantity	Factor	Unit
Vibrometer Top	<input checked="" type="checkbox"/>	<input type="checkbox"/>		+ Z	10 V	DC	<input type="checkbox"/>	Velocity	1000	mm/s / V
Vibrometer Left	<input type="checkbox"/>	<input type="checkbox"/>		+ Z	10 V	DC	<input type="checkbox"/>	Voltage	1	
Vibrometer Right	<input type="checkbox"/>	<input type="checkbox"/>		+ Z	10 V	DC	<input type="checkbox"/>	Voltage	1	
Reference 1	<input checked="" type="checkbox"/>	<input checked="" type="checkbox"/>		+ Z	10 V	DC	<input type="checkbox"/>	Voltage	1	

**Figure 127: Acquisition Channel Settings**

One sets the frequency spectra parameters in the Frequency toolbox. This toolbox changes to accommodate both Zoom-FFT and FFT measurement modes. Figure 128 displays the options available for a Zoom-FFT test. The center frequency is simply the chosen frequency around which a frequency range will be created. This frequency range determines upon the choice of bandwidth. FFT lines are chosen based upon the desired test resolution. The following formula relates bandwidth (BW), sample time ( $t_{\text{sample}}$ ) and the number of FFT lines ( $n_{\text{FFT}}$ ):

$$t_{\text{sample}} = \frac{n_{\text{FFT}}}{BW} \quad (\text{D.1})$$

If averaging is used, overlap is an option. With overlap you can significantly reduce the time for a measurement, in particular for narrow bandwidths (16:Ch 7.2).

Windowing and trigger options were primarily left at their default setting for this project, so they will not be introduced. When scanning, with Signal Enhancement and Speckle Tracking, you get an approximately even noise level for all scan points (16:Ch 7.2).

The parameters of the controller for data acquisition are set in the Vibrometer toolbox. The measurement range for velocity is set in this toolbox. The beam experiments often required the highest velocity setting of 1000 mm/s/V to keep the tests within acceptable range tolerances.

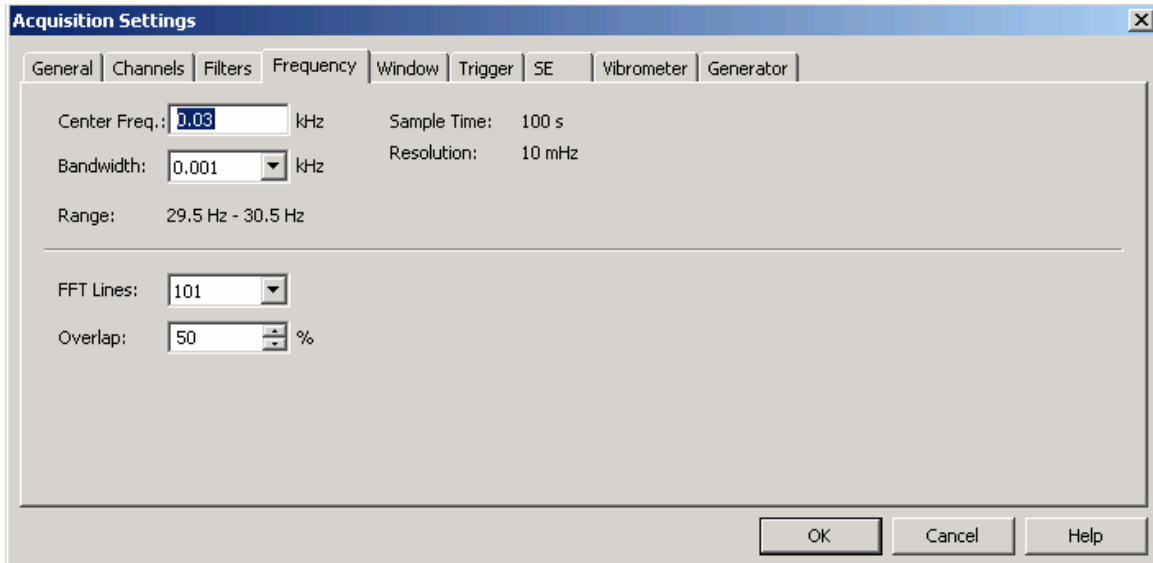


**Figure 128: Acquisition Frequency Settings**

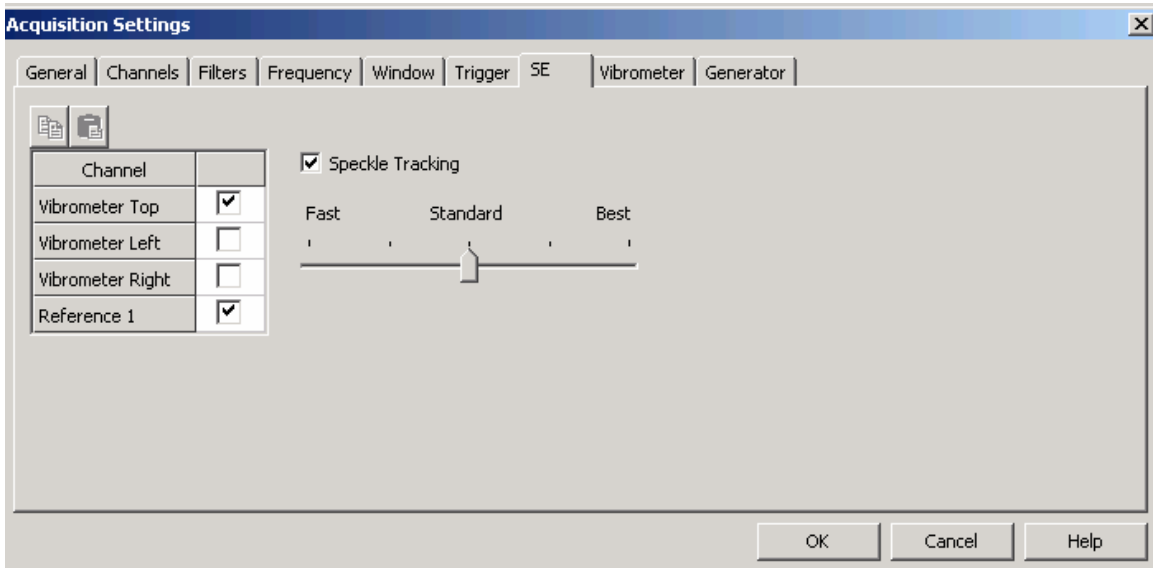


**Figure 129: Acquisition Signal Enhancement Settings**

The remaining acquisition settings are for the use of a function generator. This was the case in this project since a shaker was powered by signals from the laser vibrometer control box. Three waveform types were used throughout this experimentation; pseudo random, sweep, and sine. With pseudo random, sinusoidal signals are emitted to all FFT lines at the same time, but only in the frequency range

defined in the Frequency toolbox. The sweep waveform allows the user to enter the start and end frequencies as well as the sweep time. The sine waveform requires the user to enter only one frequency that will be repeated throughout the duration of the test. The remaining option used in this toolbox is the entry for amplitude. This determines the magnitude in Volts of the signal sent from the PSV Junction Box to the Power Amplifier.

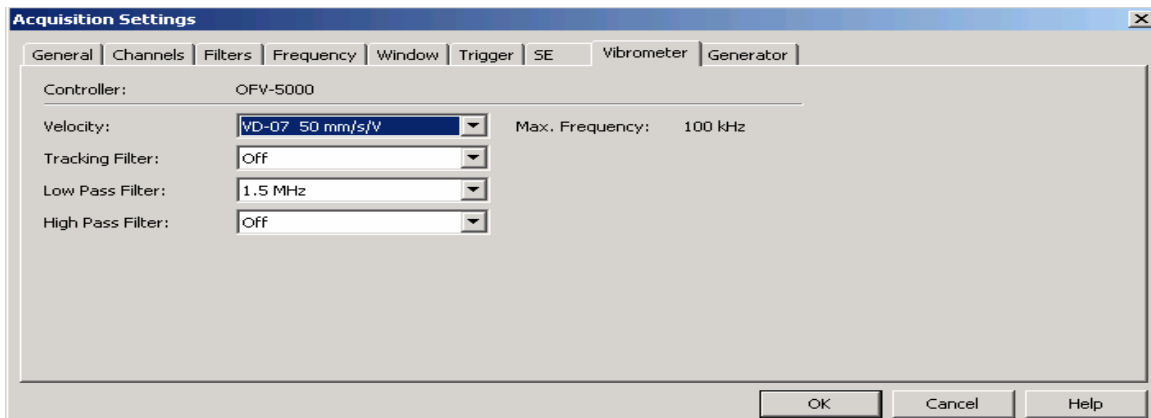


**Figure 130: Acquisition Vibrometer Settings**

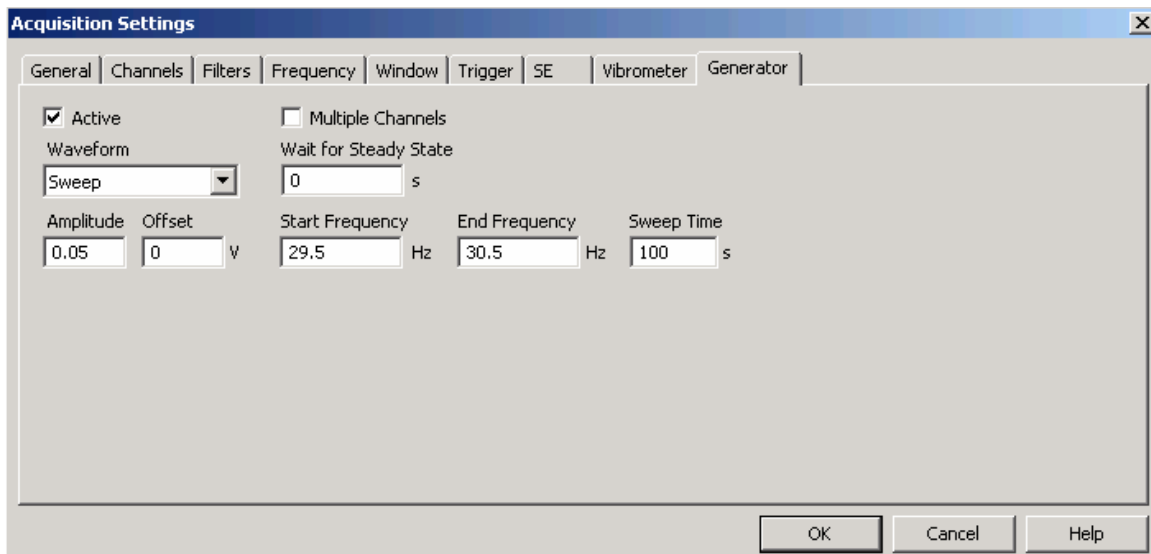


**Figure 131: Acquisition Generator Settings**

## Bibliography

1. Bismarck-Nasr, Maher N. *Structural Dynamics in Aeronautical Engineering*. Reston, Virginia: American Institute of Aeronautics and Astronautics, Inc., 1999.
2. “Dual-Mode Amplifiers.” Excerpt from APS Dynamics company website. <http://apsdynamics.com>. 2007.
3. Elert, Glen. “Frequency of Hummingbird Wings.” Excerpt from website. <http://hypertextbook.com/facts/2000/MarkLevin.shtml>. 2000.
4. “Entomopter Project.” Excerpt from Robert Michelson GTRI website. <http://avdil.gtri.gatech.edu/RCM/RCM/Entomopter/EntomopterProject.html>. 2007.
5. Herkovich, Carl T. *Mechanics of Fibrous Composites*. New York: John Wiley and Sons, 1998.
6. Jones, Kevin D., Chris J. Bradshaw, Jason Papadopoulos, and Max F. Platzer. “Improved Performance and Control of Flapping-Wing Propelled Micro Air Vehicles.” *42<sup>nd</sup> Aerospace Sciences Meeting & Exhibit*, January 2004.
7. Ju, Jaehyung, and Roger J. Morgan. “Characterization of Microcrack Development in BMI-Carbon Fiber Composite under Stress and Thermal Cycling.” *Journal of Composite Materials*, 38(22):2011, 2004.
8. “Laser Basics.” Excerpt from Polytec company website. <http://www.polytec.com>. 2007.
9. Malatkar, Pramod. *Nonlinear Vibrations of Cantilever Beams and Plates*. Virginia Polytechnic Institute, 2003.
10. Meirovitch, Leonard. *Fundamentals of Vibrations*. New York: McGraw Hill, 2001.
11. Michelson, Robert C. and Steven Reece. “Update on Flapping Wing Micro Air Vehicle Research.” 13<sup>th</sup> Bristol International RPV Conference, 1998.
12. “Modal-Test-Excitation.” Excerpt from APS Dynamics company website. <http://apsdynamics.com>. 2007.
13. Nayfeh, A.H., and D.T. Mook. *Nonlinear Oscillations*. New York: Wiley, 1979.
14. Pennycuik, C.J. “Predicting Wingbeat Frequency and Wavelength of Birds.” *Journal of Experimental Biology*, 150:171-185, 1990.
15. Pines, Darryll J. and Felipe Bohorquez. “Challenges Facing Future Micro-Air-Vehicle Development.” *Journal of Aircraft*, 43(2):290-304, 2006.
16. *Polytec Scanning Vibrometer: Software Manual*. Version 8.4. Polytec, Inc. 2007.
17. *Polytec Scanning Vibrometer: Theory Manual*. Version 8.1. Polytec, Inc. 2005.
18. Pratt, David. “Potential AFIT Research Topics.” Air Force Research Laboratory Structural Sciences Division, 2005.
19. Saada, Adel S. *Elasticity*. Malabar, Florida: Krieger Publishing Company, 1993.

20. "Vibrometers." Excerpt from Polytec company website. <http://www.polytec.com>. 2007.
21. "Vibrometry Basics." Excerpt from Polytec company website. <http://www.polytec.com>. 2007.



## **Vita**

Captain Adam P. Tobias graduated from Lyons High School in Lyons, Kansas. He entered undergraduate studies at the University of Kansas in Lawrence, Kansas where he graduated with a Bachelor of Science degree in Aerospace Engineering in December 2000. He was commissioned through Detachment 280 AFROTC at the University of Kansas.

His first assignment was at Sheppard AFB as a student at Euro-NATO Joint Jet Pilot Training in August 2001. In July 2003, he was assigned to the Long Range Missile Systems Group, Eglin AFB, Florida where he served as a systems engineer and an executive officer. While stationed at Eglin, he worked to support the development and testing of the Lockheed Martin Joint Air to Surface Standoff Missile. In August 2005, he entered the Graduate School of Engineering and Management, Air Force Institute of Technology. Upon graduation, he will be assigned to the Air Vehicles Directorate of the Air Force Research Laboratory.

REPORT DOCUMENTATION PAGE				Form Approved OMB No. 074-0188	
<p>The public reporting burden for this collection of information is estimated to average 1 hour per response, including the time for reviewing instructions, searching existing data sources, gathering and maintaining the data needed, and completing and reviewing the collection of information. Send comments regarding this burden estimate or any other aspect of the collection of information, including suggestions for reducing this burden to Department of Defense, Washington Headquarters Services, Directorate for Information Operations and Reports (0704-0188), 1215 Jefferson Davis Highway, Suite 1204, Arlington, VA 22202-4302. Respondents should be aware that notwithstanding any other provision of law, no person shall be subject to an penalty for failing to comply with a collection of information if it does not display a currently valid OMB control number.</p> <p><b>PLEASE DO NOT RETURN YOUR FORM TO THE ABOVE ADDRESS.</b></p>					
1. REPORT DATE (DD-MM-YYYY) 22-03-2007		2. REPORT TYPE Master's Thesis		3. DATES COVERED (From – To) 26-06-2006 – 22-03-2007	
4. TITLE AND SUBTITLE  EXPERIMENTAL METHODS TO CHARACTERIZE NONLINEAR VIBRATION OF FLAPPING WING MICRO AIR VEHICLES				5a. CONTRACT NUMBER	
				5b. GRANT NUMBER	
				5c. PROGRAM ELEMENT NUMBER	
6. AUTHOR(S)  Tobias, Adam, P., Captain, USAF				5d. PROJECT NUMBER	
				5e. TASK NUMBER	
				5f. WORK UNIT NUMBER	
7. PERFORMING ORGANIZATION NAMES(S) AND ADDRESS(S) Air Force Institute of Technology Graduate School of Engineering and Management (AFIT/EN) 2950 Hobson Way WPAFB OH 45433-7765				8. PERFORMING ORGANIZATION REPORT NUMBER  AFIT/GAE/ENY/07-M23	
9. SPONSORING/MONITORING AGENCY NAME(S) AND ADDRESS(ES) AFRL/VASD Attn: Dr. Philip S. Beran Bldg 146, 2210 8th St WPAFB OH 45433 DSN: 785-6645				10. SPONSOR/MONITOR'S ACRONYM(S)	
				11. SPONSOR/MONITOR'S REPORT NUMBER(S)	
12. DISTRIBUTION/AVAILABILITY STATEMENT  APPROVED FOR PUBLIC RELEASE; DISTRIBUTION UNLIMITED.					
13. SUPPLEMENTARY NOTES					
14. ABSTRACT For urban combat reconnaissance, the flapping wing micro air vehicle concept is ideal because of its low speed and miniature size, which are both conducive to indoor operations. The focus of this research is the development of experimental methods best suited for the vibration testing of the wing structure of a flapping wing micro air vehicle. This study utilizes the similarity of a beam resonating at its first bending mode to actual wing flapping motion. While computational finite element analysis based on linear vibration theory is employed for preliminary beam sizing, an emphasis is placed on experimental measurement of the nonlinear vibration characteristics introduced as a result of large movement. Beam specimens fabricated from 2024-T3 aluminum alloy and IM7/5250-4 carbon-epoxy were examined using a high speed optical system and a scanning laser vibrometer configured in both three and one dimensions, respectively.					
15. SUBJECT TERMS Flapping Wing Micro Air Vehicle, flapping-wing MAV, MAV, ornithopter, entomopter, nonlinear vibration, beam resonance, beam nonlinear vibration, carbon epoxy beam					
16. SECURITY CLASSIFICATION OF:			17. LIMITATION OF ABSTRACT	18. NUMBER OF PAGES	19a. NAME OF RESPONSIBLE PERSON
REPORT U	ABSTRACT U	c. THIS PAGE U			Anthony N. Palazotto, PhD
					19b. TELEPHONE NUMBER (Include area code) (937) 255-6565, ext 4599; anthony.palazotto@afit.edu